NAVAL POSTGRADUATE SCHOOL

MONTEREY, CALIFORNIA

THESIS

INVESTIGATION OF SHALLOW UNDEX IN LITTORAL OCEAN DOMAIN

by

Sung (Dean) H. Ahn

June 2014

Thesis Advisor: Young W. Kwon
Co-Advisor: Jarema M. Didoszak

Approved for public release; distribution is unlimited

THIS PAGE INTENTIONALLY LEFT BLANK

REPORT DOCUMENTATION PAGE

Form Approved OMB No. 0704-0188

1. AGENCY USE ONLY *(Leave blank)*	**2. REPORT DATE** June 2014	**3. REPORT TYPE AND DATES COVERED** Master's Thesis

4. TITLE AND SUBTITLE
INVESTIGATION OF SHALLOW UNDEX IN LITTORAL OCEAN DOMAIN

5. FUNDING NUMBERS

6. AUTHOR(S) Sung (Dean) H. Ahn

7. PERFORMING ORGANIZATION NAME(S) AND ADDRESS(ES)
Naval Postgraduate School
Monterey, CA 93943-5000

8. PERFORMING ORGANIZATION REPORT NUMBER

9. SPONSORING /MONITORING AGENCY NAME(S) AND ADDRESS(ES)
N/A

10. SPONSORING/MONITORING AGENCY REPORT NUMBER

11. SUPPLEMENTARY NOTES The views expressed in this thesis are those of the author and do not reflect the official policy or position of the Department of Defense or the U.S. Government. IRB Protocol number ____N/A____.

12a. DISTRIBUTION / AVAILABILITY STATEMENT
Approved for public release; distribution is unlimited

12b. DISTRIBUTION CODE
A

13. ABSTRACT (maximum 200 words)

With recent delivery of littoral combat ships, the impact of operating in shallow or littoral ocean domain (LOD) during the duration of their life cycle is of interest, and a shock trial or hardening test and validation for this class is needed. For this study, the theories of underwater shock phenomena as applied within the boundaries of LOD, specific to the Eulerian fluid domain were conducted. The results of varying ocean depth show clear distinction in UNDEX characterization at depths shallower than 300ft. Varying charge size and depth showed that charge size of less than 300lbs of HBX-1 displayed a linear relationship while changing the charge depths to near water-air or water-bottom interface also resulted in amplified characteristics of UNDEX parameters. In addition, varying lateral boundary showed that as its distance is brought inside the radius of bulk cavitation, the UNDEX behavior also became increasingly chaotic due to similar effects seen in the shallower bottom depth. Lastly, adding blocked cells prior to a full scale coupled run showed that fluid behaves more erratically as these small rigid boundaries are situated within the radius of forming bulk cavitation.

14. SUBJECT TERMS Underwater Explosion, Shallow Water, DYSMAS, Dyna_N(3D), Gemini, Pregemini, Eulerian, Lagrangian, Bulk Cavitation, Littoral Ocean Domain, UNDEX	**15. NUMBER OF PAGES** 145
	16. PRICE CODE

17. SECURITY CLASSIFICATION OF REPORT	**18. SECURITY CLASSIFICATION OF THIS PAGE**	**19. SECURITY CLASSIFICATION OF ABSTRACT**	**20. LIMITATION OF ABSTRACT**
Unclassified	Unclassified	Unclassified	UU

NSN 7540-01-280-5500

Standard Form 298 (Rev. 2-89)
Prescribed by ANSI Std. 239-18

THIS PAGE INTENTIONALLY LEFT BLANK

Approved for public release; distribution is unlimited

INVESTIGATION OF SHALLOW UNDEX IN LITTORAL OCEAN DOMAIN

Sung (Dean) H. Ahn
Lieutenant, United States Navy
B.S., Embry-Riddle Aeronautical University, 2006

Submitted in partial fulfillment of the
requirements for the degree of

MASTER OF SCIENCE IN MECHANICAL ENGINEERING

from the

NAVAL POSTGRADUATE SCHOOL
June 2014

Author: Sung (Dean) H. Ahn

Approved by: Young W. Kwon
Thesis Advisor

Jarema M. Didoszak
Co-Advisor

Knox T. Millsaps
Chair, Department of Mechanical and Aerospace Engineering

THIS PAGE INTENTIONALLY LEFT BLANK

ABSTRACT

With recent delivery of littoral combat ships, the impact of operating in shallow or littoral ocean domain (LOD) during the duration of their life cycle is of interest, and a shock trial or hardening test and validation for this class is needed. For this study, the theories of underwater shock phenomena as applied within the boundaries of LOD, specific to the Eulerian fluid domain were conducted. The results of varying ocean depth show clear distinction in UNDEX characterization at depths shallower than 300ft. Varying charge size and depth showed that charge size of less than 300lbs of HBX-1 displayed a linear relationship while changing the charge depths to near water-air or water-bottom interface also resulted in amplified characteristics of UNDEX parameters. In addition, varying lateral boundary showed that as its distance is brought inside the radius of bulk cavitation, the UNDEX behavior also became increasingly chaotic due to similar effects seen in the shallower bottom depth. Lastly, adding blocked cells prior to a full scale coupled run showed that fluid behaves more erratically as these small rigid boundaries are situated within the radius of forming bulk cavitation.

THIS PAGE INTENTIONALLY LEFT BLANK

TABLE OF CONTENTS

LIST OF FIGURES

THIS PAGE INTENTIONALLY LEFT BLANK

LIST OF TABLES

THIS PAGE INTENTIONALLY LEFT BLANK

LIST OF ACRONYMS AND ABBREVIATIONS

B	boundary
BB	bottom bounce
BC	bulk cavitation
BD	bottom depth
BK	block
DYSMAS	Dynamic System Mechanics Advanced Simulation
DOD	Department of Defense
DOF	degree of freedom
EOS	equation of states
FE	finite element
FSI	fluid-structure interface
FSA	fluid-structure interaction
FSP	floating shock platform
IABG	Industrieanlagen- Betriebsgesellschaft mbH
IHD	Indian Head Division
LB	lateral boundary
LCS	littoral combat ship
LOD	littoral ocean domain
LR	laterally reflected
MDOF	multi-degree of freedom
NPS	Naval Postgraduate School
NRB	nonreflecting boundary
NSWC	Naval Surface Warfare Center

SCI	standard coupler interface
SVCL	Shock and Vibration Computation Lab
SW	shock wave
SWI	singly-wetted interface
TNT	trinitrotoluene
UNDEX	underwater explosion
USN	United States Navy
VTO	vertical take-off or z-axis velocity

ACKNOWLEDGMENTS

I would like to first thank my wife, Tammy. Without her love, support, and patience, I would never have completed a fraction of this thesis, let alone finish all the research and course work on time. I also would like to thank Professor Young Kwon of Naval Postgraduate School's Mechanical Engineering Department for giving me an opportunity to work under his guidance. His continual encouragement and fundamental-based approach to research helped me to stay focused during the more challenging and frustrating aspects of my research. Additionally, I would like to thank Professor Jarema Didoszak of Naval Postgraduate School's Shock and Vibration Computational Laboratory. His in-depth knowledge in the field of underwater explosion and the use of DYSMAS provided the guidance and inspiration I needed to complete this research. His never-ending patience in teaching me the highly complex DYSMAS/GEMINI code and its usability were truly instrumental in every aspect of my research.

THIS PAGE INTENTIONALLY LEFT BLANK

I. INTRODUCTION

A. BACKGROUND

The theory of underwater explosion (UNDEX) phenomena has been studied extensively since post World War II. For United States Navy (USN), its motivation was to analyze damages incurred on surface and subsurface vessels during direct impact and near misses from underwater weapons. Since then, advancement in computing power, extensive understanding of the UNDEX theory and theory of finite element have led to solidifying efforts in validating shock trial analysis of newly commissioned ships via modeling and simulation prior to an actual at sea shock trial analysis. The result is software that utilizes UNDEX theory, based on theoretical works of Arons, Cole, Snay and Taylor, called Dynamic System Mechanics Advanced Simulation (DYSMAS) [1]. DYSMAS is a result of the combined efforts of German Defense Contractor, Industrieanlagen-Betriebsgesellschaft mbH (IABG) and Naval Surface Warfare Center Indian Head Division (NSWC – IHD), as well as, Lawrence-Livermore, led by the USN. It is a six degree of freedom (DOF) finite element hydrocode used to model and simulate fully coupled, fluid-structure interaction (FSA) problems of an UNDEX event on a surface or subsurface vessel.

With the recent delivery of the littoral combat ship (LCS), the impacts of operating in a shallow or littoral ocean domain (LOD) during the duration of the ship's life cycle are of interest. Thus, a shock trial or hardening test and validation for this class is needed. However, due to current Department of Defense's (DOD) budgetary constraints and rising LCS class issues, an actual shock trial analysis for LCS class has been postponed indefinitely [2]. Nevertheless, continued study of FSA within the LOD during UNDEX is needed in order to verify the sea and battle worthiness of LCS class.

From Naval Postgraduate School's (NPS) Shock and Vibration Computation Lab (SVCL), several studies have already been conducted to address the factors of UNDEX simulations of littoral or shallow water by Walters, Arbogast, and Santiago regarding explicitly modeled solid Lagrangian ocean floor, influence of shock-induced air bubble collapse and cavitation effect on surface ship model, respectively. As Walters suggests,

the distinct advantages of using Lagrangian solid bottom was the ability to model contoured bottom shapes and for the various solid bottom types created, there were significant differences between the initial bottom reflections for the different contours [1]. He further suggests that the most important bottom contour effect was the distortion to the gas bubble and its associated first pulse timing. Santiago's study of bulk cavitation (BC) effect on fluid-structure interaction (FSA) shows that the effects of cavitation closure can be quite significant and inflict another impulsive force upon the ship as reported empirically during an actual shock trial report of DDG 53, in addition to the incident wave, bubble pulsations, bottom reflection, or bottom refractions [3]. Lastly, Arbogast's work showed that the bubbles in the vicinity of marine vessels, depending on the size and location and proximity of these bubbles, created a buffering effect from shock induced by an UNDEX [4].

B. SCOPE OF RESEARCH

The importance of FSA and depth of such UNDEX theory in evaluating and analyzing shock design of a naval vessel cannot be understated. However, in order to understand the FSA, first, a solid understanding of how fluid behaves during UNDEX must be clearly sought out. As Figure 1 shows, there are numerous theoretical and experimental analysis that deals with the interdisciplinary studies of Naval Ship Shock Design and Analysis [5]. In short, it is primarily divided into structural analysis that stems from a thorough understanding of dynamic fluid characteristics and fluid-structure interactions during UNDEX through the use of finite element modeling and simulations, as well as, real world experimental validations. For this study, the theories of underwater shock phenomena as applied within the boundary of shallow water or LOD will be of focus.

Building on the knowledge of previous researches conducted here at NPS and various UNDEX studies published over the years, a more in-depth analysis and characterization of LOD is attempted. Furthermore, a clear definition of LOD, in terms of UNDEX parameters, especially the influence on BC is sought out. In addition, the implementation of various boundary conditions for both bottom and side conditions of fluid domains were compared and contrasted in the current Eulerian fluid model, gaining

better understanding of their effect on shallow water UNDEX phenomena. In short, several variations of typical benchmark LOD problems were modeled and simulated using DYSMAS to gain better insights to its resulting UNDEX parameters including the impacts that BC have on the overall response to fluid behaviors.

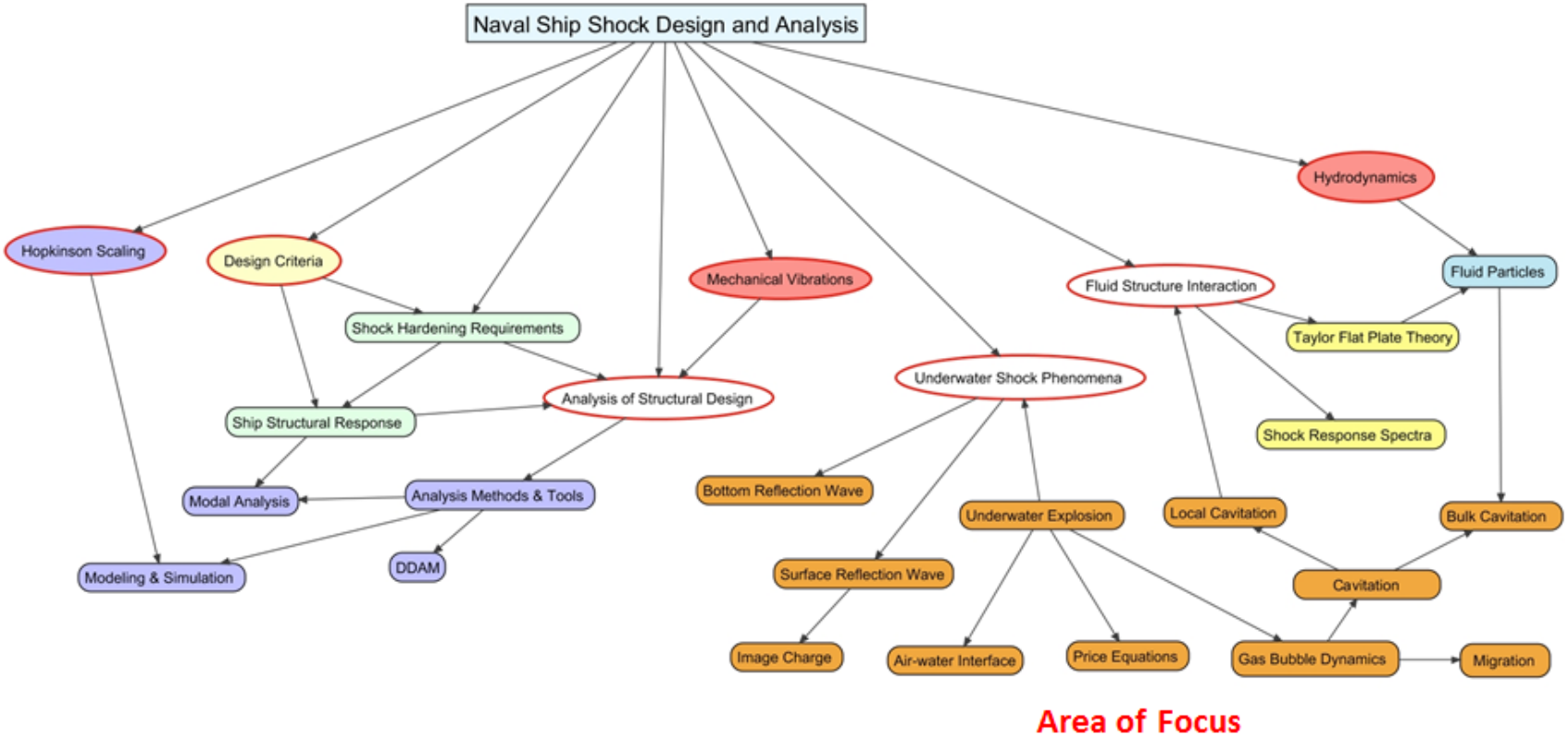

Figure 1. Naval Ship Shock Design and Analysis, from [5]

II. UNDERWATER EXPLOSION THEORY

A. INTRODUCTION TO CONVENTIONAL, NON-NUCLEAR EXPLOSION

A conventional, non-nuclear explosion is a chemical reaction in a material or substance that converts the original material into high pressure gas and temperature at extreme and catastrophic speed [6]. In general, any explosive material, regardless of its state, is an unstable compound that becomes more stable during the chemical reaction that takes place post ignition and detonation. The temperature within the explosion of a gas is usually in the order of 3,000˚ C (5,432˚ F) and the pressures are greater than 50,000atm (734,797psi) [6]. A reaction of this magnitude can only be initiated with sufficient energy provided to a specific place within the explosive prior to detonation and is done usually by means of a fuse.

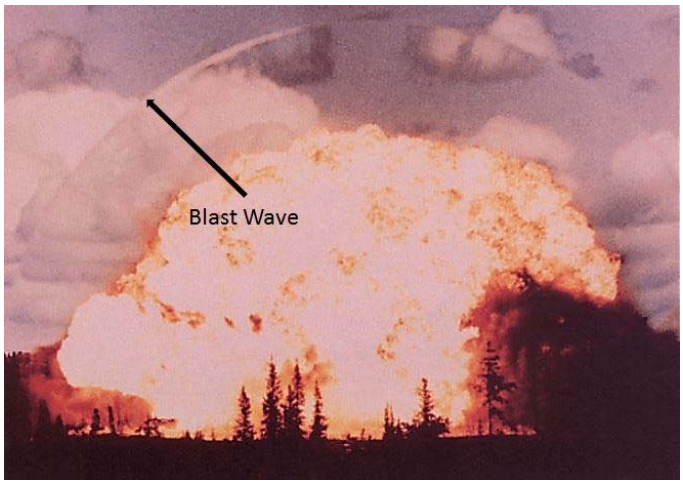

Figure 2. Conventional, Non-nuclear Explosion on Land, from [7]

During detonation process, the developing intense heat and pressure are sufficient to set up the explosive material surrounding the fuse. As a result, a very narrow boundary between the exploding material and its surrounding develops as a product of extremely high temperature, pressure and energy. This distinctly defined rapidly advancing discontinuity, known as a “detonation” or “blast wave,” travels with a velocity of several thousand feet per second and destroys everything in its path (Figure 2) [6].

The way in which blast waves or detonating disturbance propagates depends on the physical or chemical properties of explosive materials and the surrounding medium—air, water or vacuum—at which the explosion takes place. From the standpoint of destructiveness of explosive materials and impact to its surrounding, the process of detonation, propagating shock waves (SW) and energy transfer that takes place through the means of pressure or velocity changes to its surrounding becomes increasingly important.

B. UNDERWATER EXPLOSION

Conventional UNDEX is a non-nuclear explosion that takes place at the surface or subsurface of water. The characteristics of UNDEX is similar to that of conventional explosion discussed previously, except due to water as medium, the initial mass of explosive becomes unstable hot mass of gas at tremendous pressure that radiates spherically affecting its surrounding (see Figure 3(a)). The energy expenditure during UNDEX detonation accounts for predominantly the SW energy (45%) and bubbles (45%) with approximately 10% unaccounted for (see Figure 3(b)) [8]. Within the energy expenditure partition of SW and bubbles, local and BC are also accounted for some of the energy that was imparted into its surrounding water during detonation.

For this research, water is characterized as a homogeneous fluid capable of supporting only limited shearing stresses; hence, a medium and its volume of which can readjust itself to displacement of boundaries by result of flow [6]. In addition, as conservation of energy and work implies the change in its pressure on confined mass results in compression or work done to that system, which creates change in volume of such mass. Hence, when pressure is applied to a localized region, the compressibility of water makes it possible for it to transmit energy as a wave disturbance to other parts within the domain with a finite velocity which results in a local motion of water and pressure changes.

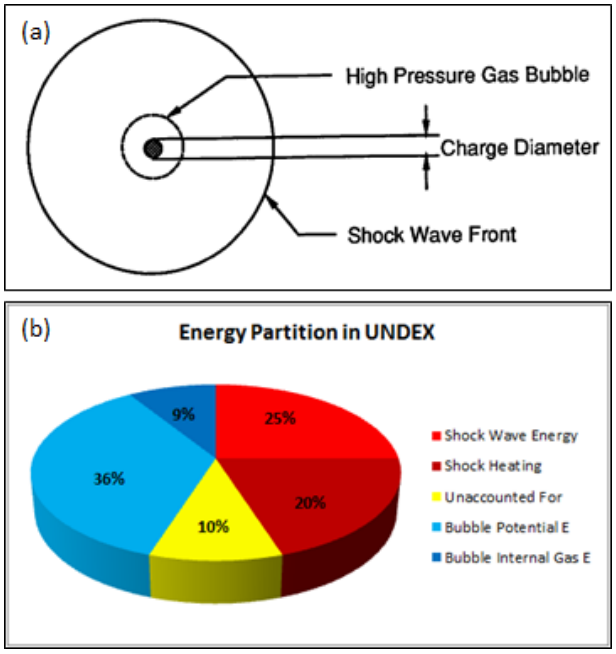

Figure 3. (a) Shock Wave and (b) Energy Partition at Time of Detonation, from [5], after [8]

If the pressure applied to localized regions within the water domain is small enough, the rate of propagation or wave of disturbances can be independent of its pressure magnitude. This propagating SW travels at about 4,900ft/sec (fps), in sea water at 18˚ C (64.4˚ F) [6]. Of note, this velocity of the propagating disturbance is also dependent on other characteristics of the water, like salinity and its density. If this wave motion is simplified to one-dimension so that plane waves are assumed, vice spherical, the wave travels without significant changes in its characteristics. However, if the detonating waves are radiated from a spherical source, there is an inverse relationship between the amplitude of the radiating SW and distance from its source. During the diverging propagation of spherical wave, motions of its surrounding water are affected due to "surge or afterflow" that takes place in reaction to propagating waves [6].

As this SW propagates, the effects it has on the surrounding medium and various boundaries like water-air and water-bottom interfaces, cause additional tensile or compressive wave that induces additional havoc to existing underwater objects. When initial SW reaches water-air interface, the differences in tensile and compressive strengths of water and air causes massive cavitation called, BC as it spallates the water

particles on the surface and separates this layer from below. The initial bubble with its detonating cycles of its expansion-collapse motion as it rises to the surface and spews out exploding material into the atmosphere due to buoyancy, it too creates another catastrophic havoc to anything in its path or in the vicinity there of. Hence, the five primary events that take place upon detonation during UNDEX are initial SW propagation, formation of BC, cyclic bubble phenomena, secondary or third pressure pulses due to boundary reflections and surface phenomenon.

1. The Shock Wave and Acoustic Wave Assumptions

The initial cause of disturbance to the water in an UNDEX is the arrival of shock pressure wave reacting between the boundaries of explosives and water [6]. This pressure distribution, usually in the order of 34,000lb/in^2 (psi) for a 300lbs of TNT, begins to rapidly decay as it propagates followed by intense peak pressure wave in an outward motion of the water (figures 4 and 5) as the extremely dense mass of exploding gas continues to spherically expand as detonation takes places. As its SW pressure diminishes, so too does the pressure in the water fall off rapidly, as shown in three different target distances of 5, 50 and 500ft from the point of detonation (Figure 4). Lasting for a few milliseconds at most, a discontinuity exists in the initial SW pressure rise that is followed by a distinct exponential decay, shown in Figure 5 [6].

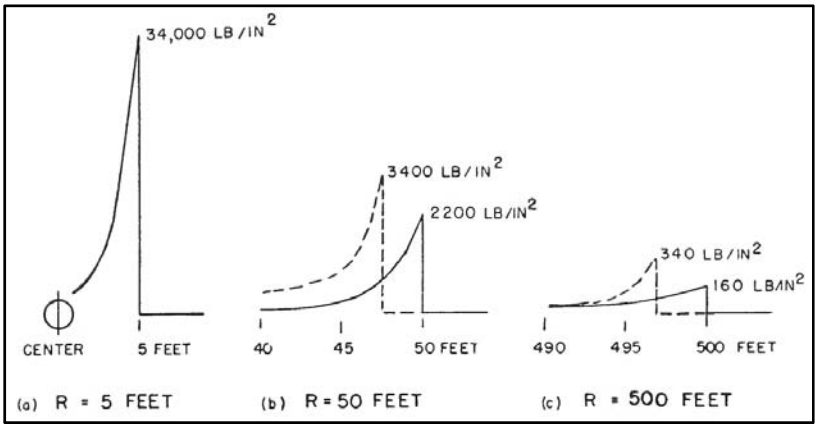

Figure 4. Pressure Distribution at (a) 5ft (b) 50ft and (c) 500ft from Detonation, from [6]

The pressure distributions of a 300lbs TNT charge, shortly after detonation at target distance of 50 and 500ft at three instants of time from the center of TNT charge are depicted in Figure 5. For comparison, the initial wave in previous Figure 4(a) is also depicted in acoustic wave form by dotted lines for (b) 50 and (c) 500ft. The obvious scaling law that emerges when different charge sizes are used is called, "principle of similarity." The principle of similarity states that "if the linear size of charge is changed by factor of k, the pressure conditions will also change at new distance and time scales k times as large as the original ones are used" [6].

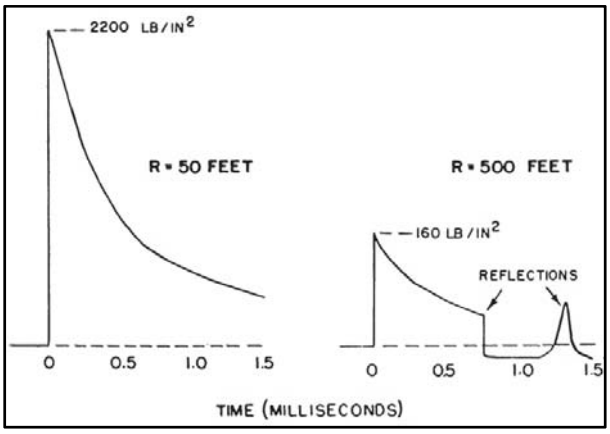

Figure 5. Shock Wave Pressure Profile at Two Distances from Detonation, from [6]

The radially propagating disturbance as a wave of compression in water called, "shock wave" has following characteristics [6]:

a. The initial velocity of propagation at or near charge and water boundary is approximately 5,000fps at detonation and drastically falls to its "acoustic" values as wave advances outward (Figure 4)

b. The pressure level in spherically propagating wave falls off more rapidly than with inverse of distance near the charge at detonation, but eventually converges to this behavior as it reaches larges distances.

c. The region of highest peak pressure is at target location closest to the charge at detonation and its wave profile broadens gradually as the wave propagates outward. Same characteristics can be observed at various target location with reduced peak pressure.

As mentioned, since the initial SW velocity will be drastically reduced and eventually converged to acoustic speed as it propagates, it is assumed that the SWs are approximated as acoustic plane waves with small compression and speed. As a result, following Equation (2.1) is derived,

$$P = \rho_o C_o u \tag{2.1}$$

which states that the added fluid pressure (P) from propagating shockwaves is a function of water's mass density (ρ_o), acoustic wave speed (C_o) and its propagating velocity (u). The medium in which SW travels, water in this case, are considered to be constant properties and as mentioned previously, this relationship assumes that water is uniform, homogenous, compressible and inviscid.

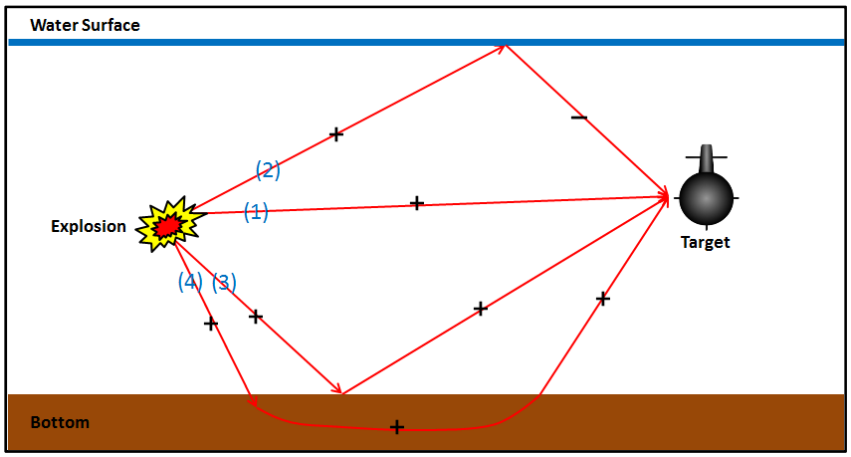

Figure 6. UNDEX Geometry and Various Paths of Detonating Shockwave, after [5]

There are basically four primary paths that a propagating shockwave can travel during an UNDEX event before reaching its target (Figure 6): (1) Direct Path (2) Surface Reflected or Rarefacted (3) Bottom Bounce and (4) Bottom Refracted Waves. Depending on the UNDEX geometry of the explosion in terms of charge depth, size and ocean depth, these shockwave travels in the order of listed and the nature of applied pressure waves are either compressive (+) or tension (-) as experienced by the target due

to varying densities at water, air or bottom interfaces. Of note, the tensile pressure wave of (2) surface cut-off is due to water's inability withstand tensile force at air-water interface; hence, creating a region of expansion in water molecule rather than a compressive stress near detonation and other traveling path of pressure wave.

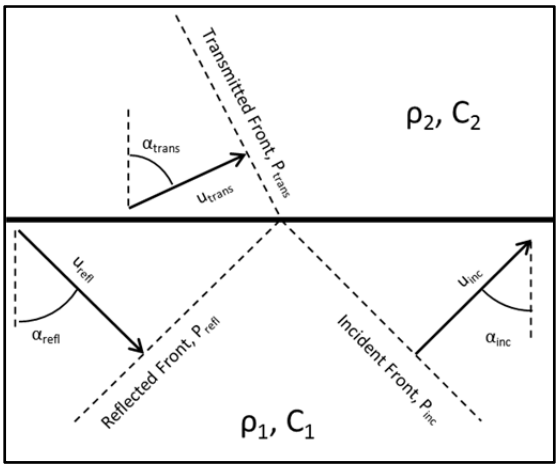

Figure 7. Arbitrary Interface Geometry, from [1]

The initial shockwave's behavior at an interface such as water-air or water-bottom (seabed) can be approximated by using combinations of Snell's law and pressure-velocity continuity at the interface [5]. An arbitrary two different medium interface is shown in Figure 7. Using Snell's law, the relationship of various medium's acoustic speed (C) and its angle of incident (α) to the approaching interface can be referenced to its normal vector of that interface or summarized in Equation 2.2 below:

$$\frac{C_1}{\sin \alpha_{inc}} = \frac{C_1}{\sin \alpha_{refl}} = \frac{C_2}{\sin \alpha_{trans}} \tag{2.2}$$

Now, if the pressure-velocity continuity is applied, equations (2.1) and (2.2) can be combined to describe the interface, yielding the following relationship between the pressure and incidental velocity, as well as, reflected, refracted or transmitted shockwaves.

$$\frac{P_{refl}}{P_{inc}} = \frac{\rho_2 C_2 \cos\alpha_{inc} - \rho_1 C_1 \cos\alpha_{trans}}{\rho_2 C_2 \cos\alpha_{inc} + \rho_1 C_1 \cos\alpha_{trans}} = \frac{u_{refl}}{u_{inc}} \tag{2.3}$$

$$\frac{P_{trans}}{P_{inc}} = \frac{2\rho_2 C_2 \cos\alpha_{inc}}{\rho_2 C_2 \cos\alpha_{inc} + \rho_1 C_1 \cos\alpha_{trans}} = \frac{\rho_2 C_2}{\rho_1 C_1}\frac{u_{trans}}{u_{inc}} \tag{2.4}$$

Therefore, when above relationships are applied to varying boundaries, the resulting pressure wave becomes either compressive or tensile waves. At rigid boundary ($\rho_2C_2 >> \rho_1C_1$), such as the water-bottom interface, the wave reflections are compressive with the magnitude of both incident and reflected waves pressure and velocity being equal, since by definition, the velocity of a rigid boundary is zero [1]. For a non-rigid boundary condition ($\rho_2C_2 << \rho_1C_1$), such as water-air interface, the same relationships applied as above results in a tensile reflection or rarefaction waves.

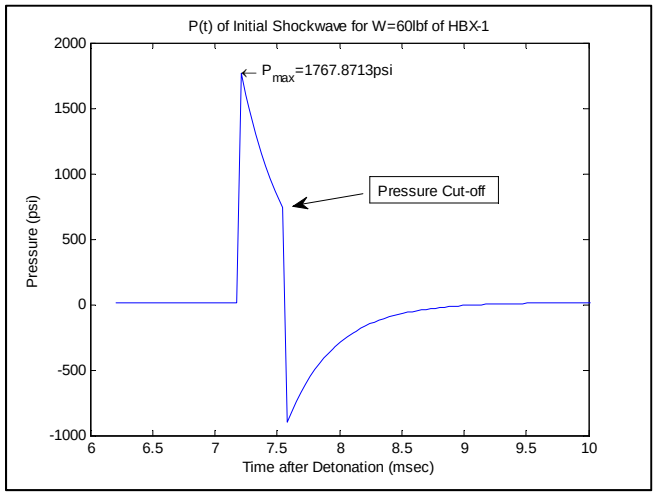

Figure 8. MATLAB Figure of Pressure History, from [1]

The simultaneous passage of a compressive and tensile wave through a point at different times causes a unique effect creating a discontinuous drop, is called the pressure cutoff shown in pressure-time history in Figure 8. At this point, the abrupt halt to the impulse induced on a target at the point of cut-off can also be observed [1]. This dependence of UNDEX behaviors on its geometry is depicted in Figure 9 and using such

geometry, pressure and vertical take-off velocity (VTO) can be calculated to analyze target behavior at various instants of time.

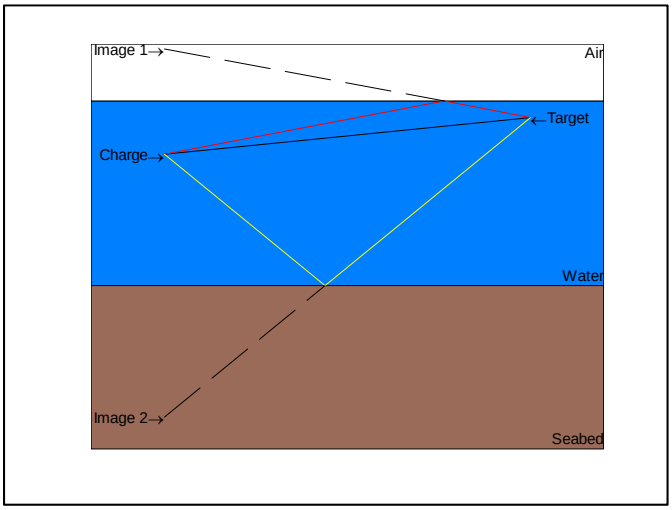

Figure 9. UNDEX Geometry, from [1]

The obvious interdependence of charge weight and wave propagation distance for spherical charge gave rise to empirical formulas to approximate several important parameters of UNDEX that have been continuously developed and tested by Cole and others since WWII [5]. The two primary formulas are the peak pressure (P_{max}) and decay constants (θ) shown in Equations (2.5) and (2.6):

$$P_{max} = K_1 \left(\frac{W^{1/3}}{R} \right)^{A_1} \tag{2.5}$$

$$\theta = K_2 W^{1/3} \left(\frac{W^{1/3}}{R} \right)^{A_2} \tag{2.6}$$

where charge weight (W) is in pounds, the wave propagation distance (R) is in feet, the peak pressure (P_{max}) in psi and the decay constant (θ) in milliseconds (msec). The constants K and A are depended on the explosive materials used and were found

experimentally prior to this research through numerous field testing during various historical researches [5].

2. Typical UNDEX Problem

A typical UNDEX problem with an explosive charge of weight, W, detonated in water at depth, D, is considered in Figure 10 and its corresponding pressure wave profile as time passes is shown in Figure 11 [9]. The water depth for this problem is assumed to be infinitely deep; therefore, negligible when it comes to bottom bounce interaction and considerations. In order to measure various parameters of UNDEX event taking place, an absolute pressure gage is located at target location of point (X, Y) or 1 to measure the pressure changes at this location. As detonation takes place, a compressive SW propagates radially or spherically from its source and travels along the line 0 – 1 in Figure 10 as it reaches the target or gage location [9].

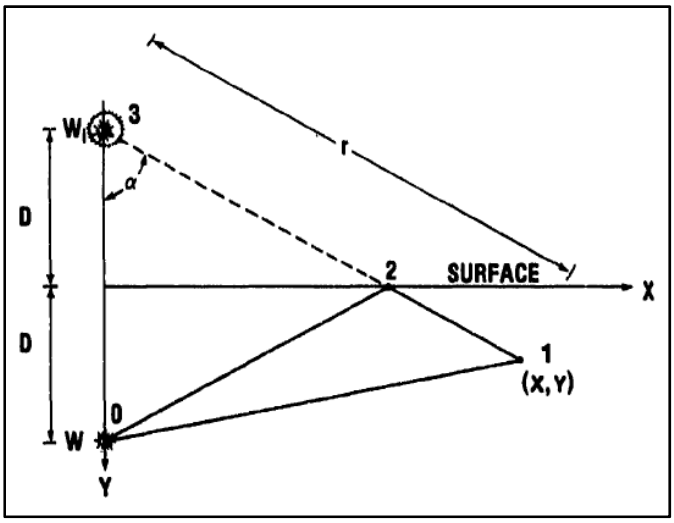

Figure 10. Incident and Reflected Wave Paths, from [9]

The absolute pressure gage shows constant pressure at its hydrostatic depth denoted by line A – B in Figure 11 prior to detonation. This pressure at this depth is sum of atmospheric and hydrostatic pressure at the gage depth and upon arrival of SW at target point, the pressure jumps to point C, followed by exponential decay along line C – D is observed [9]. As will be shown for most of the cases studied in this research, this

pressure is at or close to 14.7 psi or 1atm; for all practical purpose, at or near surface of the water. As shown previously in Figure 6 and now Figure 10, the line 0 – 2 represents the compressive path of SW as it travels to the water-air interface. Next, the SW takes the path of 2 – 1, where a rarefaction or tensile wave is observed due to difference in acoustic impedance of air and water mentioned previously.

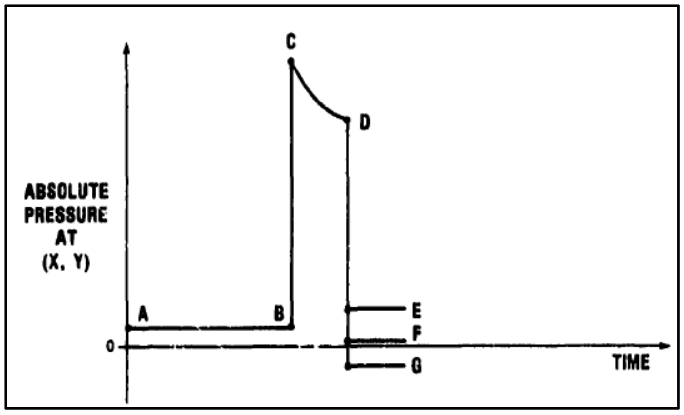

Figure 11. Absolute Pressure at a Point, from [9]

The arrival of this rarefaction or surface reflected wave at the gage location is termed surface cutoff and is illustrated in Figure 11 by a sudden drop in the absolute pressure from point D to three different locations, E, F or G, depending on the vapor pressure of the surrounding water [9]. This concept of surface cutoff is made clearer by depicting the rarefaction wave as emanating from an image charge, W_i, and propagating along line 3 – 2 – 1 in Figure 10. This method of including image charge to calculate surface cutoff characteristics is known as method of images and is valid since the distance 3 – 2 – 1 equals the distance 0 – 2 – 1. Therefore, where point D drops upon cutoff as the rarefaction wave tries to lower the absolute pressure at the gage location is depended on one of three levels [9]:

E: If pressure at E is greater than vapor pressure

F: If pressure at F is great than cavitation but less than vapor pressure

G: If pressure at G is less than cavitation pressure

3. Bulk Cavitation

The arrival of rarefacted or reflected wave near surface, also called cut-off due to water's inability to withstand tensile force at air-water interface, creates BC near air-water interface. In general, unlike seawater, pure homogenous water with no impurities is able to withstand a considerable amount of tensile stress. Due to abundance of obvious biological and non-biological impurities, seawater can withstand very little tension. As a result, the layer of sea water at or near the water-air interface ruptures and the pressure falls to the vapor pressure of water, assumed to be approximately zero for all practical purpose when dealing with UNDEX [10]. Within the areas of rupturing water layer near the surface, a collective spallation takes places vertically and tensile stresses at its lower boundary tending the water particles to return to its original, pre-shocked position cease to exist. Of note, the motion of spallation is dictated primarily by the atmospheric, hydrostatic pressure and the acceleration due to the gravity. The radial and vertical thickness of typical BC zone for a 60lbs charge of HBX-1 at a depth of 30ft is depicted in Figure 12. As shown, this charge size and depth creates a BC that is 574ft in radius and 24.6ft deep at its maximum thickness; hence, as shown, its radius is several magnitudes longer than its radius.

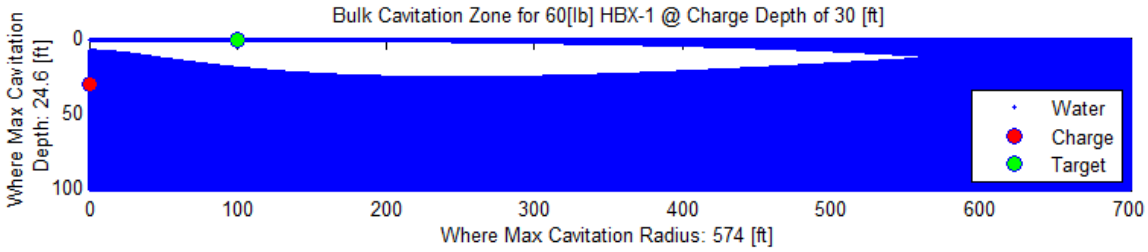

Figure 12. BC Zone for 60 lbs of HBX-1 at 30ft

Next, the spalled water layer is driven back downward by force of gravity so that ultimately it must impact the underlying water and produces a traveling source of secondary pressure wave in the water called "hammer." This traveling source and hammer created are almost equivalent to a "sonic boom" in the atmosphere and because of its focusing effects, the secondary pressure due to hammer can reach intensity as high

as initially propagating SW [10]. Interestingly, the region of cavitation between the upward traveling spalled water layer and the relatively quiescent underlying body of water have an average specific volume greater than that of seawater and this intervening region is termed the BC region due to its size and can be observed in figures 12 and 13.

Figure 13. Photograph of Upper Surface of Bulk Cavitation, from [11]

Finally, in an attempt to summarize numerous BC studies conducted and theories derived over the years since the 1960s, the critical sections within the technical paper published by Costanzo and Gordon in May 1983, titled "A Solution to the Axisymmetric Bulk Cavitation Problem" [9], as well as, sample case studies are all included in the Appendix of this study as a reference and also to be used in subsequent chapter's analysis of LOD UNDEX phenomenon for its underlying characteristics of BCs.

4. Motion of Gas Sphere and Its Empirical Bubble Formula

During the expansion and collapse of cyclic bubble, the initial peak pressure in the expanding gas sphere is decreased dramatically due to energy dissipation to its surrounding from detonation. However, the immediate state of the spherical bubble that follows still has much higher pressure than the equilibrium hydrostatic pressure at that depth [6]. This sphere or bubble has a tremendous outward velocity as its diameter increases rapidly and is proportional to the pressure magnitude at that exact time. The expansion of bubble continues for a relatively long period of time compared to other

transient UNDEX phenomenon like initial shock waves or BC. As this bubble reaches its maximum radius, the internal gas pressure decreases dramatically, while the expanding motion continues due to the inertia of water flowing outward [6]. As the internal gas pressure eventually falls below the equilibrium pressure (hydrostatic + atmospheric), this outward motion or flow stops and the bubble begins to contract at an increasing rate. The contraction or inward motion of the bubble continues until it reaches the maximum compressibility of the gas and reverses the motion once again due to reloading of pressure differences within the bubble and its surrounding. Hence, the created elastic properties of the gas and water due to detonating pressure and hydrostatic influences of surrounding water, in time creates a condition of oscillating system that repeats itself until it reaches the surface of the water [6]. This cyclic nature of bubble expansion and collapse as function of time, as well as, its displacement as it travels up towards the surface due to hydrostatic forces induced by surrounding water and gravity is depicted in Figure 14.

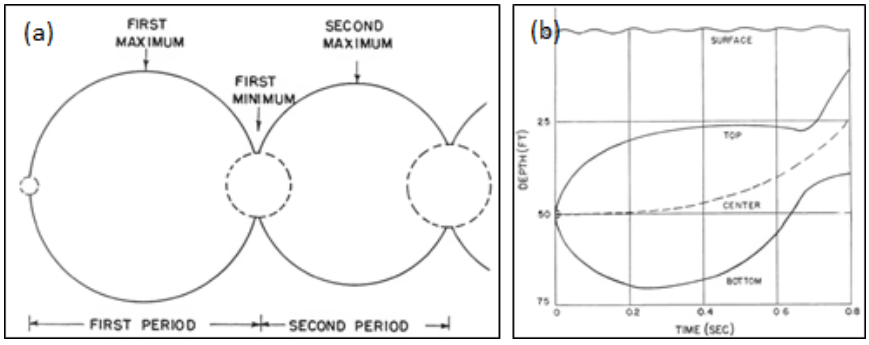

Figure 14. (a) Pulsation and (b) Displacement of Gas Bubble, from [6]

The traveling cyclic bubble pulses and its comparison to corresponding pressure profile during UNDEX are shown in Figure 15. As mentioned, the initial shockwave pressure is the greatest at minimum bubble radius at the time of detonation. As the cyclic bubble pulse travels to near water-air interface, the detonating energies are dissipated and the bubble eventually reaches the surface to create plume into the atmosphere. This nature of cyclic bubble can induce hull whipping to surface vessels if period of the bubble pulse matches its lowest natural frequency; hence, the importance of analyzing

such phenomenon during UNDEX. Within the energy partition of the shockwave bubble, the initial shockwave dominates initial energy dissipation followed by cyclic bubble pulses (Figure 16). The initial SW energy can be as high as 50% of total bubble dissipated energy while the remaining energies are attributed to traveling cyclic bubbles pulses [8].

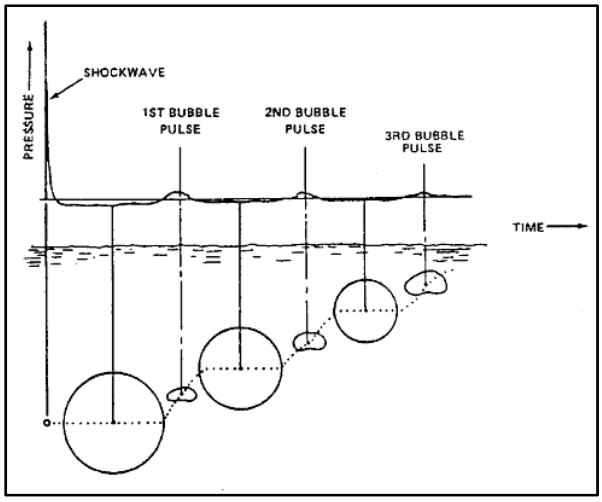

Figure 15. Traveling Cyclic Bubbles and Its Pressure Profile, from [5]

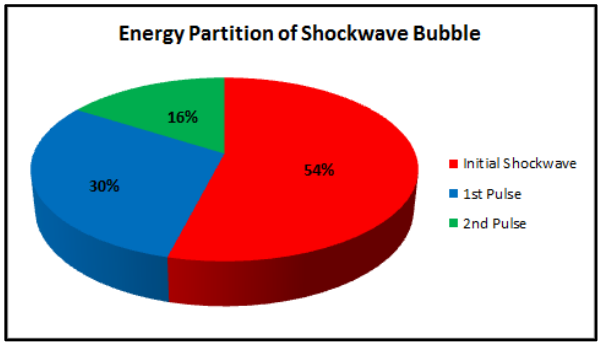

Figure 16. Energy Partition of Shockwave Bubble, after [8]

Numerous theoretical methods and approaches to modeling and analysis of gas bubbles and its oscillations have been published over the years. However, for this study, a shallow water assumption was made to limit the scope of such analysis. As a result, two parameters of gas bubble emerge during UNDEX, its maximum radius and period of initial pulse [1]. Taking into account the correction factor that must be included due to

proximity of the air-water or water-bottom interfaces in shallow water, as well as, following the same intuitions in deriving shockwave pressure equations (2.5) and (2.6), the maximum bubble radius (A_{max}) in feet is derived [5]:

$$A_{max} = K_6 \left(\frac{W}{D + 33} \right)^{1/3} \tag{2.7}$$

Next, the period of initial bubble pulse (T) is derived in seconds with its correction factor due to distance from surface, shown in Equation (2.8). The correction factor of numerical constant (α) is equal to 0.1 when Amax/D is less than 0.5 and when greater than 0.5, then α is approximated between 0.1 and 0.2 [8].

$$T = K_5 \frac{W^{1/3}}{(D + 33)^{5/6}} \left(1 - \alpha \frac{A_{max}}{D} \right) \tag{2.8}$$

5. Secondary or Additional Pressure Pulses and Surface Effects

As described previously, the bubble pulse due to cyclic expansion of gas as it travels to the surface of the water depends considerable on the water depth and proximity of the boundary surfaces at detonation. The first peak pressure of bubble pulse is usually no more than 10 to 20% of that of initial SW [6]. However, its duration is much longer and the areas under the pressure profile curve are considerably close [6]. During completion of each cyclic bubble pulse, a considerable amount of the energy initially present at detonation is lost due to energy transfer that occurs to its surrounding water as it travels and pulsate, as seen previously in figures 14 and 15. As a result, only the first bubble pulse is of practical significance since the successive pulses progressively weaken to negligent magnitude. The relations between initial SW and the first bubble pulse pressures and durations are shown in Figure 17 and Figure 18 shows close up details of the bubble pulse pressure generated from 300 pounds of TNT charges detonated at various depths in 100 feet total depth of water.

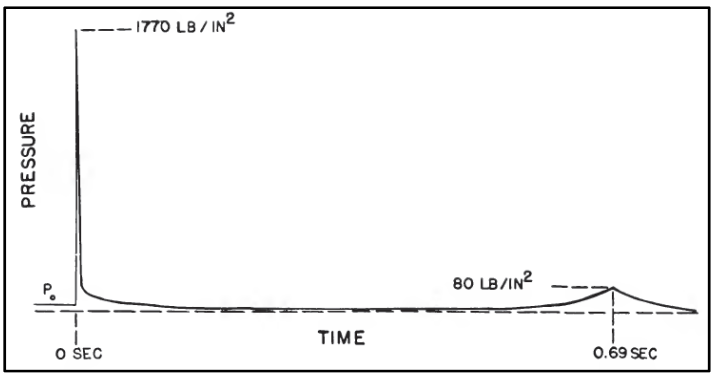

Figure 17. Pressure 60ft from 300lbs TNT Charge Detonated at 50ft, from [6]

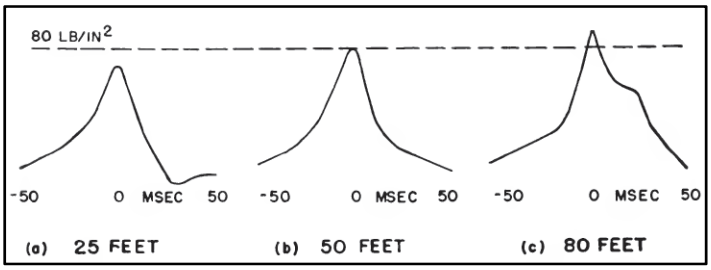

Figure 18. Various Bubble Pulses of 60ft at Various Detonated Depth, from [6]

It is observed that the profile of the first bubble pulse curve in Figure 18 becomes increasingly irregular for initial charge position close to either surface or bottom [6]. Also, for shallow water or LOD conditions, the traveling cyclic bubbles and the reflecting pressure waves from the surface or bottom give rise to interference; therefore, as would be observed in this study, the later portions of observed pressure profiles are considerably different than what would be observed in an infinitely deep water domain [6]. Lastly, the interaction on the water-air surface boundaries as initial SW and bubble reaches the surface is also important. While the initial SW creates BC at this interface, the spray dome and subsequent bubble pulses can generate multiple overlapping plumes that literally shoot or hurl the mixture of explosive materials and water vapors into the atmosphere creating additional havoc during UNDEX. This surface phenomenon which marks the end of major UNDEX events is shown in Figure 19.

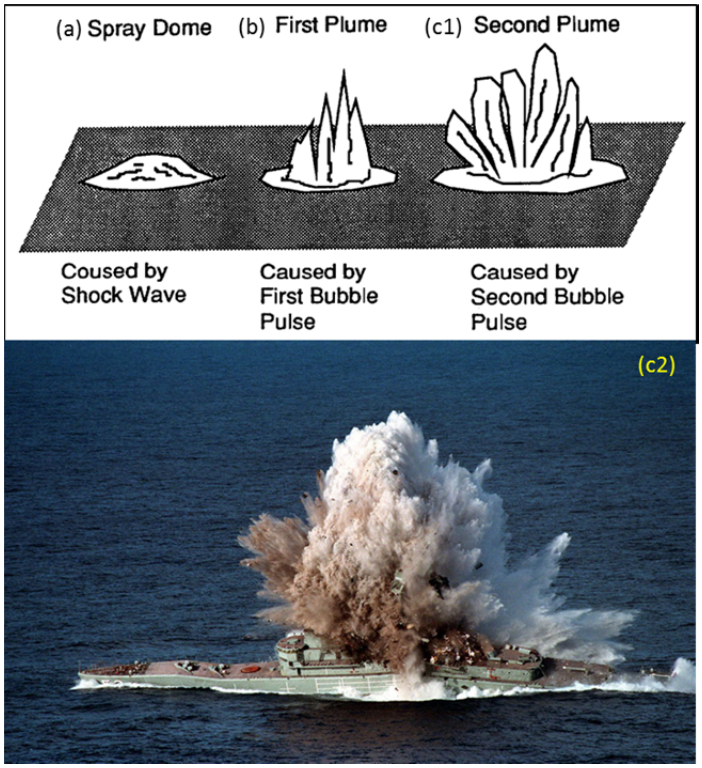

Figure 19. Surface Phenomena (a) Spray Dome or Spallation (Bulk Cavitation) Caused by Initial Shock Wave (b) First Plume Caused by the First Bubble Pulse (c1, c2) Subsequent Plume caused by Burping Bubble Pulses, from [5]

III. MODELING AND SIMULATION USING DYSMAS

A. DYSMAS

The software package used for this research is the DYSMAS finite element hydrocode. DYSMAS is a fully coupled; six degree of freedom (DOF) finite element (FE) based hydrocode that is designed to simulate three-dimensional (3D), UNDEX events to analyze fluid-structure interactions (FSA). The foundation of DYSMAS' theoretical concepts is based on FE methods and like any common FE software suite currently available, it consists of two major fluid and structural solvers, Gemini and Dyna_N(3D), that is interfaced by the Standard Coupler Interface (SCI) along with a pre- and post- processor called, DYSMAS/P [12]. The basic DYSMAS suite architecture is depicted in Figure 20.

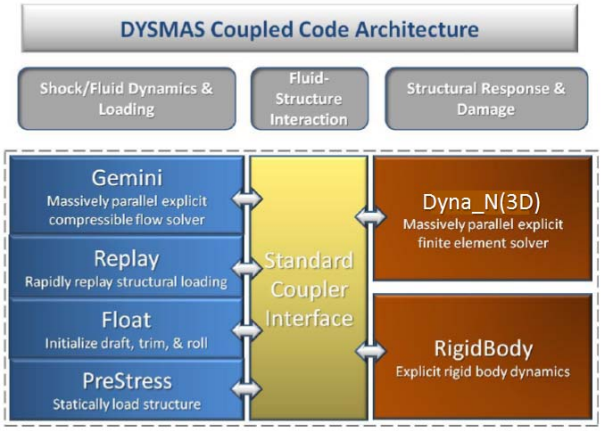

Figure 20. Basic DYSMAS Coupled Code Architecture, from [12]

The Gemini is an Eulerian fluid solver and the Dyna_N(3D) is a Lagrangian structural solver that evaluates the structural dynamic response during UNDEX. The SCI is the key coupler that connects and interfaces during a fully "coupled" simulation of both solvers by passing information between the two solvers at the end of each Eulerian time step, maintaining fully coupled interface. There are several other structural solvers that can be used in coupled DYSMAS run, such as RigidBody solver. DYSMAS/P and other

post processors like MATLAB were used for detailed analysis on the results, both graphically and numerically.

1. GEMINI

For this study, only the Gemini portion of DYSMAS was utilized in Eulerian fluid behavior analysis during UNDEX. The Gemini code is a finite-difference, Eulerian fluid equation solver that solves fluid mesh by running a higher order Godunov method algorithm to solve the fluid domain at each time step [13]. Designed specifically to simulate the shockwaves, cavitation and bubble jetting phenomena of UNDEX, Gemini is capable of solving flow fields involving several Eulerian fluid types. Using conservation of mass, momentum, and energy, the Godunov method algorithm is applied to solve each Eulerian equation for each cell within the fluid domain with a major assumption of Euler equation being that the flow is frictionless or inviscid.

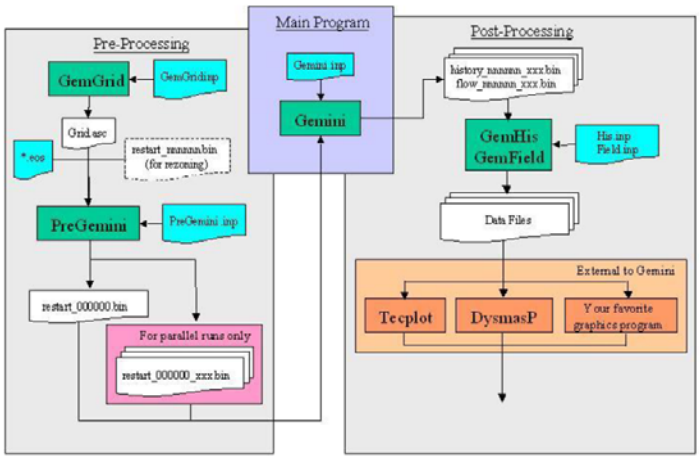

Figure 21. Basic Components of GEMINI, the Eulerian Solver, from [12]

Gemini consists of several additional components codes: GemGrid, PreGemini, Float, and Prestress are preprocessors. The user defined and required "input" files (shown in blue, Figure 21) are used to specify each component codes. The sample input files are also included in the Appendix of this report. These sub component codes are used to customize fluids domain set up for a given UNDEX problem. GemGrid is used to set up the initial Euler cell grid, up to three-dimensions and can be used for any grid

refinement that is needed around specific areas of interest in the flow field, specifically the fluid bubble, cavitation and the Lagrangian structures. PreGemini is used to fill the Euler cell grid with the user-defined Eulerian materials that utilizes the given "material files" that encompasses specific material's equation of state and initial properties, such as energy, density, and etc. In order to accurately position and prestress the Dyna_N structure in the fluid domain prior to transient analysis, the Float and Prestress processors are used.

As Gemini solves each Eulerian cell grid, it dumps and saves all flow field and historical data into a bin file, which in turn are finally processed by GemHis and Gemfield processor. GemHis processes the user specified recorded UNDEX variables and locations within the fluid domain for analysis. Gemfield generates contour plots for the similar user defined UNDEX variables of designated plane snap shot at specified time increments. Once flow field and historical data files are generated using GemHis and Gemfield, DYSMAS/P, an independent DYSMAS pre/post processing suite or MATLAB can be utilized to further analyze the Eulerian and Lagrangian solutions. Samples of all input files are included in the Appendix of this report.

B. DYSMAS/P AND MATLAB

DYSMAS/P and MATLAB were used for pre and post processing of DYSMAS simulations. The preprocessing of all Lagrangian FE models can be conducted using the DYSMAS Pre-Processor 2010 and some Eulerian characteristics like BCs were done using MATLAB. The preprocessing capabilities of DYSMAS/P can be used for the creation of the FE model's structure, assignment of material properties, boundary conditions, body forces, motions, and fluid-structure interface segment definitions. The structural model is then written into the specific input cards required Dyna_N, in turn used as additional input files during coupled runs. The DYSMAS/P postprocessor allows the user to analyze the entire fluid-structure dynamic response, allowing user to extract specified data and a snap shot of specified time steps for graphical and numerical analysis. MATLAB was also used in numerical post processing of DYSMAS solutions.

C. BASIC DYSMAS SIMULATIONS SETUP

The basic DYSMAS simulation set up entailed nearly the same basic steps and approaches on all simulated cases with minor differences depending on the type of run as fluid only or fluid-structure coupled run. For this study, fluid only runs were conducted. Following steps, in the order as listed and corresponding input files were utilized:

1. Utilize DYSMAS/P and MATLAB for preprocessing as needed for Lagrangian FE structure model and specific Eulerian fluids characteristics
2. Generate Euler grid using Gemgrid
3. Fill the fluid domain using Pregemini & Material Files
4. Check fluid field prior to Gemini execution using Gemfield
5. Run Gemini (For coupled run, Gemini will be specified as such, invoking fully coupled 3D run using Dyna_N(3D))
6. Process Gemini/Dyna_N(3D) solutions using Gemhis and Gemfield
7. Detailed post processing and qualitatively validate results prior to using DYSMAS/P and MATLAB for final post processing

Like any other FE methods or software, the "art" of utilizing FE was also considered throughout the process, especially during the mesh or grid set up, validation of initial results and distinguishing the best use of computational power versus time for each simulations.

D. EULER GRID, FLUID DOMAIN SETUP AND CHARGE PARAMETERS

During grid setup using Gemgrid, the most important decision made were where to refine grid and where to maintain as default coarse grid of approximately 0.656 ft per grid cell. According to Didoszak and from previous studies conducted at NPS, DYSMAS simulations are highly sensitive to the mesh size surrounding the explosion [14]. It was found that the smaller the mesh or grid size, the closer in accuracy in the simulation for both empirical and experimental predictions for various UNDEX parameters. Obviously, these assumptions had to be taken into consideration with a grain of salt, because mesh refinement is not the solution to all FE problems. In addition,

Gemini's free boundary conditions did not adequately allow fluid to flow in and out of fluid domain quickly enough, if the fluid domain was too small in comparison to the maximum bubble diameter. Lastly, when setting bottom boundary conditions, anything less than "wall" or rigid gave unexpected errors in flow field and historical results. This finding and realization was particularly useful and had to be considered in shallow water simulations and solutions where overall fluid depth was restricted considerably compared to deep open ocean scenarios.

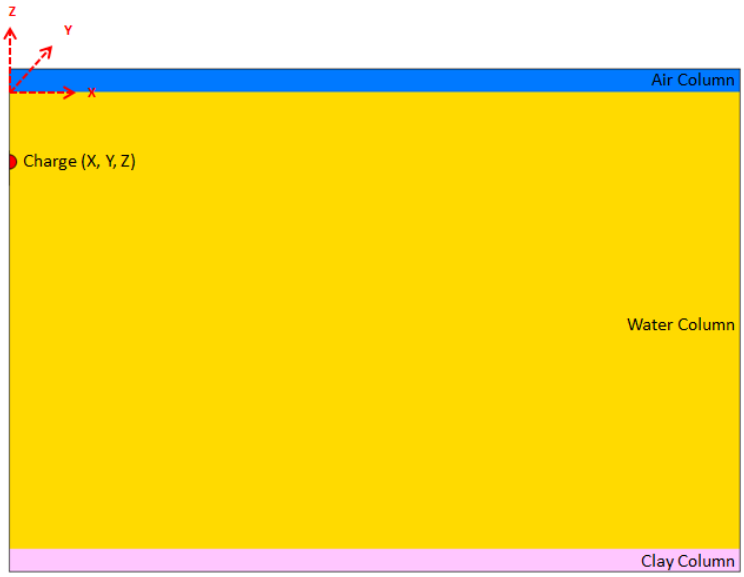

Figure 22. Typical Fluid Domain Setup for Gemini

Following the grid set up, the fluid domain was initialized and populated through the Pregemini input file. As typical Eulerian fluid domain setup is depicted in Figure 22 and the critical step in this procedure was the seeding of the fluid domain with the correct materials at the appropriate states and depth or geometry and verifying it with Gemfield prior to Gemini execution. In order to populate the fluid domain with different materials such as explosives, air, water, etc. Pregemini was utilized with given various material files. Within the material files contained specified equation of state and variables (pressure, energy, and density) that can also be manipulated, if needed, for specified materials at user's discretion. As part of the fluid domain set up within the Pregemini input file, except where specifically noted, a standard charge of HBX-1 was used. The

charge weight and depth were varied or kept constant according to the specificity of each simulation conducted.

E. SUMMARY OF SIMULATION SETUP

Taking all previously discussed factors of UNDEX theory and lesson learned from initial simulations and previous studies, the deciding values, properties and setup for each simulation started from the basic guidance and logics established in this section. This basic set up was then further explored and developed into complex and more realistic Eulerian fluid model as each DYSMAS solutions were qualitative validated in accordance with UNDEX theories discussed in previous sections of this report prior to final simulation runs. Each case studies and simulation set up, including its parameters and contributing factors can be found throughout subsequent chapters of this report and the complete outline of case studies can be found in the Appendix of this report.

IV. INTRODUCTION LITTORAL OCEAN DOMAIN

Recent proliferation of asymmetric threats, such as, diesel subs, mines, fast patrol boats, coastal integrated defense in littoral areas and even drones makes littoral ocean domain (LOD) a battle space that USN must carefully consider and analyze in the future maritime battle scenarios [15]. The term, "littoral" water (as depicted in Figure 23) has been used to extensively to describe such domain, where shallow water and its depth, as well as, shoreline and possible fresh water composition and tidal waves play a critical role in battle space management and the type of vessels or forces that USN can deploy to this domain.

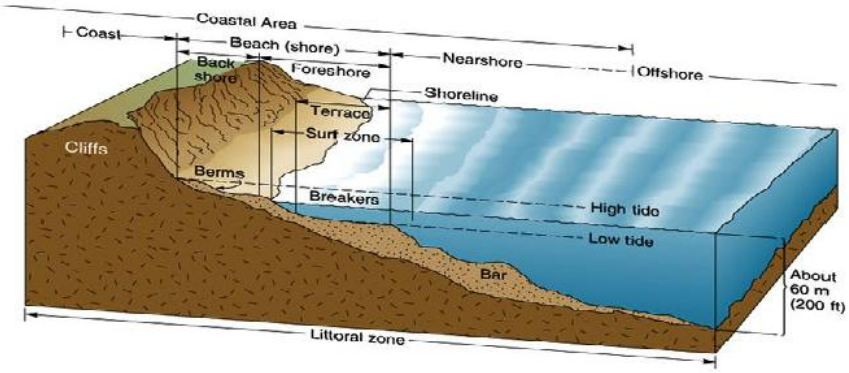

Figure 23. Littoral Ocean Domain, from [16]

The term "Littoral" and "Shallow" water domains are synonymous for this study and any body of water not of open-ocean, less than or equal to 500 feet depth and close to shore is in this category. Figure 24 shows the vast majority of ocean domain as open ocean and from a depth perspective, the LOD is only a fraction of water domain above the continental shelf. However, the vast majority of economic transaction and military conflicts are conducted in LOD and this number continues to grow [17]. Taking it further, the LOD will be bounded generally anywhere but open ocean and within the domains of depth ranges from 150 to 300 feet or approximately 10 to 20 times the average draft of USN's Littoral Combat Ship (LCS, 12.8 feet / 3.9 meters) and presence of tidal currents, gradual decent of ocean bottom shelf to open ocean depth, presence of

sedimentary debris throughout water and numerous bottom sediment types to include clay, sand and rocks are some of many characteristics that LOD embodies.

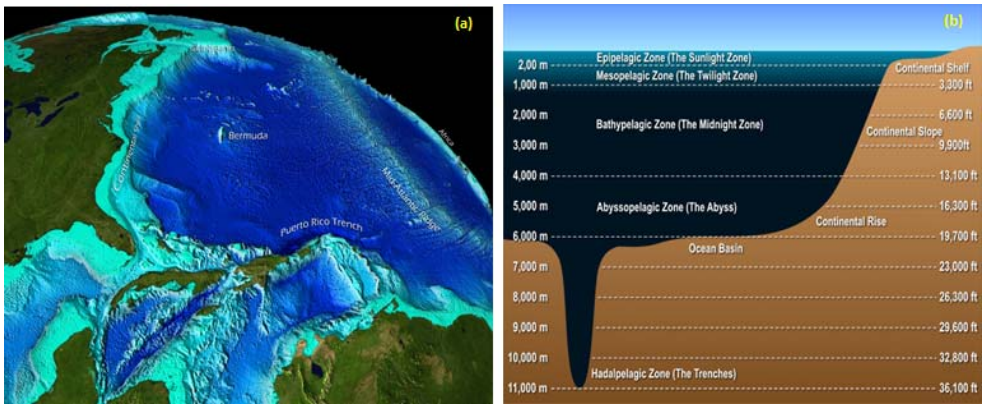

Figure 24. World Ocean Domain, from [18]

A. LITTORAL OCEAN DOMAIN RELATED TO UNDEX

To further simplify LOD UNDEX problems, only two types of bottom sediments will be considered for this study—clay and sand—for its reflectivity or absorption of energy when induced to forces incurred during UNDEX. The distinct differences in behavior of cohesive clay bottom type and non-cohesive sand will not be explored during this study, rather its reflectivity or absorption of energy. Sand in general will absorb more energy from UNDEX due to its increased porosity between sand particles. Also, the angle of decline or incline in shallow water areas, like beaches or shoreline coming in from the deep abyss will be assumed to be small or negligible. Therefore, only the depth and side boundary conditions will be explored for UNDEX phenomenon in this research.

There are four primary forces that can be induced to a surface vessel operating in an LOD. They are initial detonating shock pressure wave, the "hammer" shockwave created by the BC formation and dissipation, the bottom bounce (BB) or laterally reflected (LR) pressure waves and rising cyclic gas bubbles due to explosive materials. While all four forces are similar to that of what is experienced in an open ocean, the effect of bottom bounce, LR pressure wave and additional shockwave due to cavitation in LOD is what sets this domain apart. The rise and effect of gas bubble is purely

determined by the size of initial bubble radius; therefore, depending on the charge size and initial bubble radius, the subsequent cyclic bubbles may or may not exist. The most distinctive feature that differs in LOD BC formation or dissipation is the follow on disorderly, additional expansion and collapse of BC. For extremely shallow depth below 100ft, the bottom-reflected shock or BB arrives before cavitation collapse starts, and as a result, it interacts with BC in a complex manner, narrowing its region and hastening its collapse to its original state [11]. Additionally, it induces additional cavitation in the vicinity of the bubble and gives rise to a more disorderly collapse involving the original cavitation region, as well as, additionally induced cavitated areas. The shallower depths also play a role in formation of and subsequent cyclic behavior in the detonating bubble. Again, if the depth of LOD is smaller than the radius of first period cyclic wave of detonation, the debris within the detonating sphere will spew out in its first expansion creating a one large plume rather than several subsequent plumes.

B. UNDEX BENCHMARK PROBLEM FOR LITTORAL OCEAN DOMAIN

Using DYSMAS, a benchmark UNDEX problem for this study is created and validated (Figure 25). This fluid or Eulerian domain contains three distinct layers of Eulerian materials to include clay bottom, sea water and a layer of air. The origin of axis lies at water-air interface right above the charge, and the depth and lateral distances of domain are varied in order to meet specific objectives for each run cases. Both charge and target locations are prescribed at some point in the domain, (X, Y, Z). In addition, HBX-1 will be used as the charge for the remainder of this study, due to carefully documented characteristics of its composition and UNDEX behaviors. HBX-1, also known as High Blast Explosive was developed during WWII as desensitized modification of Torpex explosives and its composition includes 38% TNT, 40% RDX, Aluminum Wax and Lecithin [19]. RDX, also known as Research Department Explosive is an explosive nitroamine widely used in military and industrial applications.

The setting of boundary conditions for each run was of critical importance; since, they determined the approximated interactions between various interfaces of UNDEX geometry and the way shockwaves and energy will travel accordingly. The ocean bottom

and lateral boundary (B1 though B4), such as channel walls, were assumed to be a rigid body initially to simplify the modeling requirements. For DYSMAS, there are essentially three boundary settings: free, wall and 0 to 99% reflectivity. The condition "free" includes gravity correction, relevant for the z-direction only. The condition "wall" specifies a reflecting or rigid boundary condition. Lastly, the numbers between 0 and 1 can be used for partially reflecting boundary conditions [12].

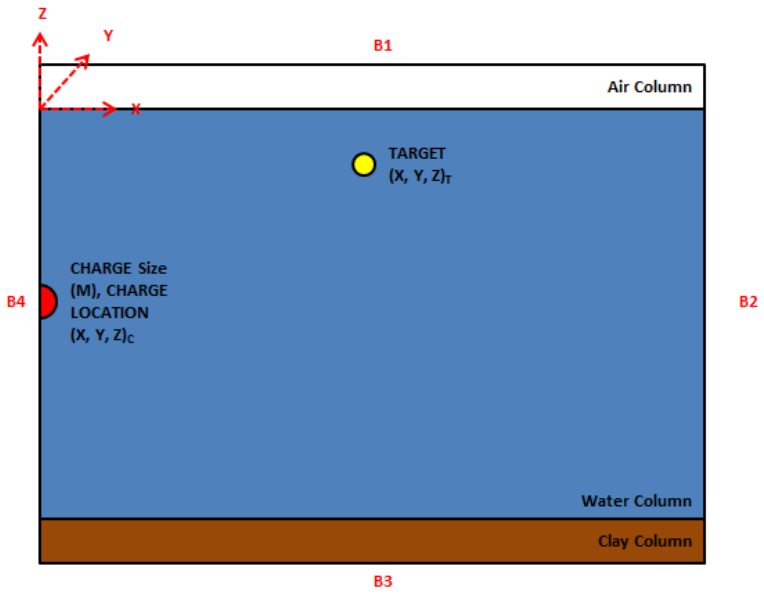

Figure 25. UNDEX Benchmark Problem, Defining Littoral Ocean Domain

To confirm initial assumptions made regarding LOD in reference to UNDEX parameters, several initial case studies were conducted with DYSMAS by first simply varying ocean depths. Initial depths were varied from 1000ft to 100ft, and additional depth ranges were further broken down and simulated to observe or validate UNDEX characteristics within that range. The simulated cases from 1 through 14 are summarized below in Table 1. The UNDEX characteristics were analyzed using several results obtained from each run to include: flow field, shockwave characteristics, vertical take-off velocity and BC.

Case #	Run Mode	Euler Dimesions (X, Y, Z) [ft]	Target Depth [ft]	Target Distance [ft]	Charge Type [ft]	Charge Weight [lbs]	Charge Depth [ft]	Bottom Type	B1 [zmax]	B2 [xmax]	B3 [zmin]	B4 [xmin]	Grid Size [ft]
1	2D, Euler	800, 1, 1000	0.820	100	HBX-1	25	50	Clay	Free	Free	Wall	Wall	0.656
2	2D, Euler	800, 1, 900	0.820	100	HBX-1	25	50	Clay	Free	Free	Wall	Wall	0.656
3	2D, Euler	800, 1, 800	0.820	100	HBX-1	25	50	Clay	Free	Free	Wall	Wall	0.656
4	2D, Euler	800, 1, 700	0.820	100	HBX-1	25	50	Clay	Free	Free	Wall	Wall	0.656
5	2D, Euler	800, 1, 600	0.820	100	HBX-1	25	50	Clay	Free	Free	Wall	Wall	0.656
6	2D, Euler	800, 1, 500	0.820	100	HBX-1	25	50	Clay	Free	Free	Wall	Wall	0.656
7	2D, Euler	800, 1, 400	0.820	100	HBX-1	25	50	Clay	Free	Free	Wall	Wall	0.656
8	2D, Euler	800, 1, 300	0.820	100	HBX-1	25	50	Clay	Free	Free	Wall	Wall	0.656
9	2D, Euler	800, 1, 200	0.820	100	HBX-1	25	50	Clay	Free	Free	Wall	Wall	0.656
10	2D, Euler	800, 1, 175	0.820	100	HBX-1	25	50	Clay	Free	Free	Wall	Wall	0.656
11	2D, Euler	800, 1, 150	0.820	100	HBX-1	25	50	Clay	Free	Free	Wall	Wall	0.656
12	2D, Euler	800, 1, 125	0.820	100	HBX-1	25	50	Clay	Free	Free	Wall	Wall	0.656
13	2D, Euler	800, 1, 100	0.820	100	HBX-1	25	50	Clay	Free	Free	Wall	Wall	0.656
14	2D, Euler	800, 1, 75	0.820	100	HBX-1	25	50	Clay	Free	Free	Wall	Wall	0.656

Table 1. Case Studies for Defining Littoral Ocean Domain

1. Flow Field Analysis

The overall flow field results for deep (greater than 500ft) and shallow (less than 300ft) ocean, or LOD, are depicted in figures 26 and 27. Both flow fields depict pressure contour plots or "flow field" at time steps of (a) 10msec (b) 35msec (c) 50msec and (d) 75msec. These time steps were chosen to coincide with the most significant UNDEX events taking place. Both figures 26 and 27 at time (a) 10msec show identical initial shockwave expansion as it intercepts the water-air interface. Once in contact, the characteristic of both cases take a different turn. The expansion and initiation BC can be clearly seen in subsequent field plots at time 35 and 50msec, with initial nucleation of collapse (Figure 26(b)) and hammer shockwave (Figure 26(c)). The traveling hammer shockwave can also be seen in Figure 26(d) as it propagates deep into the ocean. At this point, the same hammer shockwave have already reached the surface and dissipated. As mentioned in previous chapter, hammer shockwave is magnitude of the pressure pulse generated by the collision of the accreting lower and upper cavitation boundary at closure.

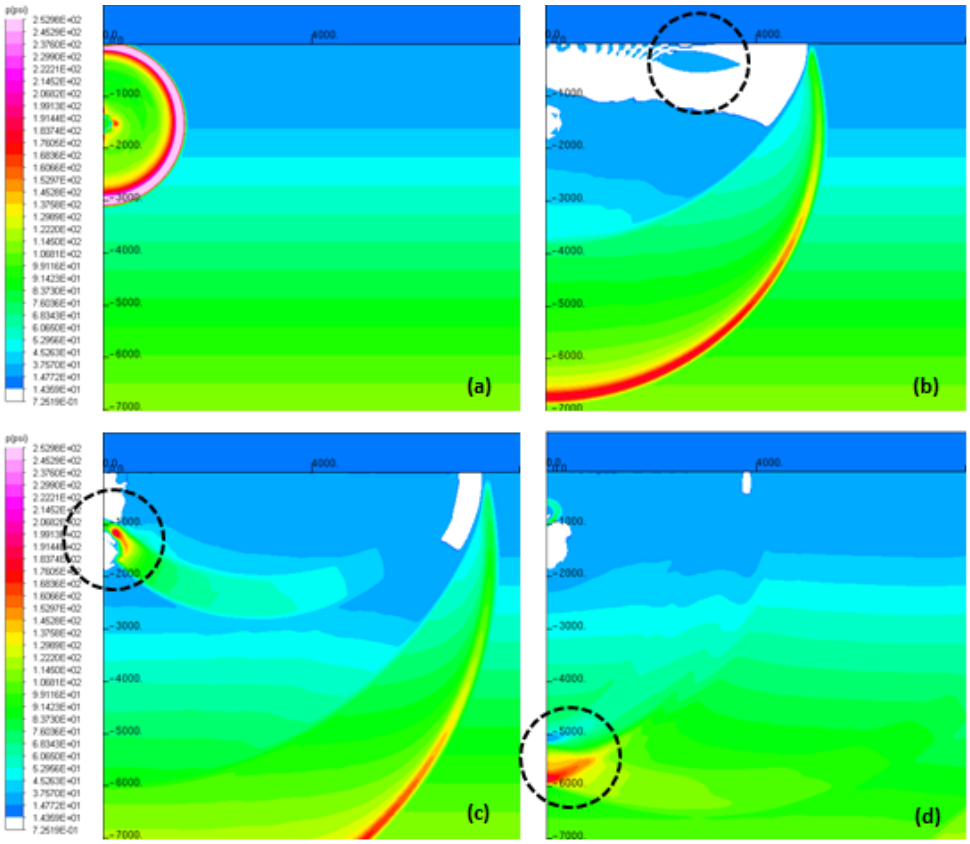

Figure 26. 500ft Ocean Depth at Time Step (a) 10 (b) 35 (c) 50 (d) 75msec

The flow field results for 200ft ocean depth are depicted in Figure 27. There are several contrasting differences to previous 500ft depth flow field results. First, the bottom bounced (BB) reflected shockwave are shown in Figure 27(b). The magnitude of this BB shockwave at reflection is identical to initially radiating shockwave. As it travels back up towards the surface, the BB shockwave intercepts the "hammer" shockwave from collapsing BC, shown in Figure 27(c). Last, as BB shockwave passes through the hammer shockwave and hit the water-air interface, it invokes additional BC that can be seen in Figure 27(d). Clearly the chaotic nature of shallower depth UNDEX can be contrasted from the 500ft flow field results and start to emerge.

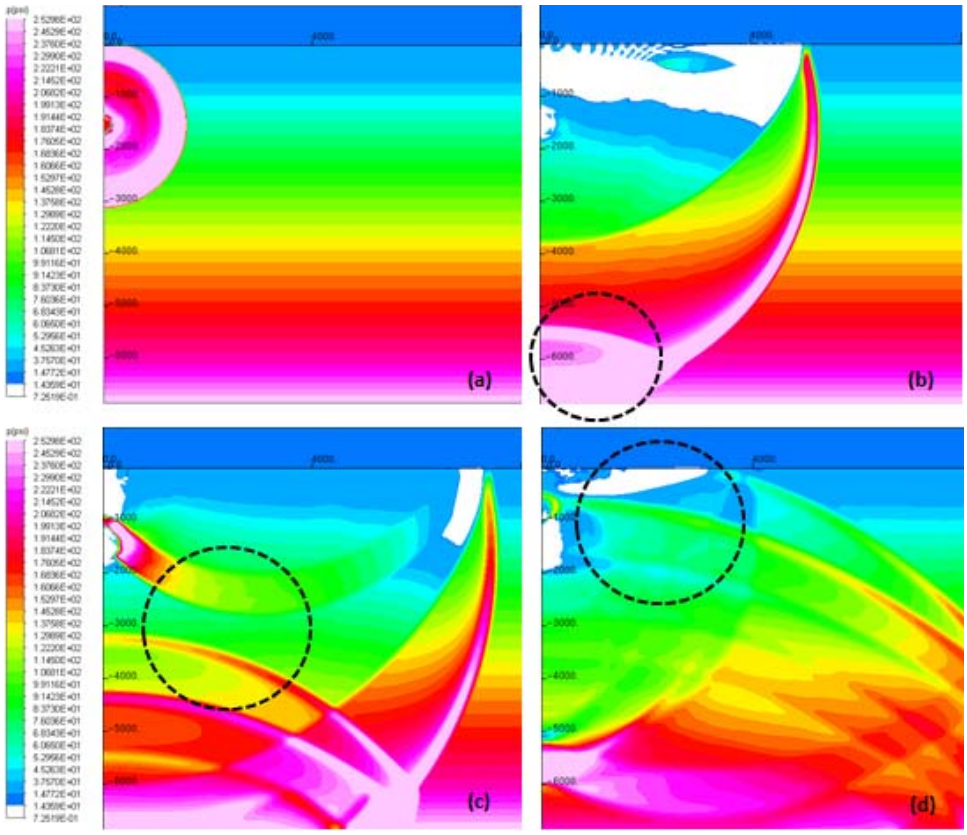

Figure 27. 200ft Ocean Depth at Time Step (a) 10 (b) 35 (c) 50 (d) 75msec

Again, the 500ft depth UNDEX results were representative of all depth cases deeper than 300ft and 200ft depth results were representative of cases shallower than 300ft. From these flow field results, there are four differing characteristics of deep and shallow water UNDEX. First, the way in which initial shockwave travels and interacts with "other" reflecting waves differ. Unlike open ocean, as initial shockwave reflects off shallow bottom, LB or water-air interface and heads towards a point of intersection of all three waves, additional cavitation and shockwaves are created. Second, the BC collapse of shallow water is more violent or higher in pressure fluctuations during "hammer" shockwave propagation due to additionally induced cavitation or shockwaves. Third, the BB shockwave during shallow water UNDEX induces additional energy back into the fluid field creating additional BCs and shockwaves that can be as close as the initial shockwave and energy. The additional BC can be seen in Figure 27(d) as the BB shockwave crashes into the water-air interface, inducing another set of spallation and

additional formation of cavitations. Lastly, the additional BCs that are formed during BB's collision of water-air interface create an additional "hammer" shockwave that also can be as high as the initial closure pulse. Another flow field results are shown in Figure 28 for shallow water UNDEX to show the violent and multiple cavitations forming due to interactions of several reflected shockwaves from the bottom. As shown, the white portion of flow field indicates BC formations. Clearly, the additionally induced BC formation and its chaotic behavior can be seen and at times greater than that of initial BC in size and scope.

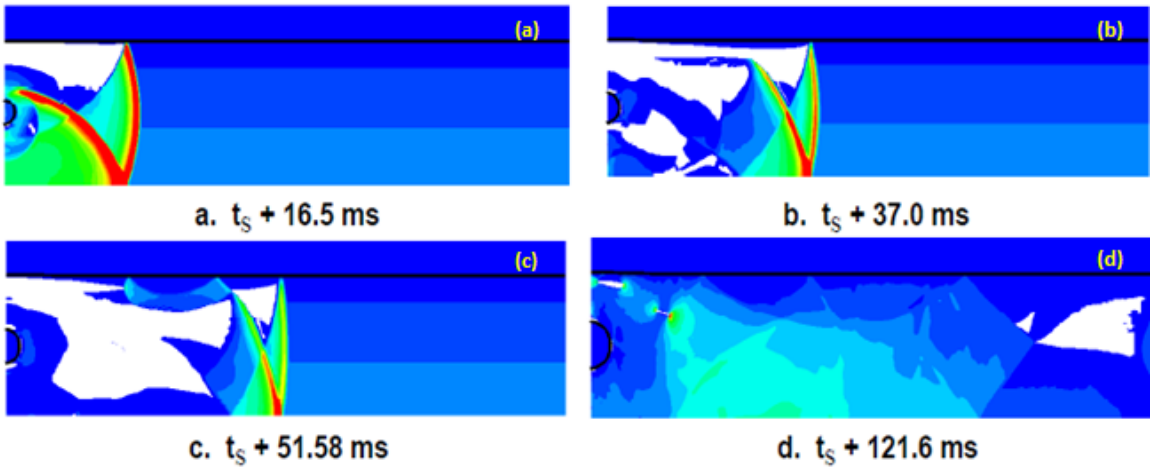

Figure 28. UNDEX of 1102lbs TNT at Charge Depth of 66ft, Water Depth of 131ft, from [11]

2. Target Pressure Analysis

The open ocean and LOD's target pressure profile during UNDEX are depicted in figures 29 and 30. Both figures show that the initial shockwave pressure at target location to be approximately 55psi. In Figure 29, this initial shockwave pressure is followed by an immediate cutoff pressure at 8psi with reverberation within the layer of target depth and air-water interface, and finally a second shockwave peak pressure at approximately 22psi representing the "hammer" shockwave pressure during the initial BC closure. To get a perspective on shockwave pressures, 14.7 psi is the atmospheric pressure that is felt at sea level and 55 psi of initial peak pressure is from a 25lbs charge of HBX-1 at a depth of 50ft of sea water. 55psi is close to what you will feel at

approximately 120ft deep water, stationary. The rest of the time period show negligible pressure peaks compared to initial and hammer shockwave, although are clearly present.

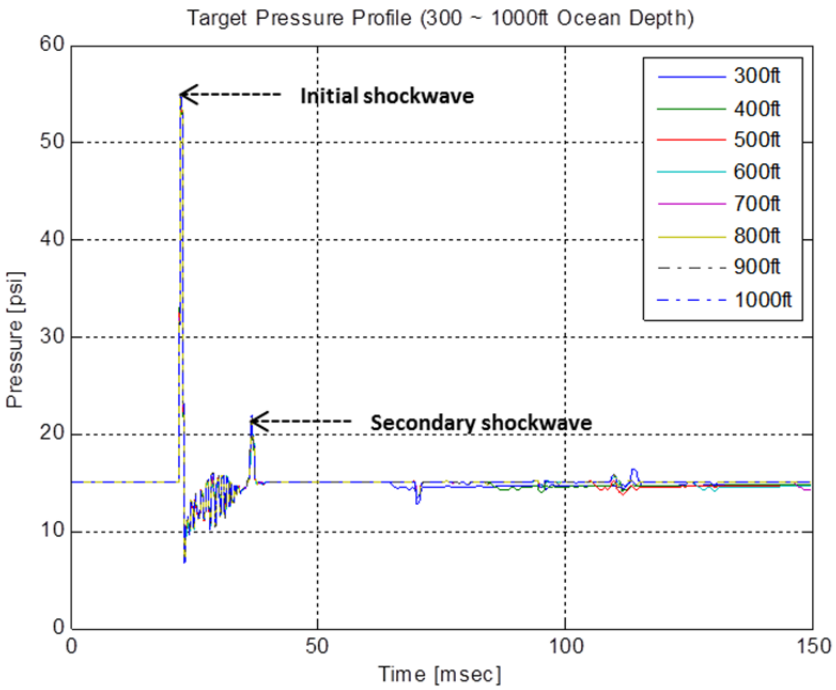

Figure 29. Target Pressure Profile (300 to 1000ft Ocean Depth)

As seen on the overall flow field plots previously, Figure 30 shows additional pressure waves generated due to BB waves and additional BC closures. For 75, 100 and 125ft of water depth, the additional shockwave present due to BB and additional BC are found to be up to 90% of what initial shockwave experienced. For the 100ft case, the BC collapse pulse and BB SW that follow are almost identical. The pressure fluctuations are clearly more observable throughout the course of the shallow pressure time domain. The pressure fluctuations felt as individuals may or may not cause structural damage depending on the magnitude and material properties of structures present. However, accumulation of dynamic nature of additional shockwave can and will increase the likelihood of the structural damage due to dynamic loads.

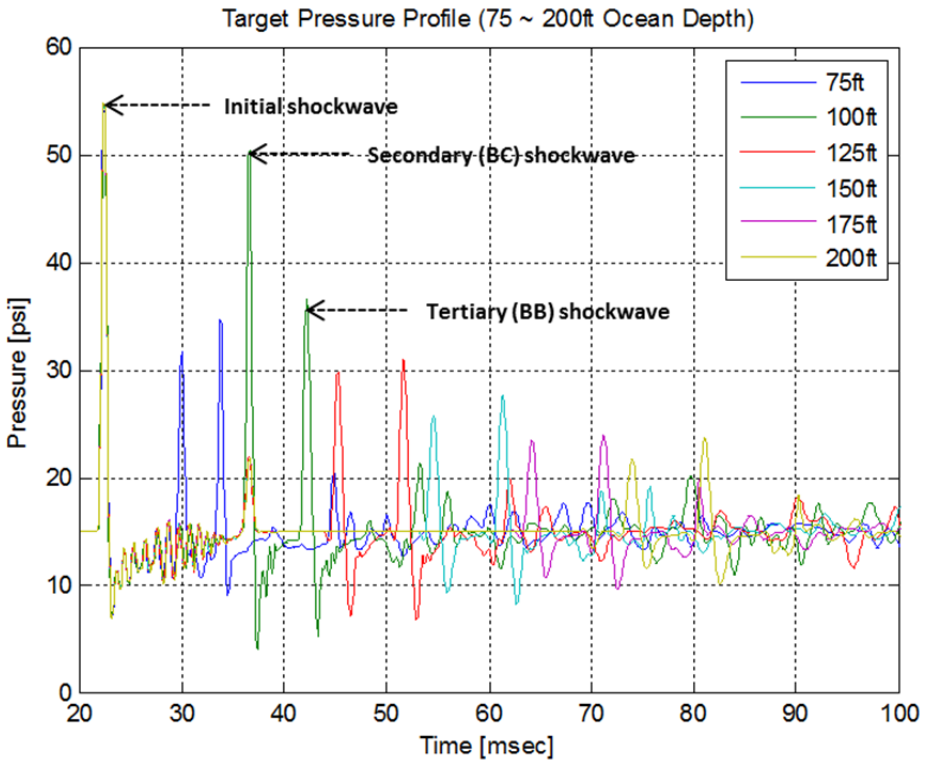

Figure 30. Target Pressure Profile (75 to 200ft Ocean Depth)

3. Vertical Take-Off Velocity Analysis

Next, the vertical take-off velocities (VTO) are analyzed for the open ocean and shallow water UNDEX events (figures 31 and 32). In short, VTO represents magnitude of z-direction velocity experienced at target location during UNDEX. The abrupt increase in velocity at a constant rate followed by a varying decay of magnitude shows close resemblance to initial shockwave characteristics. The VTO for ocean depths of 300 to 1000ft is shown in Figure 31 while Figure 32 depicts VTO for ocean depth of shallower depths, less than 300ft. Both VTO results show the peak of velocity at 1.75ft/s before decaying back close to its stationary state or into negative velocity due to additional fluid movements created by additionally reflected shockwaves or formed cavitations. For deeper water, rest of the remaining VTO during period of UNDEX seems to decrease, approaching close to negative 2ft/s.

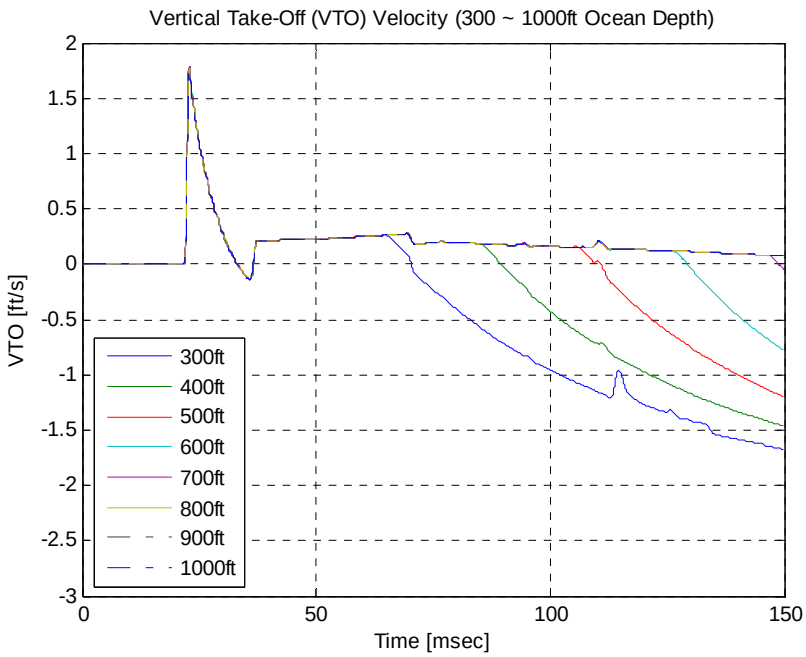

Figure 31. Vertical Take-Off Velocity (75 to 200ft Ocean Depth)

An entirely different phenomenon takes place for shallower depth in Figure 32. Although the peak VTO is identical as mentioned, the additional VTOs felt due to BB and additional BC formation and collapse can be seen. Again, closely resembling shockwave pressure, the addition VTO experienced at target locations is found to be up to and even as greater than 50% of the initial VTO. The numerous additional VTO peaks and chaotic nature of shallower depth is apparent and closely resembles previously analyzed flow fields and shockwaves. In short, shallower the depth, VTO is felt more violently and duration is longer. As observed in pressure profiles previously, the distinct characteristics of less than 300ft starts to emerge for both UNDEX parameters.

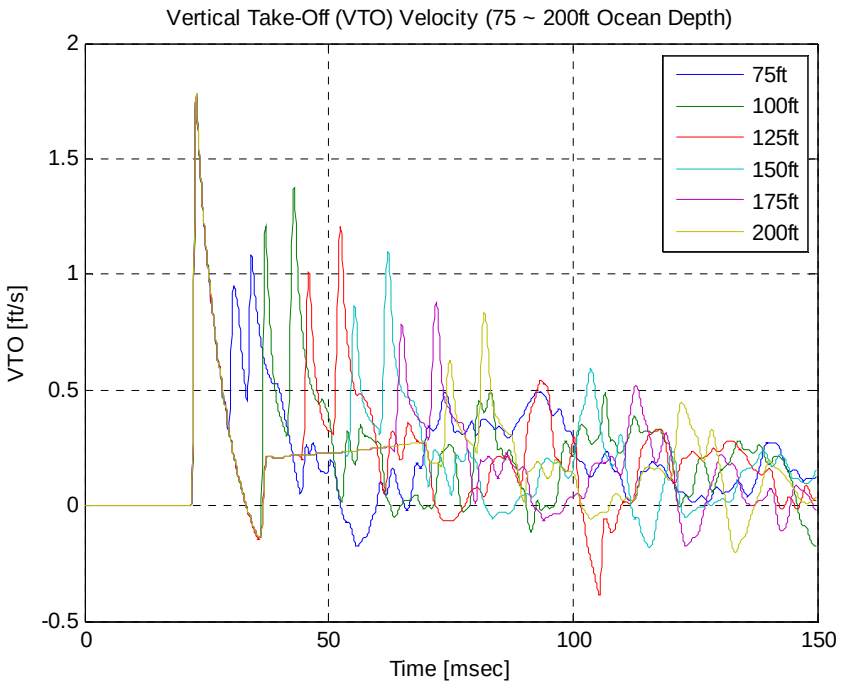

Figure 32. Vertical Take-Off Velocity (75 to 200ft Ocean Depth)

4. Bulk Cavitation Analysis

Lastly, the BC's overall characteristics and size are analyzed. The total volume of BC formed during open ocean and shallow water UNDEX are shown in figures 33 through 35. The open ocean cases, Figure 33, show a peak BC volume of approximately 6×10^5 ft^3 (4.5×10^6 Gallons). This is a tremendous amount of water moved by a 25lbs charge of HBX-1; hence, like the initial shockwave of 55 psi, one can gauge at the tremendous energy that is imparted to the water during just the initial part of an UNDEX event. For all 300 to 1000ft depth oceans, or cases without bottom reflection, the peak and total BC volumes are almost identical. By 35msec, BC starts to collapse and by 50 to 60msec, complete dissipation of initial BC can be observed both in flow field plots previously and BC volume plots.

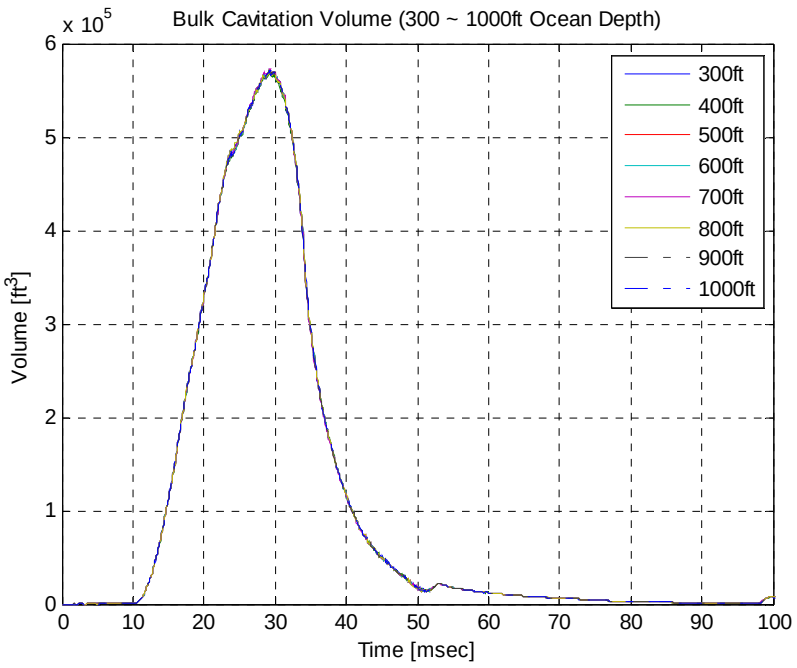

Figure 33. Bulk Cavitation Volume (300 to1000ft Ocean Depth)

The shallow water BC characteristics paint a different story as briefly mentioned in previous section. The increased cavitated zones induced by the BB wave and are clearly evident in shallow water (figures 34 and 35). From 75 to 200ft of water, the total BC formed in 75ft of water surpasses all other depth's BC formed individually, as shown with red dotted horizontal line in Figure 34. In 100ft of water, the BC peak is observed to be 6 x 10^5 ft^3, over four million gallons. Four million gallons is approximately equivalent size of present day water tower that exists throughout various cities. This dramatic increase in additional BC formation for shallower depth can be attributed to many factors, but for this study, focus will be on characterizing shallow depth and effects of boundaries at the bottom and lateral position of water domains that are present in shallow ocean or LOD.

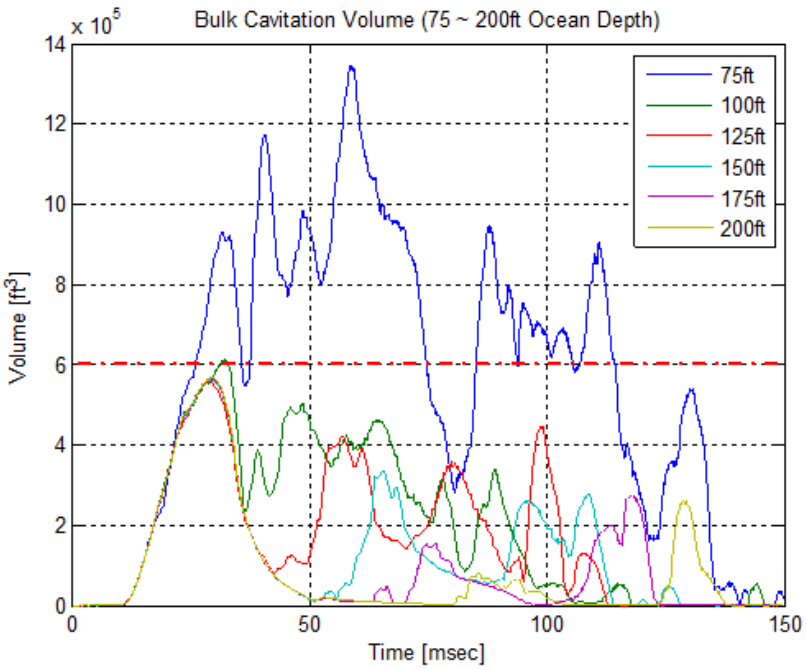

Figure 34. Bulk Cavitation Volume (75 to 200ft Ocean Depth)

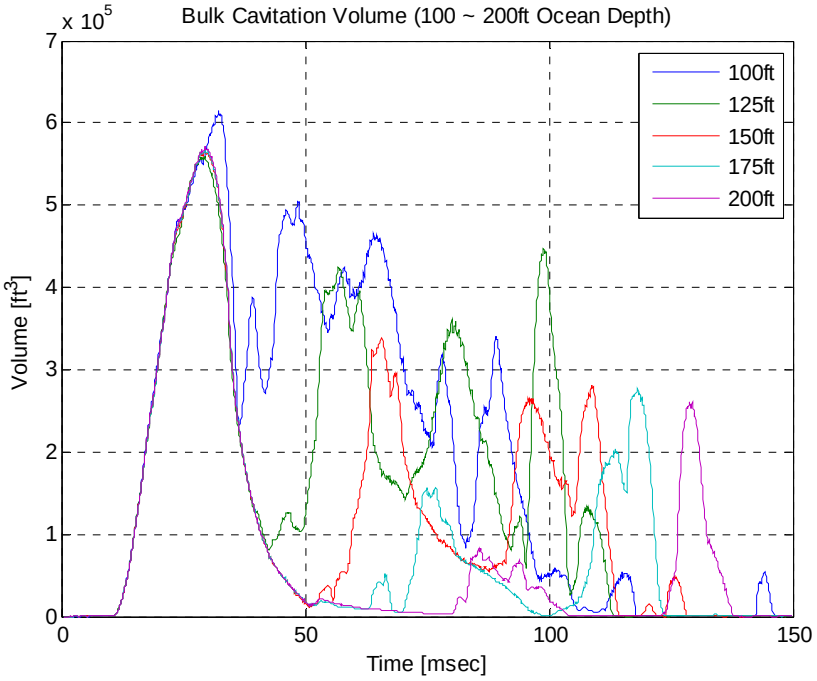

Figure 35. Bulk Cavitation Volume (100 to 200ft Ocean Depth Cases)

V. INVESTIGATION OF CHARGE SIZE AND DEPTH

Before moving further, the effects of charge size and depth must be addressed and validated for LOD. To do so, the same UNDEX fluid domain was used as in previous cases, except the ocean depth was maintained at 500ft deep while charge sizes and depths were varied. The depth at 500ft was chosen to analyze ocean depth of greater than 300ft, but not quite deep enough to see the negligible changes in UNDEX characteristics caused by charge size and depth. The ocean domain for this case studies are shown in Figure 36 and Table 2, where cases 15 through 24 are summarized for its detailed set up.

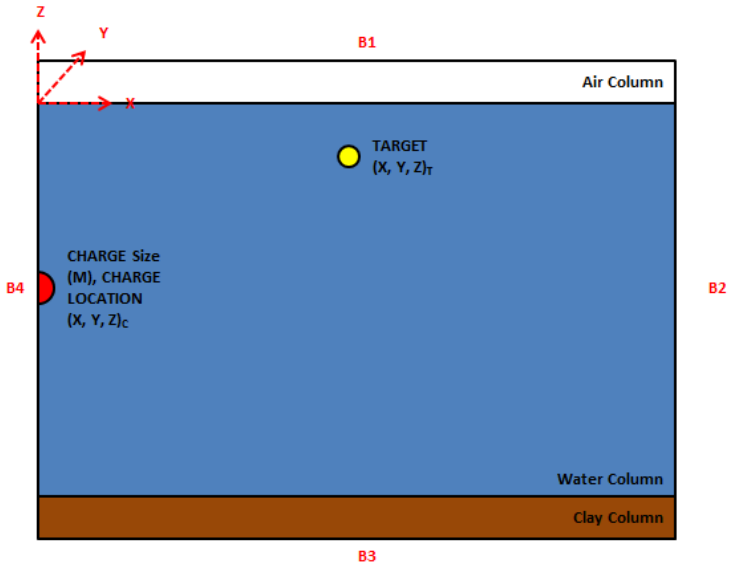

Figure 36. Littoral Ocean Domain for Charge Size and Depth Case Studies

Case #	Run Mode	Euler Dimesions (X, Y, Z) [ft]	Target Depth [ft]	Target Distance [ft]	Charge Type [ft]	Charge Weight [lbs]	Charge Depth [ft]	Bottom Type	B1 [zmax]	B2 [xmax]	B3 [zmin]	B4 [xmin]	Grid Size [ft]
15	2D, Euler	800, 1, 500	0.820	100	HBX-1	100	50	Clay	Free	Free	Wall	Wall	0.656
16	2D, Euler	800, 1, 500	0.820	100	HBX-1	200	50	Clay	Free	Free	Wall	Wall	0.656
17	2D, Euler	800, 1, 500	0.820	100	HBX-1	300	50	Clay	Free	Free	Wall	Wall	0.656
18	2D, Euler	800, 1, 500	0.820	100	HBX-1	400	50	Clay	Free	Free	Wall	Wall	0.656
19	2D, Euler	800, 1, 500	0.820	100	HBX-1	500	50	Clay	Free	Free	Wall	Wall	0.656
20	2D, Euler	800, 1, 500	0.820	100	HBX-1	100	100	Clay	Free	Free	Wall	Wall	0.656
21	2D, Euler	800, 1, 500	0.820	100	HBX-1	100	200	Clay	Free	Free	Wall	Wall	0.656
22	2D, Euler	800, 1, 500	0.820	100	HBX-1	100	300	Clay	Free	Free	Wall	Wall	0.656
23	2D, Euler	800, 1, 500	0.820	100	HBX-1	100	400	Clay	Free	Free	Wall	Wall	0.656
24	2D, Euler	800, 1, 500	0.820	100	HBX-1	100	500	Clay	Free	Free	Wall	Wall	0.656

Table 2. Case Studies for Varying Charge Size and Depth

A. VARYING CHARGE SIZE (100 – 500LBS OF HBX-1)

1. Flow Field Analysis

The overall flow field result of varying charge sizes are shown in Figure 37. The time step chosen represents three distinctly important events taking places: (a) propagation of initial shockwave (b) maximum radius of BC and (c) BC collapse where hammer shockwave is generated. Again, as the initial shockwave slams into the water-air interface, the BC develops, maturing into maximum radius by 55msec and eventually collapse at 75msec as the initial shockwave continues to propagate into the depth and remaining ocean domain. The chosen 500ft ocean depth does not interfere with initiation and collapse of BC and secondary and tertiary UNDEX events are not readily observed during the remainder of chosen time step of 150msec, hence not included. For rest of the charge size cases, the differences in the flow field results were maximum BC radius and time of BC closure, obviously due to its sizes.

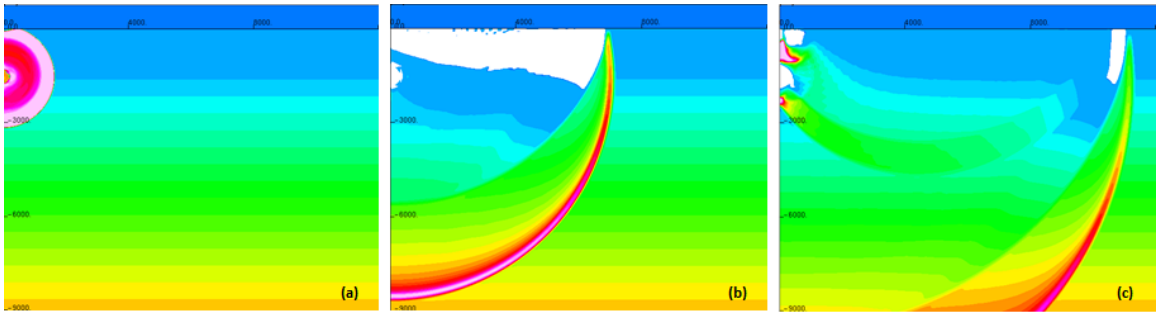

Figure 37. Flow Field at Time Step (a) 10 (b) 55 (c) 75msec

2. Target Pressure Analysis

The results of target pressure for varying charge sizes are depicted in figures 38 and 39. Figure 38 shows the maximum pressure of 500lbs HBX-1 at approximately 1,000psi. Next, Figure 39 shows maximum pressure peaks of 100 to 400lbs HBX-1. The difference of peak pressures between 400 and 500lbs HBX-1 is close to 700psi, while differences of peak pressure between 100 and 400lbs HBX-1 is close to 200psi. These drastic and almost exponential differences in pressure peak between 500 and 400lbs

charge is of significant, since it can be used to bound problems via similitude to pick an ideal weight that is most suitable for a given case studies.

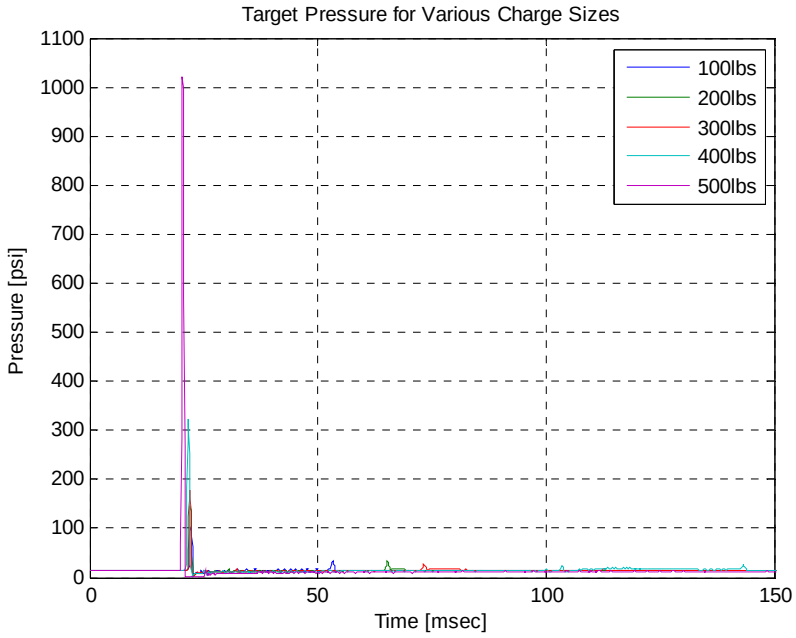

Figure 38. Target Pressure Profile (100 to 500lbs Charge Weight)

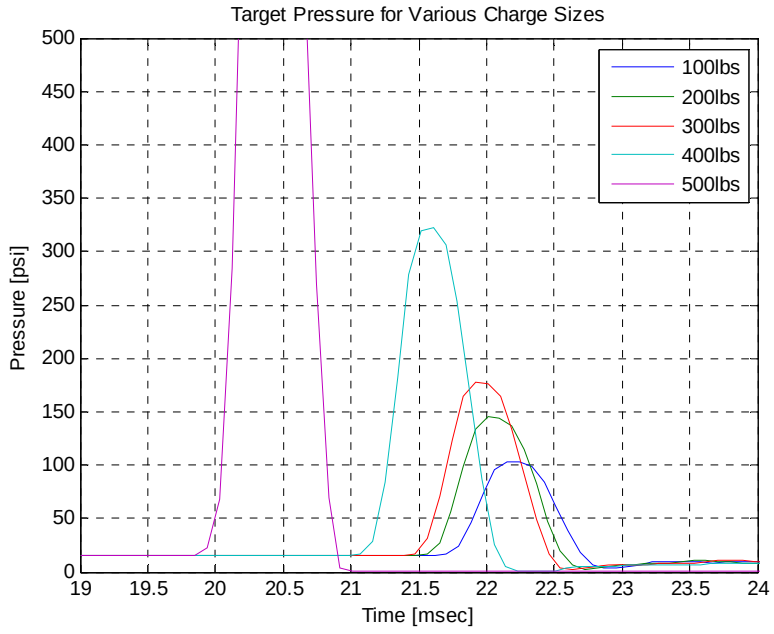

Figure 39. Initial Target Pressure Profile (100 to 500lbs Charge Weight)

3. Vertical Take-Off Velocity Analysis

The VTO results for various charge sizes are depicted in Figure 40. The maximum VTO for 500lbs peaks at approximately 37ft/s while 400lbs or less charges peak at 12ft/s or less. Similar to pressure peaks observed previously, the differences in the VTO between 100 to 400lbs charges and 500lbs charges are quite drastic. Other characteristics that are noticeable are minor VTO that starts to take shape after 50msec for 400lbs or less charge sizes. These minor VTO can be attributed to the smaller BC collapsing and inducing additional fluid movements that can be observed during the time step of simulations. For 500lbs charge, the sheer size fluids moved and BC formed during detonation takes a lot longer to return to its original state than the designated 150msec time frame, hence, the magnitude of its VTO.

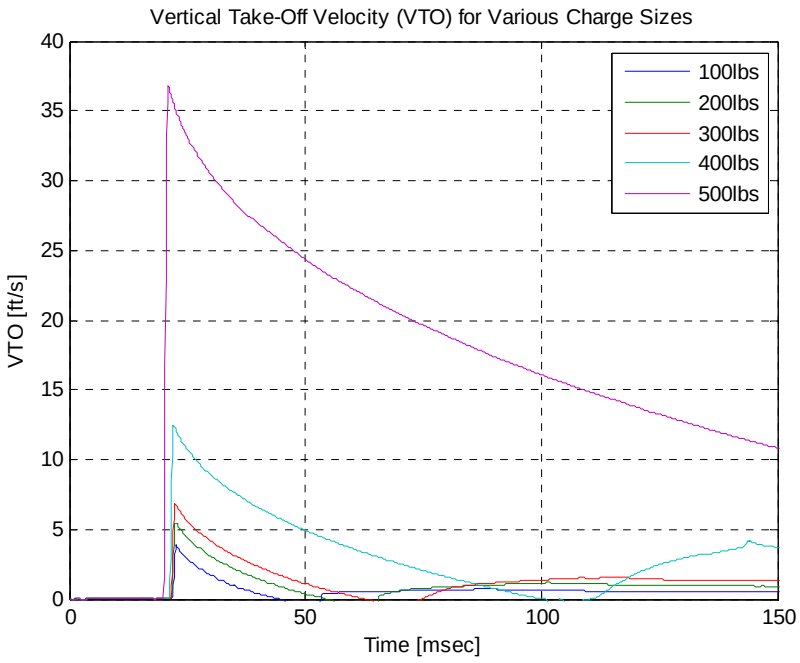

Figure 40. Vertical Take-Off Velocity (100 to 500lbs Charge Weight)

4. Bulk Cavitation Analysis

The BC formation and dissipation for various charge weight is shown in Figure 41. Again, the drastic differences in BC volume between 100 to 400lbs charge weight

compared to 500lbs charge cannot be ignored. The shape and speed of cavitations are consistent with previous cases studied. The sheer amount of water that is cavitated due to energy imparted into the water via propagating initial shockwave is close to $3x10^7$ ft^3 ($2x10^8$ Gallons) for 500lbs charge, while 400lbs charge cavitates close to $7.5x10^6$ ft^3 ($6x10^7$ Gallons) water domain. It is important to keep in mind that at this point, the effect of BB or LB's reflected waves and their cause of additional cavitation are not even considered due to chosen 500ft ocean depth. At this depth, for the chosen charge weight, the BC collapses prior to any interfering additional reflected shockwave present.

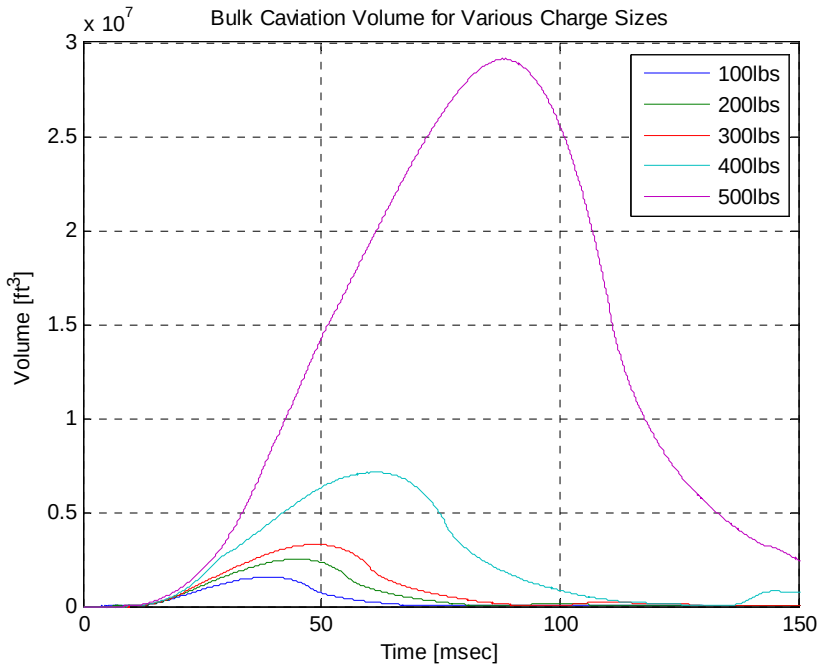

Figure 41. Bulk Cavitation Volume (100 to 500lbs Charge Weight)

B. VARYING CHARGE DEPTH (100 – 500FT OF 100LBS HBX-1)

1. Flow Field Analysis

The overall flow field result of varying charge depths are shown in figures 42 and 43. Figure 42 depicts a 300ft charge depth case and Figure 43 depicts 500ft charge depth case where the charge itself is at the water-clay (bottom) interface. The time step chosen to represent four distinctly important events taking places are: (a) propagation of initial

shockwave (b) initial shockwave reaching water-air interface (c) maximum BC radius and (d) additional cavitation formed due to BB shockwaves.

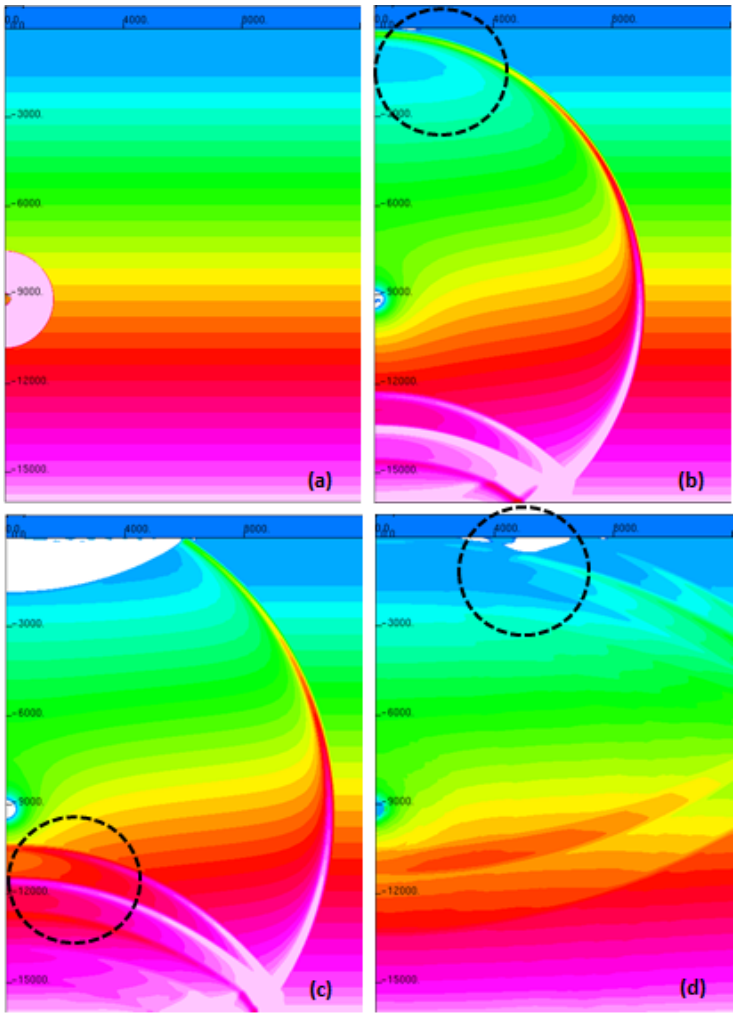

Figure 42. Flow field at Time Step (a) 10 (b) 60 (c) 73 (d) 150msec (300ft Charge Depth)

Unlike previous cases, the shockwave in Figure 42 takes a lot longer to reach the water-air interface due to its charge depth. As a result, the overall pressure, VTO and BC events are delayed up to 60msec. Further, the shockwave pressure and its magnitude that reached the water-air interface has drastically reduced, shown in Figure 42(b), since its energy has been continuously dissipating into the water as it travels up to the surface. The usual BB shockwaves that are reflected passes the charge depth (Figure 42(c)) and

reaches water-air interface after the BC have collapsed. The collapse of additional cavitation formed by BB shockwave can be seen in Figure 42(d). Next, for 500ft charge depth, two distinctly different events take place, shown in Figure 43. First, since the charge is embedded into the bottom clay, as detonation takes place, the initial shockwave and BB shockwaves are merged to form a single shockwave that propagates up to the surface of the water. As this emerging shockwave travels up to the water-air interface and collides, the BC formed is much greater than any other charge depth combined.

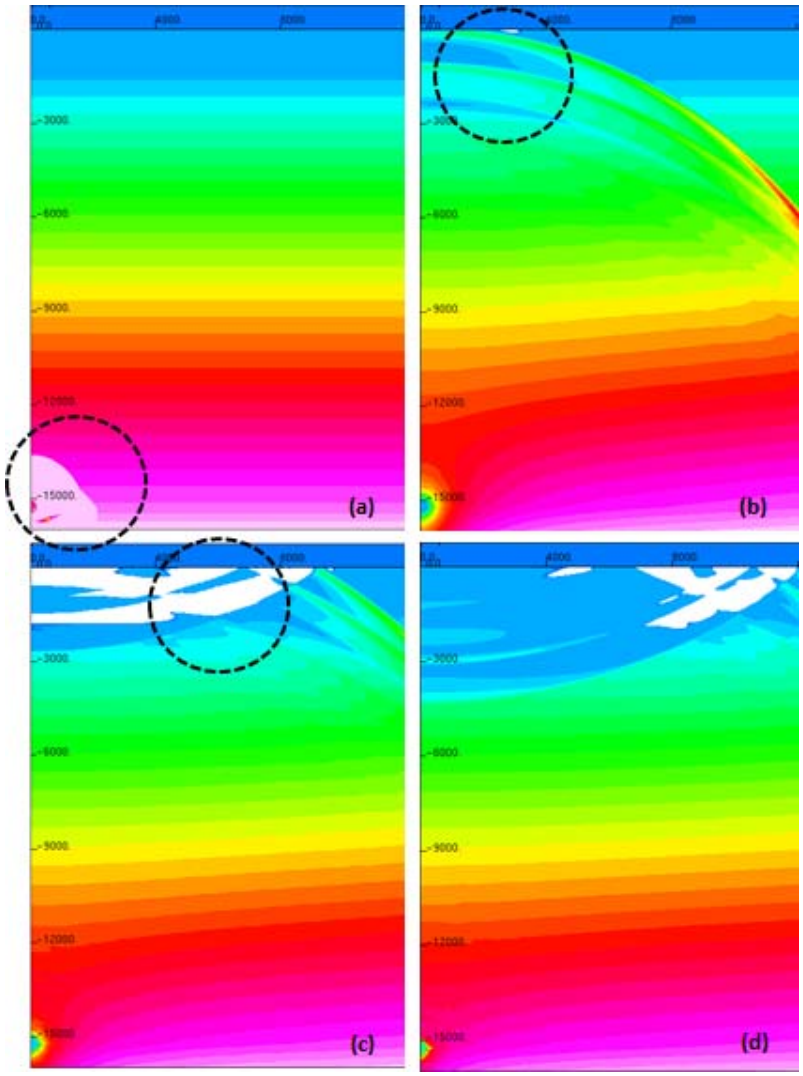

Figure 43. Flow field at Time Step (a) 10 (b) 102 (c) 119 and (d) 130msec (500ft Charge Depth)

From the flow field results, this huge BC can be seen in Figure 43(c) and (d). As this BC continues to grow, a similar characteristic can be observed in terms of additional cavitation formed during shallow water cases observed previously. In short, due to a combined shockwave in lieu of two initial and BB shockwaves, the BC formed for this case is almost double in its original size if the charge depth was deeper than its half-way point of water domain or submerged into the bottom clay. For charge depth closer to water-air interface, similar phenomenon can be observed, except the absence of BC due to 50% of detonation energy expanded directly into the atmosphere.

2. Target Pressure Analysis

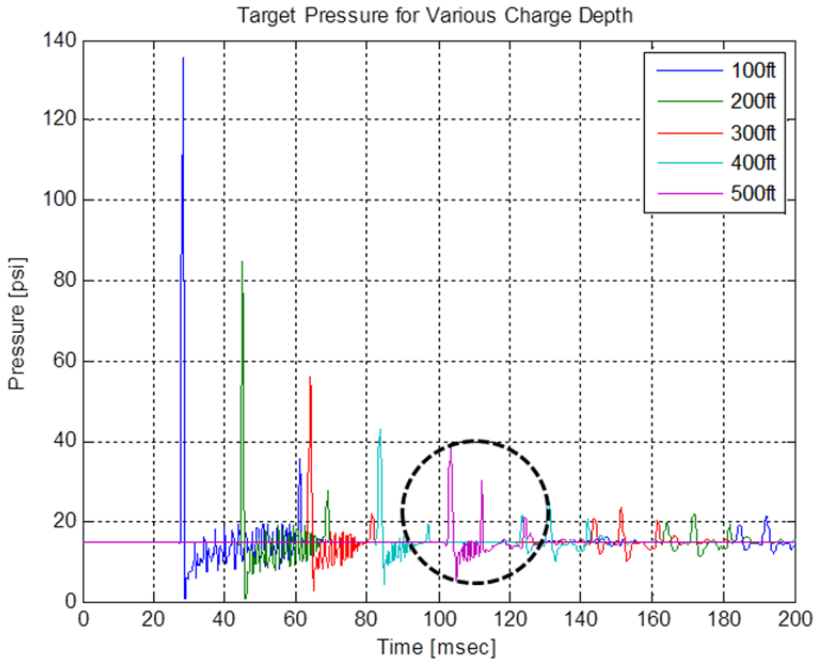

Figure 44. Target Pressure Profile (100 to 500ft Charge Depth)

The overall target pressure profiles are depicted in Figure 44 for various charge depth cases. The pressure peak of 100ft charge depth shows maximum pressure of approximately 135psi and 500ft charge depth shows a maximum pressure peak at approximately 40psi. As mentioned previously in overall flow field results, as the charge depth is increased and with it, the distance to water-air interface is also increased; hence,

the actual magnitude of shockwave's energy that collides with the interface is greatly reduced since it must travel through greater volume of water. As a result, the total volume and timing of BC formation is greatly reduced and delayed, except for 500ft charge depth case. Taking closer look at the 500ft charge depth case, the secondary shockwave is much greater than that of its counterpart (Figure 45). As described previously through overall flow field results, this is due to the emergence of two shockwaves: initial shockwave and BB shockwaves. This secondary shockwave is similar in magnitude of 100ft charge depth cases. The tertiary and rest of the shockwaves observed are consistent in magnitude and time duration except for 500ft charge depth case. For this case, tertiary and rest of the shockwaves are actually missing since these shockwaves were combined to form greater secondary shockwave.

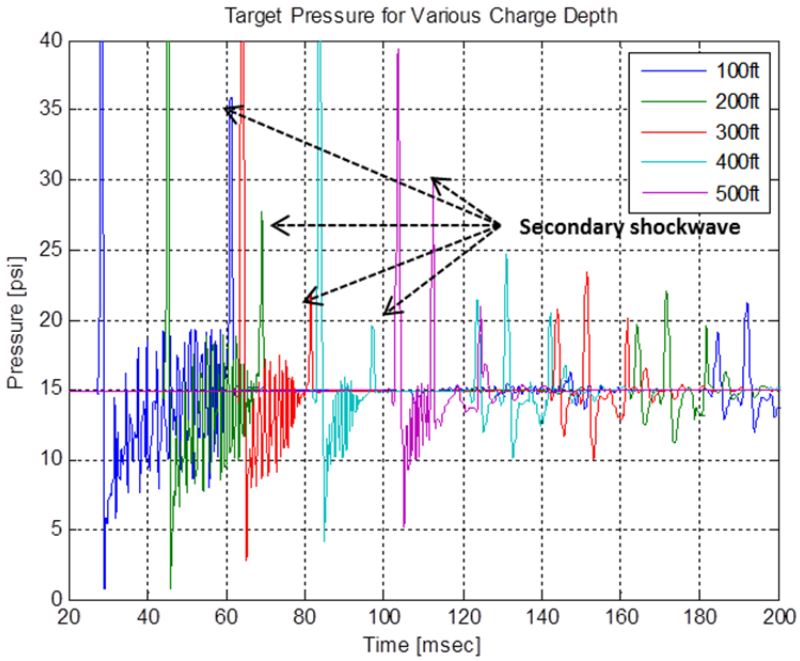

Figure 45. Close-Up Target Pressure Profile (100 to 500ft Charge Depth)

3. Vertical Take-Off Velocity Analysis

The VTO for various charge depth cases are depicted in Figure 46. Consistent with previous UNDEX parameters, the decrease in VTO as charge depth is increased can

be observed. The 100ft charge depth's VTO is close to 5ft/s while 500ft charge depth is shown to exhibit VTO of close to 1.75ft/s. Not surprisingly, the differences to the 400ft charge depth's VTO is minimal when compared back to the bottom depth case of 500ft. Another characteristic of VTO that can be observed is that as the initial VTO comes back to the original state, this overall state is increased for shallower depth. For example, VTO for 100ft returns back to greater than 0.5ft/s and hovers at this state of velocity through the remainder of its timeframe. This characteristic is also true for the remaining cases, except for the bottom depth case, as pointed out in Figure 44. Instead of initial VTO spike and returning to constant secondary state, there is a secondary spike in VTO followed by tertiary fluctuated spikes. Again, these secondary and tertiary spikes are attributed to the additional cavitation formation at initial shockwave interception of water-air interface, rather than later time for rest of the depth cases. Lastly, the tertiary VTO spike settles out at a lower magnitude than what the previous cases exhibited.

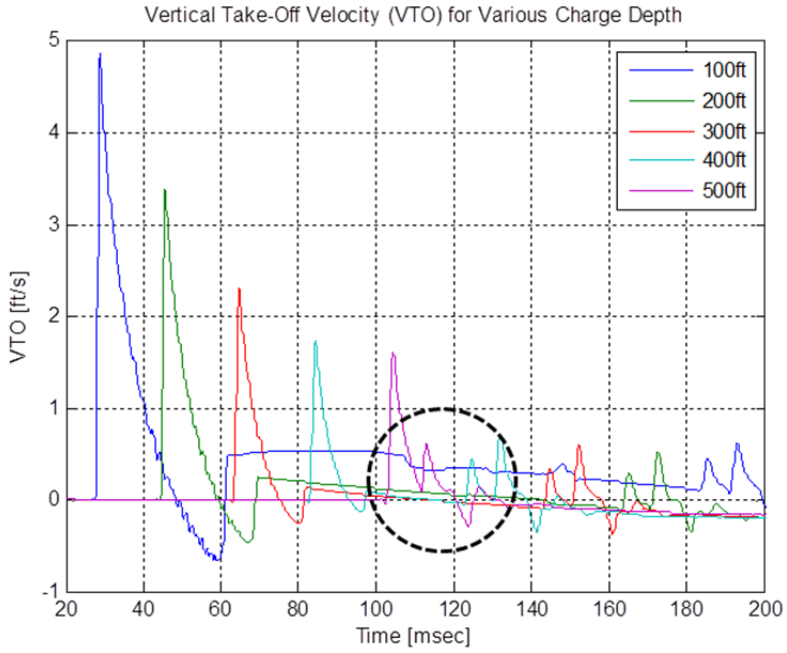

Figure 46. Vertical Take-Off Velocity (100 to 500ft Charge Depth)

4. Bulk Cavitation Analysis

The BC volume formation is depicted in Figure 47. The overall formation and dissipation of BC is consistent with what was observed in previous cases where BC is initiated at initial shockwave's interception of water-air interface, reaches its maximum radius at some point depending on the charge size and additional cavitations are formed depending on the presence or lack of bottom. The BC volume for charge depth of 100 and 200ft follows this consistent pattern observed previously; however, the rest of the cases differ. For a charge depth of 300 and 400ft, an additional "hump" can be observed at the posterior section of BC formation and dissipation. This is due to BB shockwave catching up to the BC dissipation and as it interferes with the BC collapse, the BB shockwave induces additional cavitation to be formed. This phenomenon is greatly amplified in the 500ft charge depth case where initial BC and additional cavitation are formed simultaneously, causing greater volume of overall BC. As observed, the overall max BC formed for the bottom depth case is close to 2.3×10^6 ft^3 (1.7×10^7 Gallons), while the 100ft charge depth case's overall max BC volume is drastically less than the former at 1.8×10^6 ft^3 (1.3×10^7 Gallons). While the amount of overall BC formed is not as important as additional cavitations formed due to additional shockwaves that can be created, the sheer volume of additional BC created due to charge depth differences cannot be ignored. Hence, the collapse of BC formed by the 500ft charge depth will have greater residual shockwaves originated from its hammer pulse.

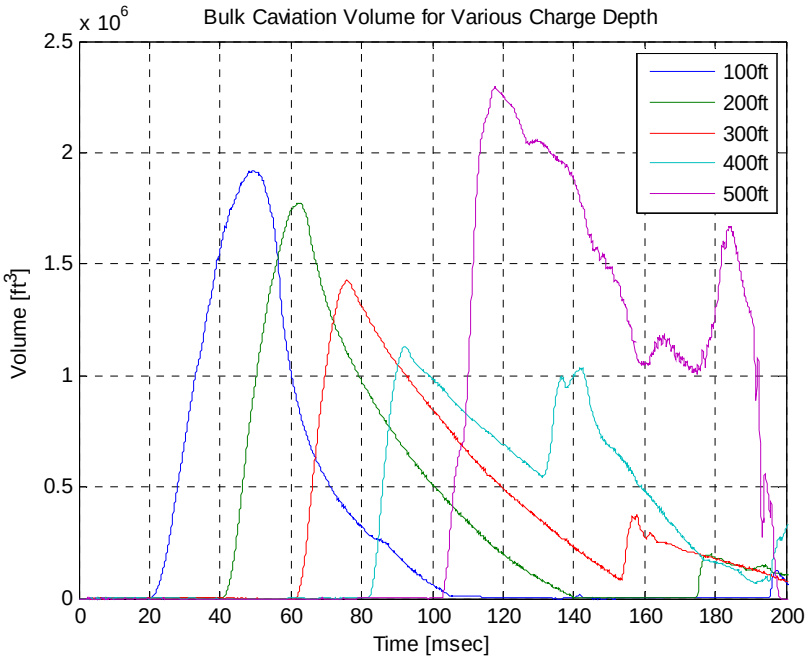

Figure 47. Bulk Cavitation Volume (100 to 500ft Charge Depth)

VI. INVESTIGATION OF LATERAL BOUNDARY CONDITIONS

In LOD, the lateral boundary (LB) condition (B2) play a role in truncating BC formation, as well as, drastically enhancing the role of reflected wave, much like the BB effect observed previously. Cases such as channels, test ponds and areas of LOD where lateral spaces are limited, are critical to in-depth analysis of this case due to its effects on UNDEX parameters. To take a look at such phenomenon, the placement and reflectivity of lateral wall boundaries were varied during UNDEX (Figure 48). The placement of LB conditions (B2.1, 2.2, and 2.3) were a matter of where the BC's edge was located and accordingly placed inside, at the edge or outside of the maximum BC radius. These represent the physical boundaries that the target and charge placements are as prescribed in the Case 25 to 28 in Table 3. In addition, reflectivity of boundary case 26 (B2.1), within the maximum BC radius, was varied to analyze its effect and influences on UNDEX parameters.

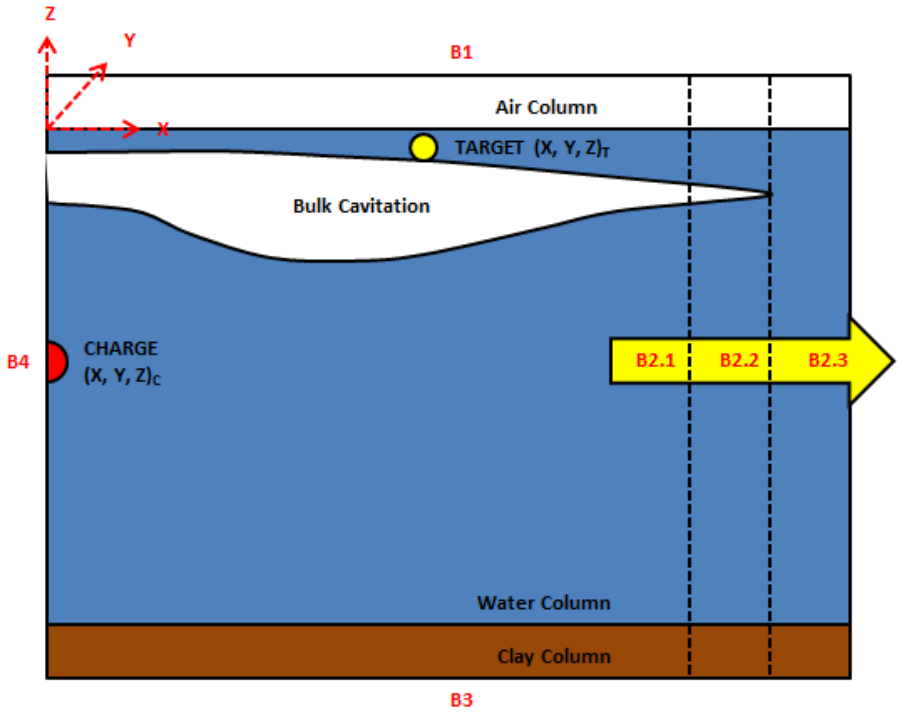

Figure 48. Lateral Wall Boundary Conditions (B2.1, B2.2 and B2.3)

Case #	Run Mode	Euler Dimesions (X, Y, Z) [ft]	Target Depth [ft]	Target Distance [ft]	Charge Type [ft]	Charge Weight [lbs]	Charge Depth [ft]	Bottom Type	B1 [zmax]	B2 [xmax]	B3 [zmin]	B4 [xmin]	Grid Size [ft]
25	2D, Euler	230, 1, 300	0.820	100	HBX-1	25	50	Clay	Free	Free	Wall	Wall	0.656
26	2D, Euler	164, 1, 300	0.820	100	HBX-1	25	50	Clay	Free	Wall	Wall	Wall	0.656
26.1	2D, Euler	164, 1, 300	0.820	100	HBX-1	25	50	Clay	Free	0.50	Wall	Wall	0.656
26.2	2D, Euler	164, 1, 300	0.820	100	HBX-1	25	50	Clay	Free	Free	Wall	Wall	0.656
27	2D, Euler	197, 1, 300	0.820	100	HBX-1	25	50	Clay	Free	Wall	Wall	Wall	0.656
28	2D, Euler	230, 1, 300	0.820	100	HBX-1	25	50	Clay	Free	Wall	Wall	Wall	0.656

Table 3. Case Studies for Varying Lateral Boundary

A. VARYING LOCATIONS

The next set of numerical results show initial and follow on shockwave pressure, vertical take-off velocity and BC volume experienced at target location and depth. As mentioned in Table 3 for case studies 25 through 28, the lateral target location is at 100ft and 0.820ft deep, for all practical purpose in regards to mesh size at 0.656ft, this depth is at shallow surface depth near water-air interface.

1. Flow Field Analysis

The overall pressure flow field results are shown in figures 49 to 52. Figure 49 is the base case where LB was set well outside the maximum BC radius with free boundary condition. The snapshots of flow field were taken at time step 10, 30, 50 and 111msec where significant UNDEX events took place. Consistent with previous cases, the flow field results show expected behaviors of (a) radiating initial shockwave, (b) initiation and dissipation of BC, (c) BC's "hammer" shockwaves and (d) influence of other reflected waves from bottom or lateral boundaries. In Figure 49(d), the BB SWs are shown passing the charge depth as it intercepts the water-air interfaces. The "free" LB condition set at x-maximum of this domain seems to have no observable effect on the radiating shockwave within flow field.

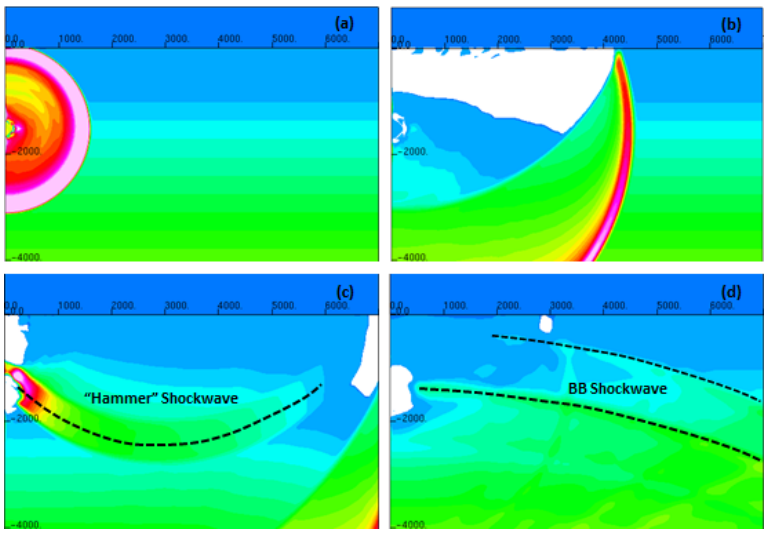

Figure 49. Case 25 (Base), Time Step (a) 10 (b) 30 (c) 50 (d) 111msec

Next, case 26 involved setting the LB conditions inside the maximum BC radius to observe its effect on UNDEX during the identical time steps of case 25. No differences were observed at time step 10msec where initial shockwave intercepts the water-air interface, shown in Figure 50(a). However, subsequent time steps clearly show distinction on the effect of wall boundary condition set inside the BC radius. First, Figure 50(b) shows BC at a maximum radius similar to that of the base case, but with shallower maximum depth. Second, Figure 50(c) shows the presence of secondary shockwave that is reflected off the LB as it travels back towards the charge location, creating turbulence and additional cavitation following its path as it intercepts the hammer pressure shockwaves. At this point, the additional cavitation following this wave is also collapsing, creating another shockwave, although smaller in magnitude. As this reflecting wave intercepts the left boundary condition and again reflected back into the water domain, the BB waves are seen disrupting this process as it begins to dissipate completely post time step of 111msec, shown in Figure 50(d).

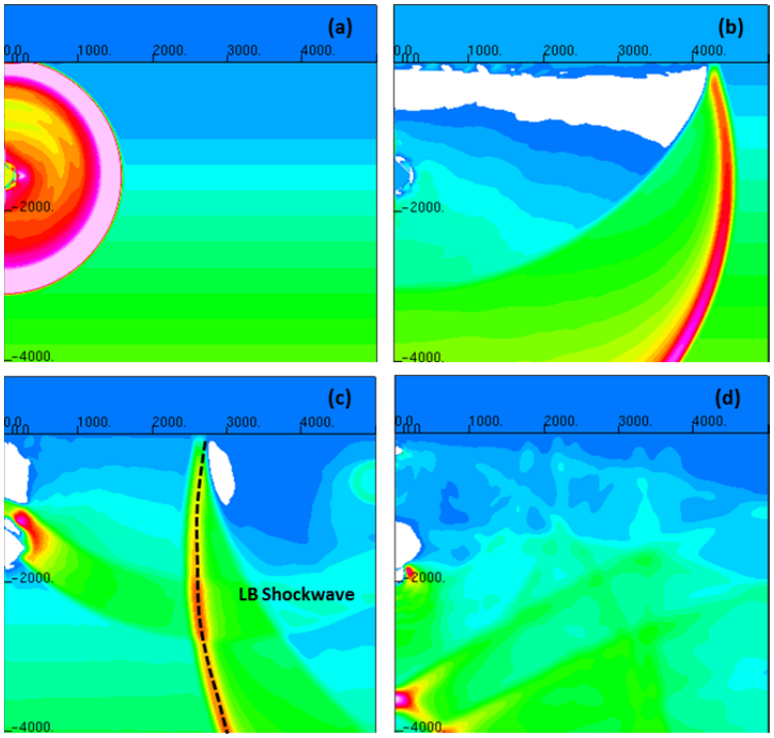

Figure 50. Case 26 (Inside BC), Time Step (a) 10 (b) 30 (c) 50 (d) 111msec

Case 27 shows the LB placement at the edge of the BC radius (Figure 51). The flow field at time step 10 and 30msec are identical to base case in both shockwave propagation and BC's max radius and depth. At time step 50msec of Figure 51(c), the reflected LB SW begins to emerge with trails of additional cavitation forming. This LB shockwave is delayed due to the boundary's placement and the magnitude seems to be similar to that of case 26. Lastly, Figure 51(d) shows the several BB and LB shockwaves intercepting to initiate additional turbulence and cavitation formations.

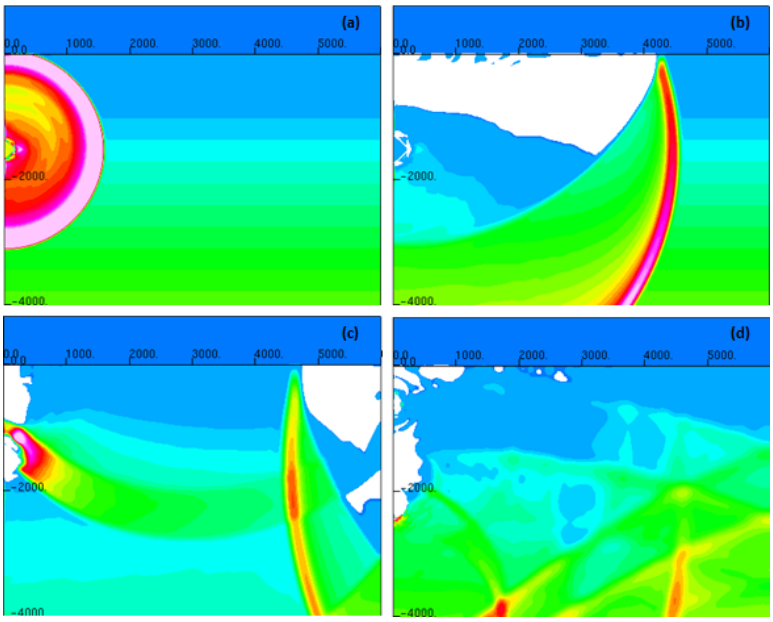

Figure 51. Case 27 (Edge of BC), Time Step (a) 10 (b) 30 (c) 50 (d) 111msec

The results of LB placement well outside of the BC radius (case 28) are shown in Figure 52. The flow field at time step 10 and 35msec are identical to the base case in both shockwave propagation and max radius and depth of BC. At time step 50msec, shown in Figure 52(c), the delayed LB reflected wave have yet to intercept the hammer pressure wave generated as initial BC collapses. Once again, following closely to the laterally reflected wave, an initiation of additional cavitation is clearly visible in Figure 52(c). Lastly, intercepting laterally reflected and the BB SWs are shown in Figure 52(d). As expected this interception takes place at a time step longer than any other cases discussed due to the location of LB conditions and compared to previous cases the additionally induced cavitation seems to have dissipated completely by this time step of 111msec. To further analyze various UNDEX parameters numerically, a point target location was chosen at 100ft lateral distance and surface depth from the charge location.

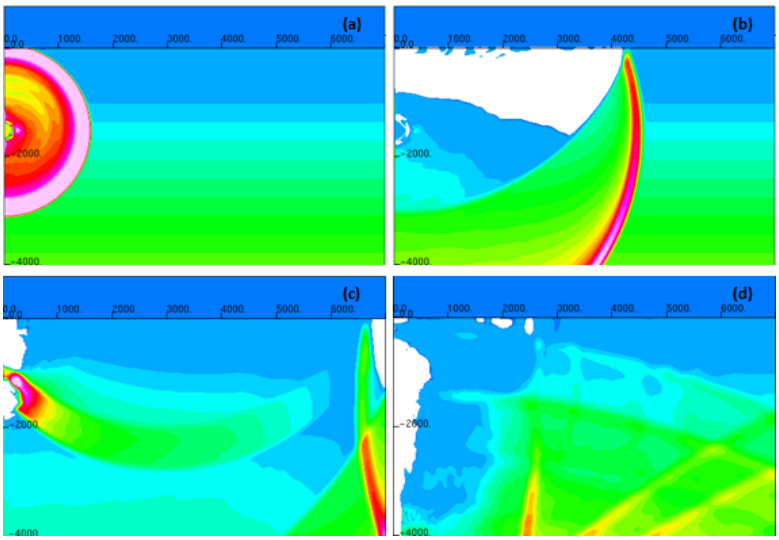

Figure 52. Case 28 (Outside of BC), Time Step (a) 10 (b) 30 (c) 50 (d) 111msec

2. Target Pressure Analysis

The resulting shockwaves at the target location are analyzed for various LB conditions (figures 53 to 55). The first distinct spikes at approximately 25msec are initial compressive shocks as it reaches the target, immediately followed by tensile SW as water-air interface expands and spallates to initiate BC formation, the BC closure or "hammer" SW and followed by laterally returning reflected shockwave's interception of target location. The BC collapsing shockwave is considered to be secondary and laterally reflected wave is considered tertiary during this case study. The other shockwaves observed post 110msec is BB SWs. The location and magnitude of these SWs are consistent theoretically. However, the timing and where both LB and BB reflected SW is located during the entire pressure time step can cause undue damage to the ship by invoking modal response. Another characteristic to point is the fact that the magnitude of the LB and BB shockwaves are at time even greater than that of BC collapsing SWs.

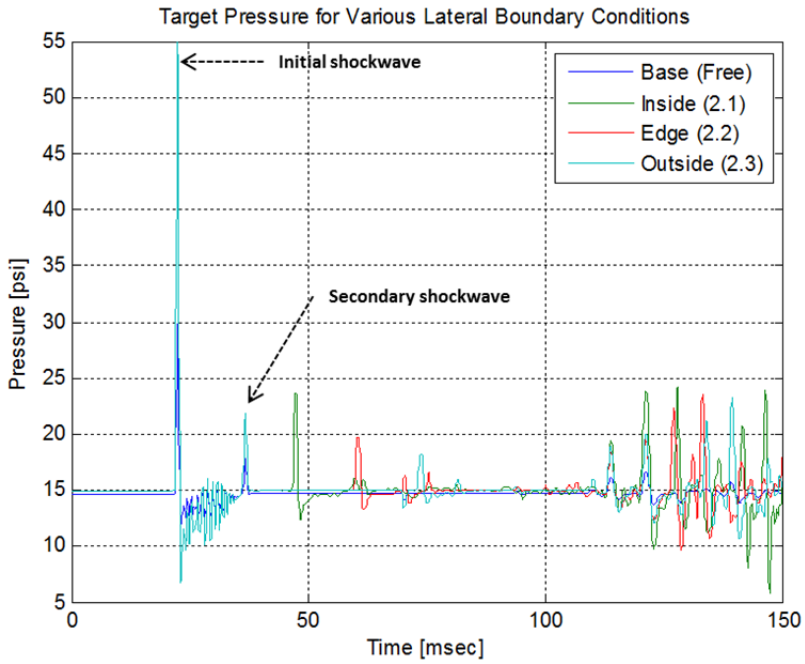

Figure 53. Target Pressure for Various Lateral Boundaries

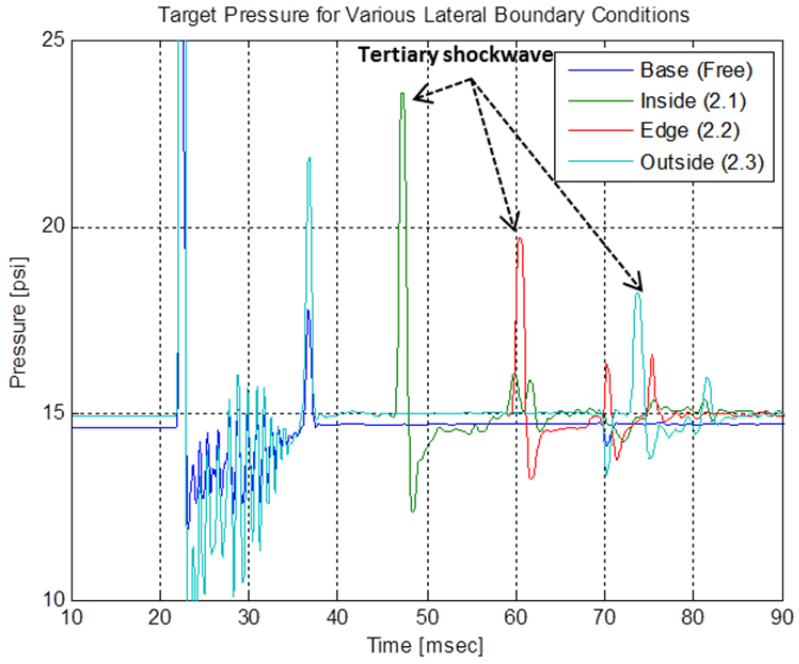

Figure 54. Initial, Secondary and Tertiary Target Pressure for Various Lateral Boundaries

The initial shockwave magnitude for all LB cases are identical in magnitude at approximately 55psi and shaped similarly; however, what follows after the BC collapse, differs depending on the size of the water domain or location of LB conditions. Between approximately 25 and 35msec where BC collapses, the magnitude of cyclic trapped shockwave between the surface and target location is largest for LB condition located outside BC max radius (Figure 54). Next, the magnitude of BC collapse shockwave also differs with this boundary condition at 22 psi. What follow next are three tertiary pressure peaks showing laterally reflected waves for all three boundary conditions with closest boundary showing highest and earliest magnitude of reflected shockwave. Lastly, the group of tensile and compressive shockwave after 110msec show various shockwaves as both BB and LB reflected shockwave intersect to cause additional cavitations and shockwaves where it reaches peak magnitudes of greater than hammer shockwave (Figure 55).

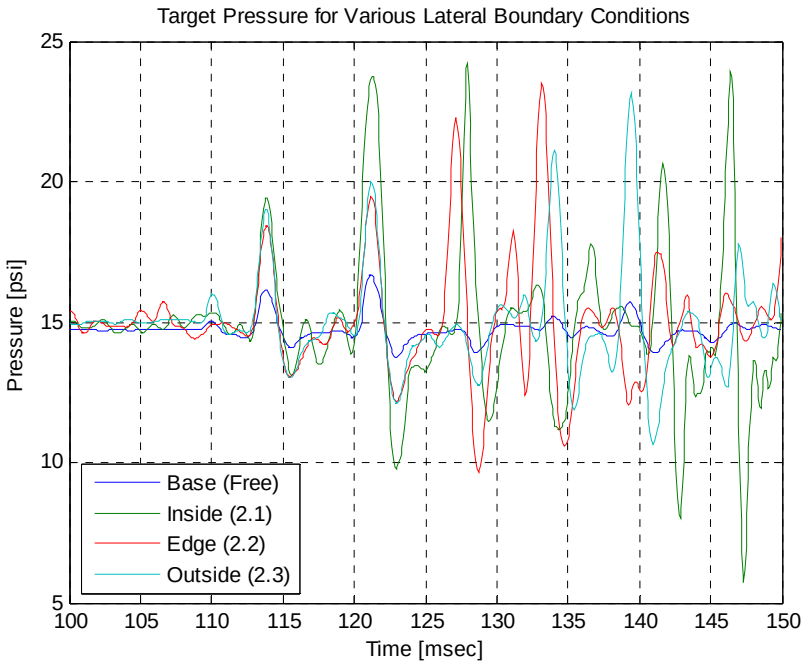

Figure 55. Bottom Bounce Target Pressure for Various Boundaries

3. Vertical Take-Off Velocity Analysis

The VTO for various LB conditions are shown in Figure 56. The initial upward velocity peaks at 1.75ft/s for all LB conditions. What follows next mirror the pressure profile seen in previously. As the initial peak VTO settles to near zero velocity, the hammer shockwave at approximately at 37msec induces another VTO back to .25ft/s. As VTO reattempts to settle, the three additional peak pressure waves induced by LB between 49 to 75msec causes three additional peaks of VTO. The VTO settles once again, and then picks up approximately 120msec when collision of LB and BB reflected SWs cause additional BC and dynamic motion of water within the domain. It is important to note that VTO does not return below zero from approximately 35 to 130msec and continues to be induced with additional forces and its velocity caused by BC, collisions of LB and various reflected wave.

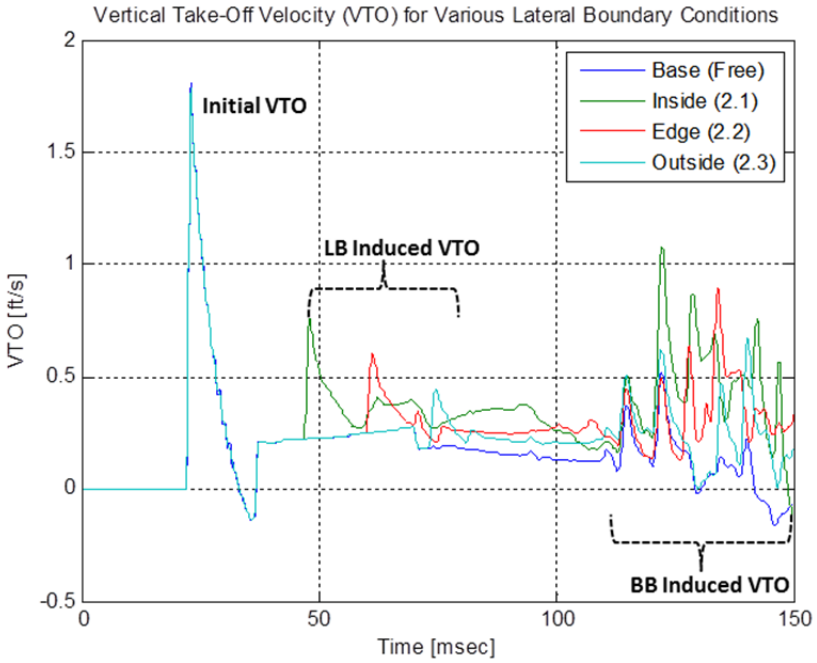

Figure 56. VTO for Various Lateral Boundaries

4. Bulk Cavitation Analysis

The BC volumes at various LB conditions compared to the base condition are depicted in Figure 57. Observing the initial BC formation and dissipation from time steps 0 to 50msec, there are several distinct differences in various LB conditions. First, base and LB2.3 conditions are practically identical in nature except there is a distinct "hump" (1.25×10^5 ft^3) initiated at 50msec and also post 135msec. This phenomenon, also observed in Figure 52(c), is the initiation of additional cavitation at LB at time of initial shockwave reflection. This "hump" in BC volume is not observed in base case obviously due to different LB condition setting as "free" condition. Second, looking at the LB2.1 and LB2.2, a similar hump is visible at an earlier time step (near 37msec) due to closer in proximity of the wall. Lastly, the overall BC volume of LB2.1 is much greater than rest compared to the base and other LB cases. Like shallower depth BB shockwave inducing enormous volume of additional cavitation, the same effects are observed here for LB conditions well within the BC's max radius.

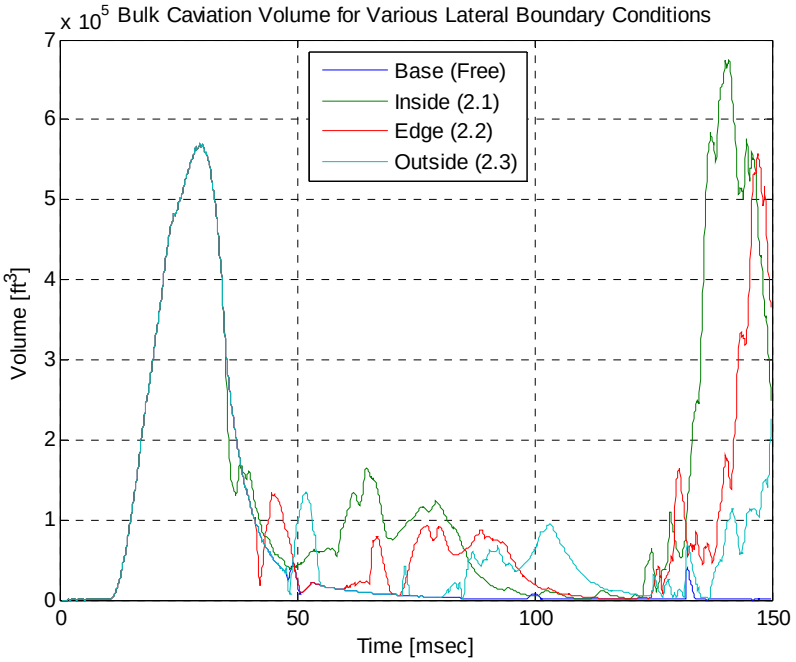

Figure 57. Bulk Cavitation Volume for Various Lateral Boundaries

The next range of time step from 50 to 100msec shows the effect of LB's interferences and additional cavitation formed as the lateral shockwave intercepts the hammer shockwave. Clearly, the magnitude and speed of the additional cavitation formed are much higher for LB2.1. The post 100msec ranges show drastic increase in additional cavitation formation due to BB inclusion of already chaotic water domain. Consistent in behavior to the 50 to 100msec range, the LB that is the closest to the charge had the largest additional cavitation formed surpassing the initial cavitation volume for all cases. It is surprising to note that the LB conditions have almost the same effect in inducing additional cavitation as the BB has on BC.

B. VARYING REFLECTIVITY INSIDE THE BC RADIUS

In order to further investigate the degree of shockwave propagation as it pertains to the percentage of reflectivity of the LB conditions, case 26 (LB2.1) were simulated once again using 50% and free boundary conditions. For case 27 (LB2.2) and 28 (LB2.3) the effects of such change in reflectivity due to greater distance, in reference to max BC radius, were not as drastic as case 26. All other parameters were maintained as previously described in Table 3.

1. Flow Field Analysis

The flow field results for 50% reflective LBs are shown in Figure 58. Comparable to base case 26, where boundary condition was set as 100% reflective (wall), the general features of radiating initial shockwave, BC formation, reflected shockwave and its interception of BB waves and BC collapse wave are nearly identical. Case 26 is the base case in this section where its LB conditions is set as wall and case 26.1 is set at 50% reflectivity. As expected, the magnitude of shockwave for the 50% reflective wall is clearly lower than the case 26 but its shockwave travels at a pattern consistent with case 26. The flow field at 111msec is drastically different than that of base case 26. As Figure 58(d) shows, the magnitude in which BB wave interacts with laterally reflected waves are a lot higher than the base case. Since, 50% of laterally reflected energy was absorbed by the LB; the intercepting wave has less energy to neutralize BB waves as it traveling up to the water-air interface. In short, as BB waves travels up and passes the

charge depth, the energy dissipation is a lot lower for 50% lateral wall reflective case 26.1. The result is increased UNDEX forces applied to object in its path and on surface of water.

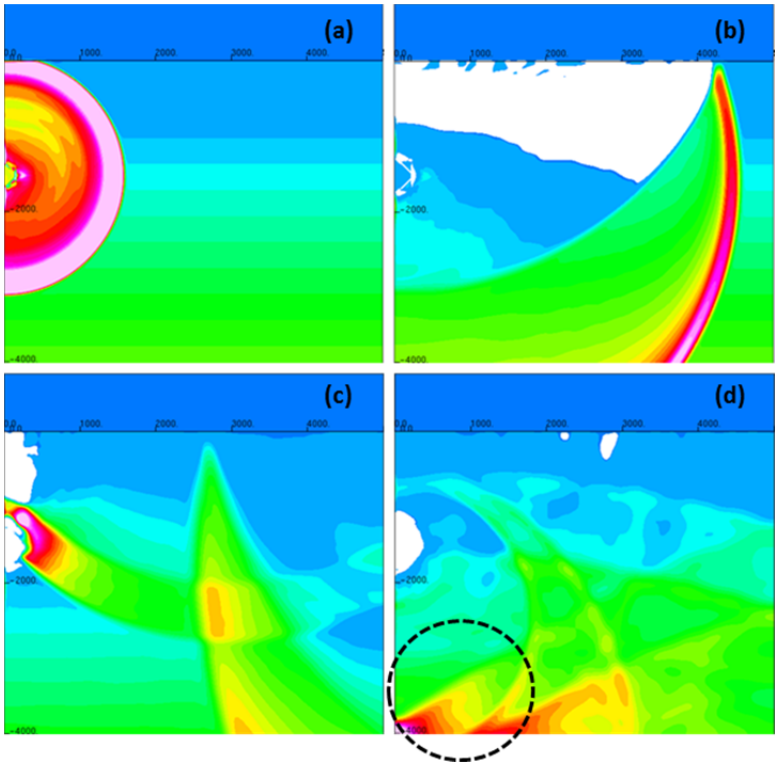

Figure 58. Case 26.1 (Inside of BC, 50% Reflectivity), Time Steps (a) 10 (b) 30 (c) 50 (d) 111msec

Next, the flow field result for Case 26.2 is shown in Figure 59. Case 26.2 depicts case 26 with free or no reflective LB conditions well within the max radius of BC. The flow field result is almost identical to the base case 25 for all chosen time step, except for 111msec. At approximately 100ft deep below charge depth there is a pressure spike where BB SWs meet the downward traveling BC hammer SW (Figure 59(d)). As seen, where these two pressure waves collide, there is a noticeable spike that is similar to when the laterally reflected wave and BB wave intercept. Although this seems minor, the distinct and unexpected difference in pressure spike can cause additional forces applied to the floating object within the timeframe of UNDEX event.

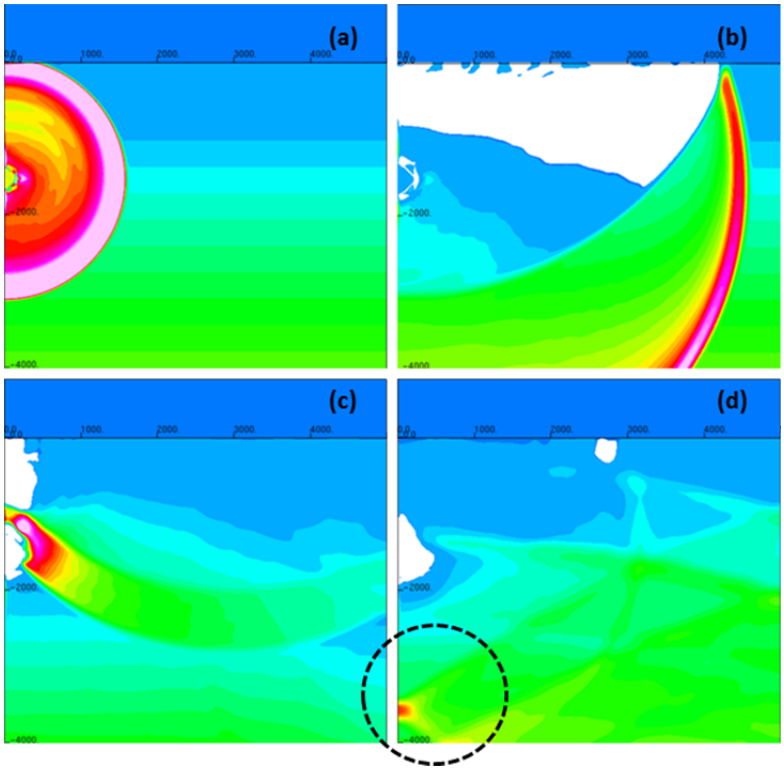

Figure 59. Case 26.2 (Inside of BC, No Reflectivity), Time Steps (a) 10 (b) 30 (c) 50 (d) 111msec

2. Target Pressure Analysis

The pressure profile for cases 25, 26, 26.1 and 26.2 are shown in figures 60 to 62. Observing these pressure profiles of four different cases, the tertiary LB SW following BC hammer shockwave is clearly absent except for case 26 and 26.1 where LBs were set as a rigid wall and 50% reflective wall. The observed shockwaves are expected for both cases in terms of their location and magnitude. A closer look at timeframe from 20 to 50msec (Figure 61) shows base case 25 and case 26.2 pressure profiles are indeed identical for both BC collapse shockwaves of 17.5psi and absence of LB reflection spike near 48msec. Likewise for case 26 and 26.1, the pressure profiles also closely resemble each other, being identical in BC collapse pressure spike of 22psi at 37msec and presence of laterally reflected wave near 48mse, with wall LB setting having the higher pressure spike at 23psi.

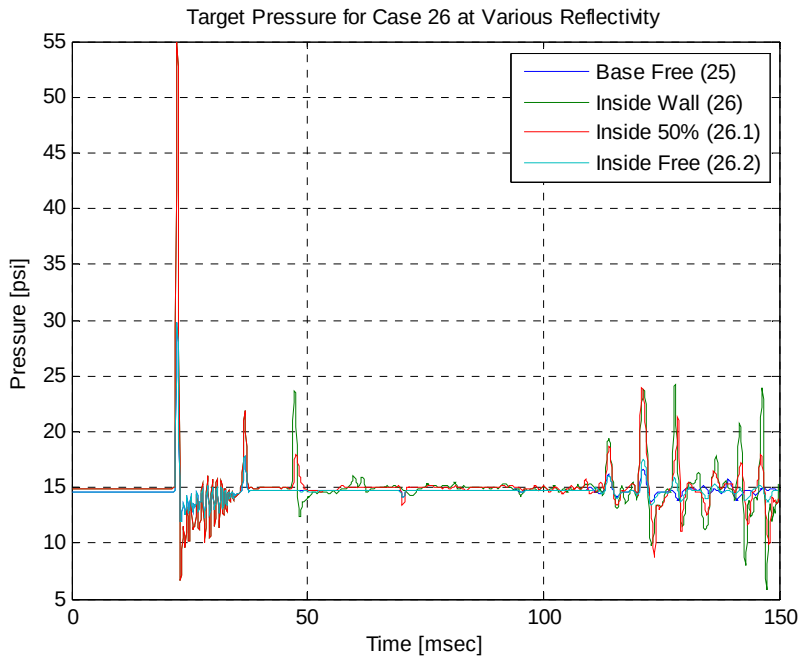

Figure 60. Target Pressure for Varying Boundary Reflectivity

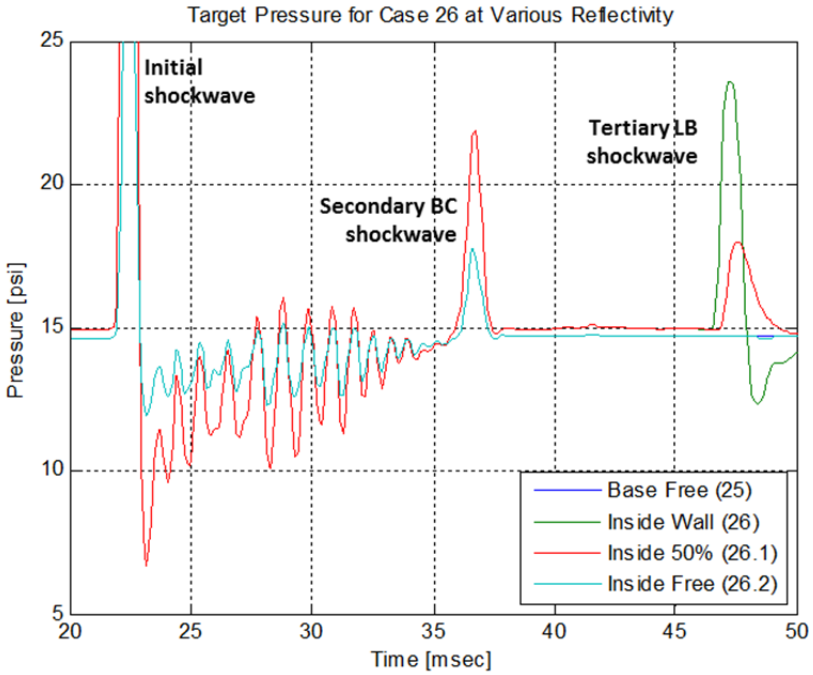

Figure 61. Initial and Secondary Target Pressure for Varying Boundary Reflectivity

Taking a closer look at time step ranges from 100 to 150msec where BB SWs start to emerge, again the presence or lack of LB conditions play a crucial role in invoking additional shockwaves during this time frame. Both cases 25 and 26.2 show similar pressure fluctuations between 13.5 and 17psi. Cases 26 and 26.1 show pressure fluctuations between 6 and 24psi. The differences between wall and free LB conditions are distinct with possibility of LB condition invoking higher pressure fluctuations and within the changes, the reflectivity setting closely resembles how much fluctuations are observed for cases 26 and 26.1.

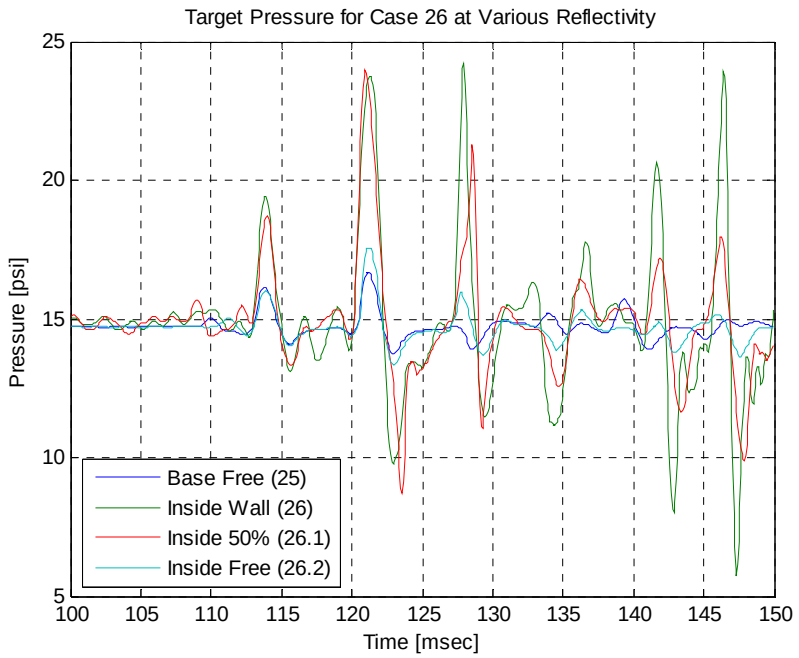

Figure 62. Bottom Bounce Target Pressure for Varying Boundary Reflectivity

3. Vertical Take-Off Velocity Analysis

The VTO results are shown in Figures 63. The initial spike in VTO peaks at 1.75ft/s for all cases. The secondary or LB induced VTO for all cases are different to some degree, but the presence of spike is apparent for presence of LB setting at 50% or wall. For cases 25 and 26.2, the spike is absent; however, there is a minor difference between the two. Again for BB induced VTO, there are distinct differences between

presence of LB conditions and higher magnitudes are observed for cases where 50% or wall setting is present. Lastly, compared to cases 27 and 28 (Figure 56), the absence of varying LB induced spikes, as well as, reduced fluctuation in BB induced VTO are also apparent for this case (Figure 63).

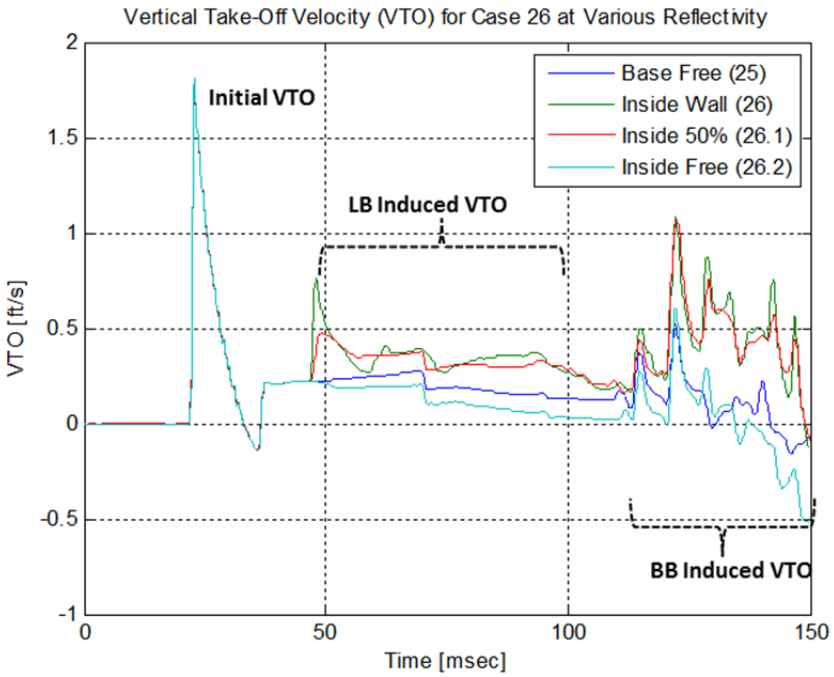

Figure 63. VTO for Various Lateral Boundary Reflectivity

4. Bulk Cavitation Analysis

Taking flow field results into considerations, the BC volume formations were also analyzed numerically and shown in Figure 64. The changing BC volume of case 26.1 and 26.2 were compared to base case 25 and case 26 (Figure 57). There are two distinctly unexpected characteristic observed for cases 25 and 26.2 (free) vs. 26 and 26.1 (50% or wall). As mentioned, case 25 is base case with free boundary and case 26.1 is the same except the location of the LB. In case 25, the boundary is located well outside the BC max radius and case 26.1 the boundary is located inside the BC max radius. The volumetric formation of BC result shows that results of case 25 and 26.2 are not identical. During the initial collapse of BC near 40 to 50msec, the results show case 26.2 to

collapse a lot faster than that of case 25. Additionally, near 30msec and beyond, the case 26.2 shows greater volume spike than case 25. This is during the secondary pressure spike where BC hammer is present (approximately 35msec) and from the observed results, case 26.1 and 26.2 had the most impact in their BCs. For time step ranges of 50 to 100msec, where LB reflective shockwaves are present, case 26 and 26.1 had the most impact. This was expected due to presences of reflective setting in their LB conditions. Lastly, time step ranges from 125 to 150msec show cases 26 and 26.1 with most additional cavitation formed due to same reasoning behind presence of reflective LB conditions.

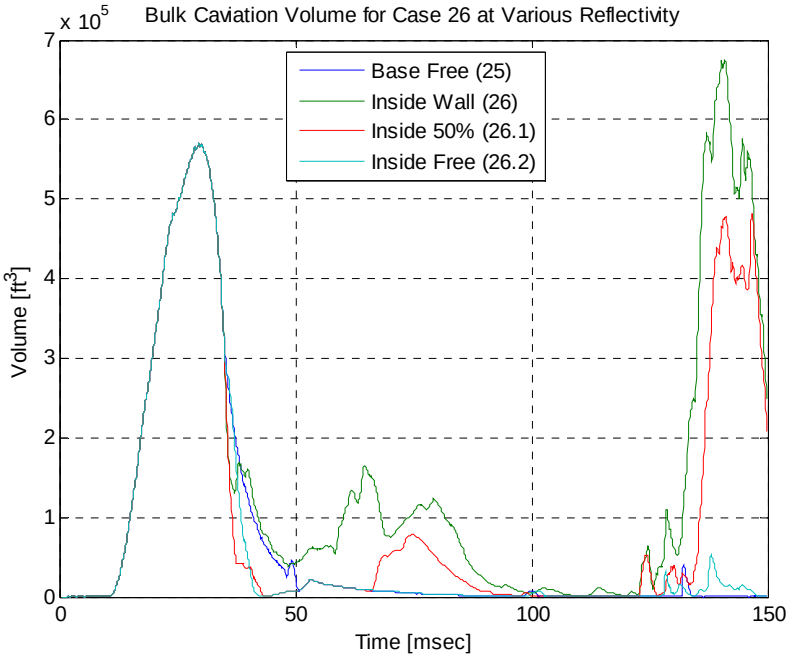

Figure 64. Bulk Cavitation Volume for Various Lateral Boundary Reflectivity

THIS PAGE INTENTIONALLY LEFT BLANK

VII. PRECURSOR TO FULLY COUPLED RUNS

A. THE BLOCKED CELL METHOD

The presence of foreign body and its effect on UNDEX parameters in LOD is of interest for this chapter. Likewise, UNDEX parameter's impact on the FSA is also of interest. As a precursor to including rigid body or Lagrangian solid in the Eulerian domain for fully coupled run, use of "blocked cell" method was utilized. The blocked cell method is set and invoked during Pregemini phase, where inclusion of such object in the Eulerian domain acts as a rigid body in lieu of an actual Lagrange structure in its place, without actually running a fully coupled run. The placements of foreign bodies in three locations as blocked cells (BK) are shown in Figure 65. Generality exists to show that placements of foreign surface object near origin, at midpoint and at the edge of BC radius will have an observable impact on UNDEX parameters; hence, making these cases worth the look prior to fully coupled simulations. As before, the target, charge and DYSMAS set up are as described in Table 4.

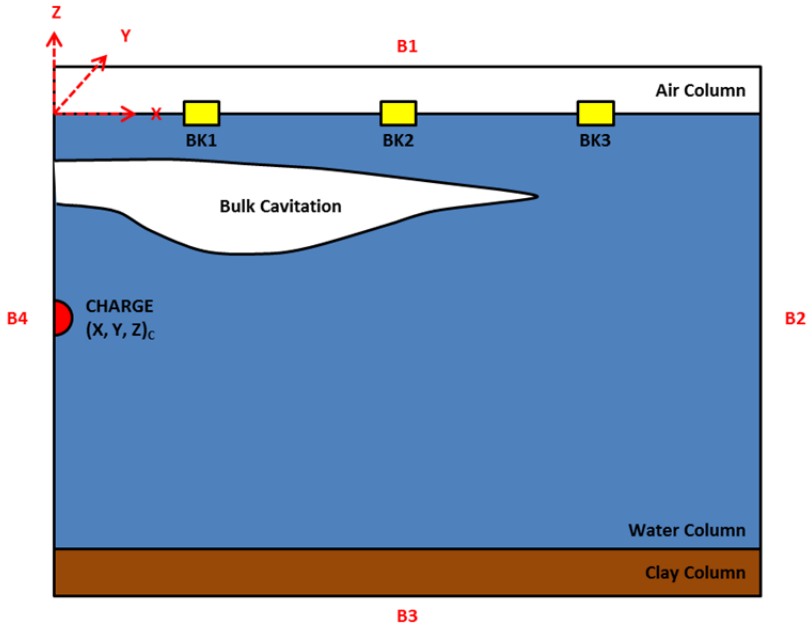

Figure 65. Blocked Cell Methods

Case #	Run Mode	Euler Dimesions (X, Y, Z) [ft]	Target Depth [ft]	Target Distance [ft]	Charge Type [ft]	Charge Weight [lbs]	Charge Depth [ft]	Bottom Type	B1 [zmax]	B2 [xmax]	B3 [zmin]	B4 [xmin]	Grid Size [ft]
29	2D, Euler	300, 1, 300	10	15, 105, 255	HBX-1	25	50	Clay	Free	Free	Wall	Wall	0.164
30	2D, Euler	300, 1, 300	10	15	HBX-1	25	50	Clay	Free	Free	Wall	Wall	0.164
31	2D, Euler	300, 1, 300	10	105	HBX-1	25	50	Clay	Free	Free	Wall	Wall	0.164
32	2D, Euler	300, 1, 300	10	255	HBX-1	25	50	Clay	Free	Free	Wall	Wall	0.164

Table 4. Case Studies for Blocked Cell Methods

B. SUMMARY OF RESULTS AND ANALYSIS

1. Flow Field Analysis

The flow field results for cases 29 through 32 are depicted in figure 66 through 69. The base case, without any blocked cell is shown in Figure 66. No unusual observation was made and all time steps with significant UNDEX events following the same pattern as previous cases studied: (a) initial SW propagation (b) BC reaching maximum radius and depth (c) collapse of BC and initiation of hammer SWs (d) emergence of BB SW as it travels to intercept water-air interface to invoke additional cavitation. Two things that stand out are the characteristics of residual cavitations shown in Figure 66(d).

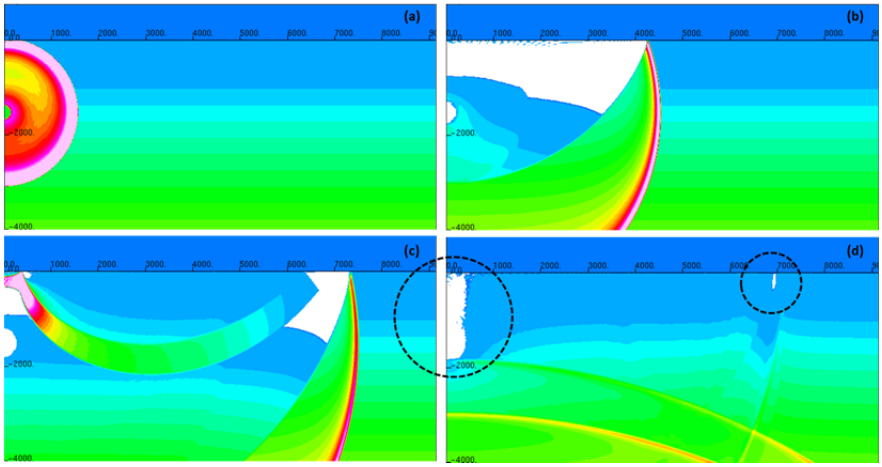

Figure 66. Case 29 (Base), Time Step (a) 10 (b) 30 (c) 50 (d) 100msec

Case 30 with blocked cell closest to the detonation is depicted in Figure 67. The distinctly different characteristics are (a) observation of local cavitation near and around the blocked cell, (b) disruption in BC formation by the blocked cell, (c) presence of additional hammer SWs originating from collapse of local cavitation of blocked cell and speed at which initial BC collapses.

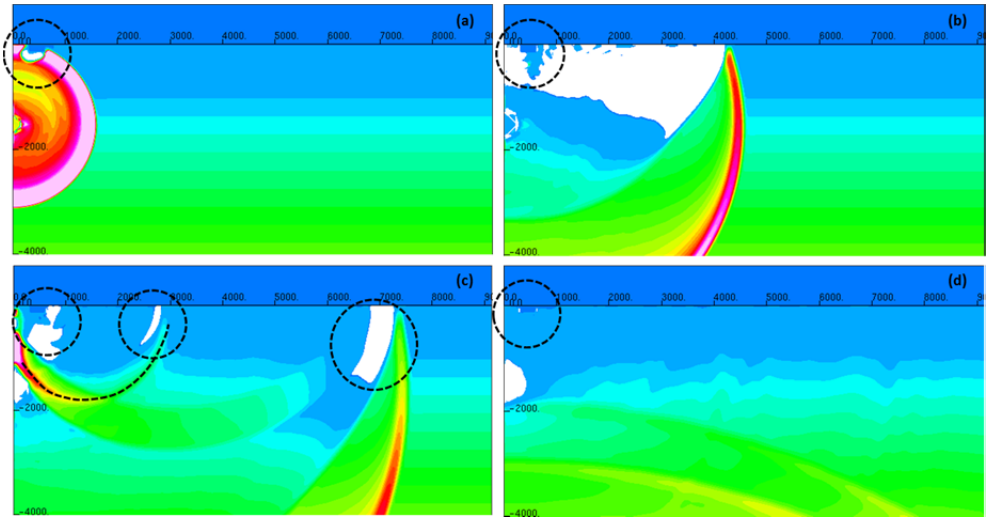

Figure 67. Case 30 (BK1), Time Step (a) 10 (b) 30 (c) 50 (d) 100msec

Case 31 with blocked cell at midpoint to BC radius is depicted in Figure 68. The distinctly different characteristics are (a) lack of local cavitation near and around the blocked cell, (b) disruption in BC formation by the blocked cell as it fully matures and local cavitation, (c) presence of additional hammer SWs originating from collapse of local cavitation of blocked cell merging with the initial BC collapse and (d) emergence of laterally reflected SW originated from the local cavitation hammer shockwave.

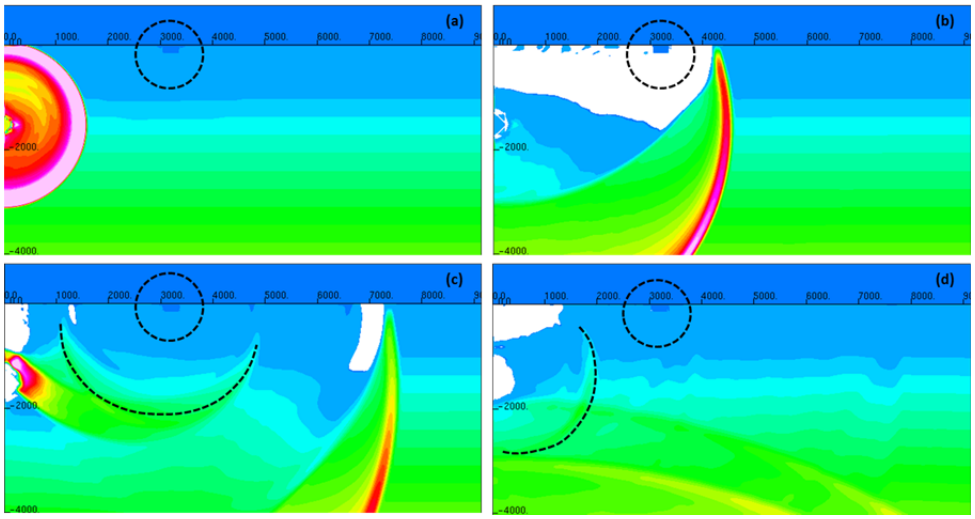

Figure 68. Case 31 (BK2), Time Step (a) 10 (b) 30 (c) 50 (d) 100msec

Case 32 with blocked cell located well outside the max radius of BC is depicted in Figure 69. Once again, the distinctly different characteristics are (a) lack of local cavitation near and around the blocked cell, (b) lack disruption in BC formation and presence of local cavitation, (c) lack of additional hammer SWs originating from collapse of local cavitation and (d) emergence of laterally reflected SW originated from unknown source. The origin of this laterally reflected wave can be speculated from local cavitation collapse from blocked cell, but with time step and location of blocked cell for the case 32, this is unlikely.

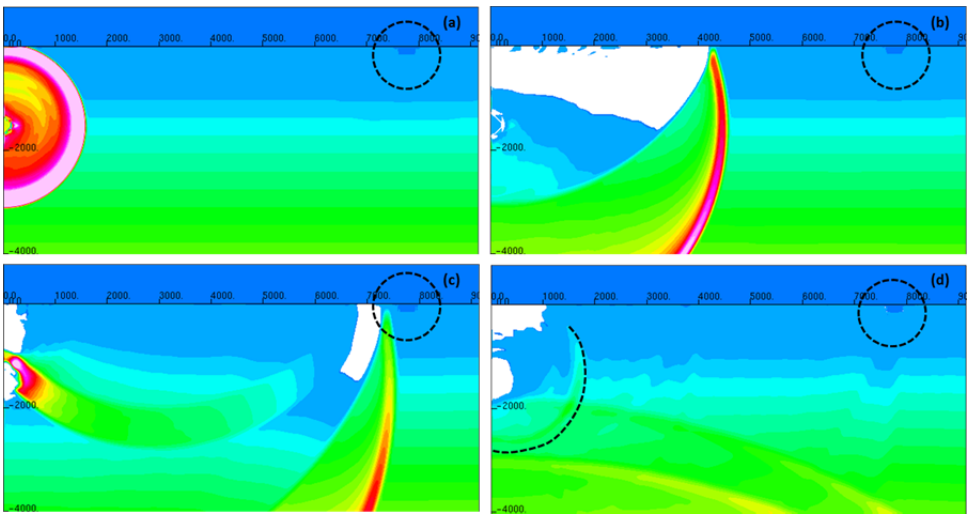

Figure 69. Case 32 (BK3), Time Step (a) 10 (b) 30 (c) 50 (d) 100msec

2. Target Pressure Analysis

The target pressure profiles for each blocked cell location are depicted in figures 70 through 72. Figure 70 is target pressure profile for BK1 compared to the base case without any blocked cells. As can be seen, although there are no impacts to the magnitude of initial shockwave of nearly 700psi near 10msec, a significant differences in BC collapse shockwave's time and magnitude can be observed. While the base case's BC collapsing shockwave reaches close to 400psi, the BK1 only experiences close to 100psi. BK1 also experiences BC closure almost 10msec faster than base case. As observed in the flow field results, the presence of BK1 also expedites the BC collapse.

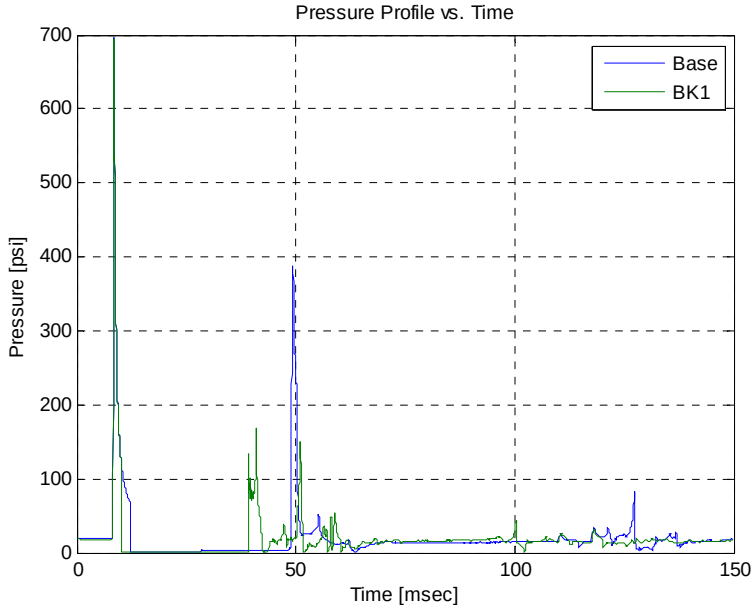

Figure 70. Pressure Profile for BK1 and Base Case

Target pressure profile for BK2 and base case is depicted in Figure 71. Once again, the initial shockwaves are almost identical in magnitude and timing with close to 240psi at time 25msec. Unlike previous case, this time the BC collapse shockwave is higher for the BK2 at close to 85psi while base case hovers at 25psi. Post 100msec show presence of additional cavitations formed when shockwaves originating from the collapse of local cavitation is reflected off the lateral boundaries, shown in flow field of Figure 68.

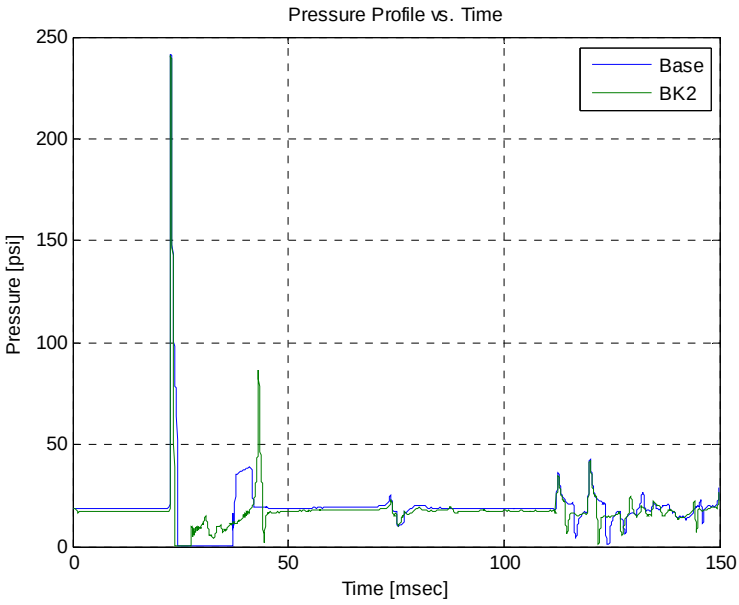

Figure 71. Pressure Profile for BK2 and Base Case

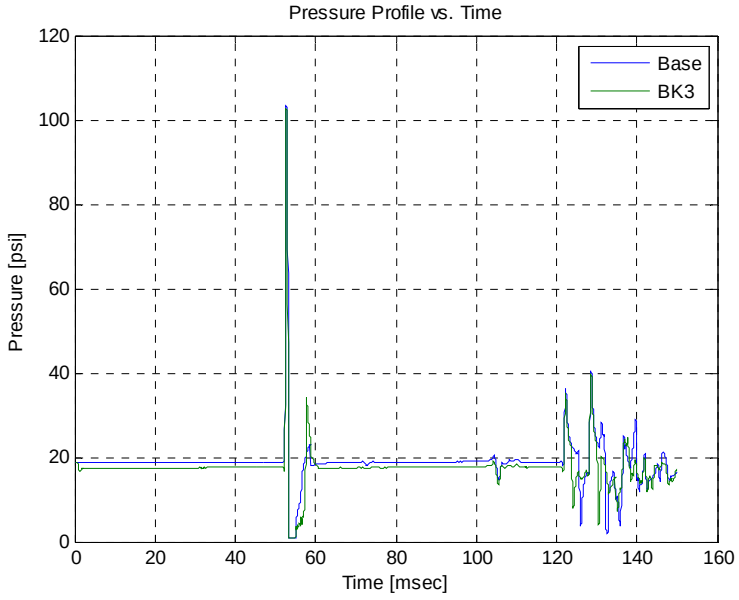

Figure 72. Pressure Profile for BK3 and Base Case

Target pressure profile for BK3 and base case is depicted in Figure 72. Once again, the initial shockwaves are almost identical in magnitude and timing with close to 100psi at time 46msec. Similar to previous case, this time the BC collapse shockwave is higher for the BK3 at close to 35psi while base case hovers at 20psi. Post 120msec also

show presence of additional cavitations formed when shockwaves originating from the collapse of local cavitation is reflected off the lateral boundaries, shown in flow field of Figure 69.

3. Vertical Take-Off Velocity Analysis

The VTO for each blocked cell location are depicted in figures 73 through 75. The VTO for base case and BK1 are depicted in Figure 73. Both cases' VTO peaks at 11ft/s followed by an immediate collapse and fluctuation near and around 3ft/s. The VTO fluctuations for the base case seems to be more dramatic in that lack of blocked cell that can hinder movement will freely let water to slush around the domain. Conversely, the presence of blocked cells greatly decreases the movement of the water around it since the energy is transferred to and from blocked cell invoking a beginning of FSA phenomenon.

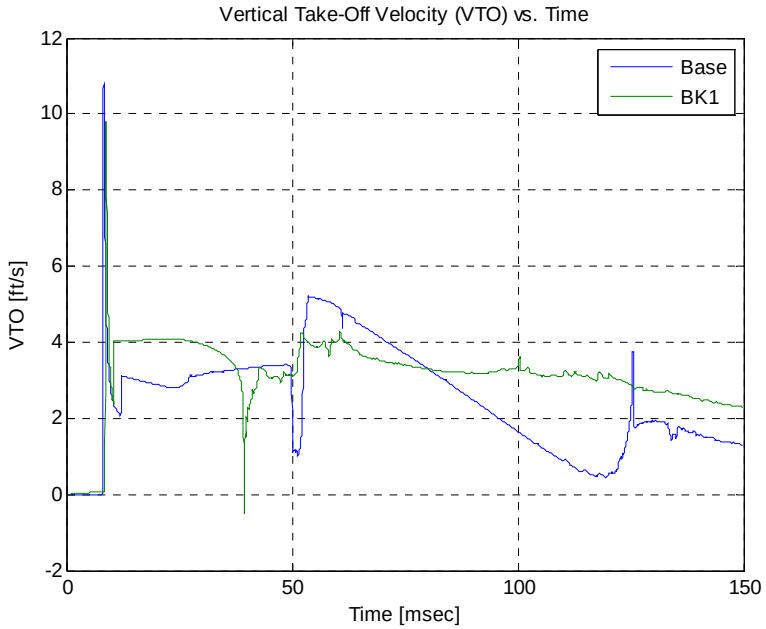

Figure 73. VTO for BK1 and Base Case

The VTO for the base case and BK2 are depicted in Figure 74. Both cases' VTO peaks at 1.5ft/s followed by an immediate collapse and fluctuation near and around 0.25ft/s. The VTO fluctuations for the BK2 seem to be more dramatic with dip of -1.5ft/s

at approximately 40msec. The dip at 40msec is counterintuitive since the blocked cell is not moving, but further investigating flow field results (Figure 68), show that this is due to traveling shockwave originated from the collapsing local cavitation.

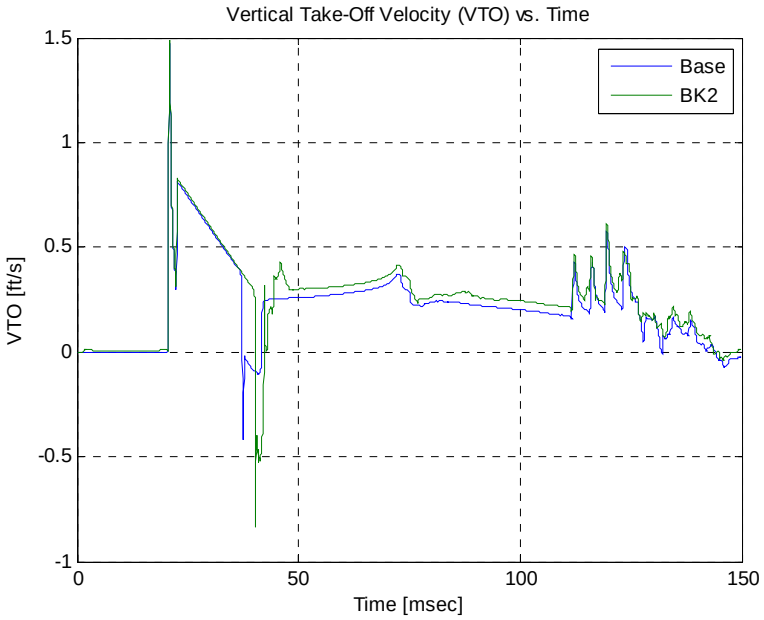

Figure 74. VTO for BK2 and Base Case

Lastly, VTO for base case and BK3 are compared in Figure 75. For this case, the presence of initial shockwaves at 0.3psi at 55msec and presence of shockwave originating from collapse of local cavitation are close to being identical, except, for BK3, the VTO continues to increase throughout the time step. Since blocked cells are treated as a rigid material and reflecting surface, BK3's characteristic can only be explained as error in Gemini's solution [12]. Numerous attempts were made to fix this error through remeshing Eulerian domain and placement of the blocked cells, as well as, target position. At this time, an acceptable solution does not exist although the pattern and presence of initial and additional shockwave are consistent with previous cases.

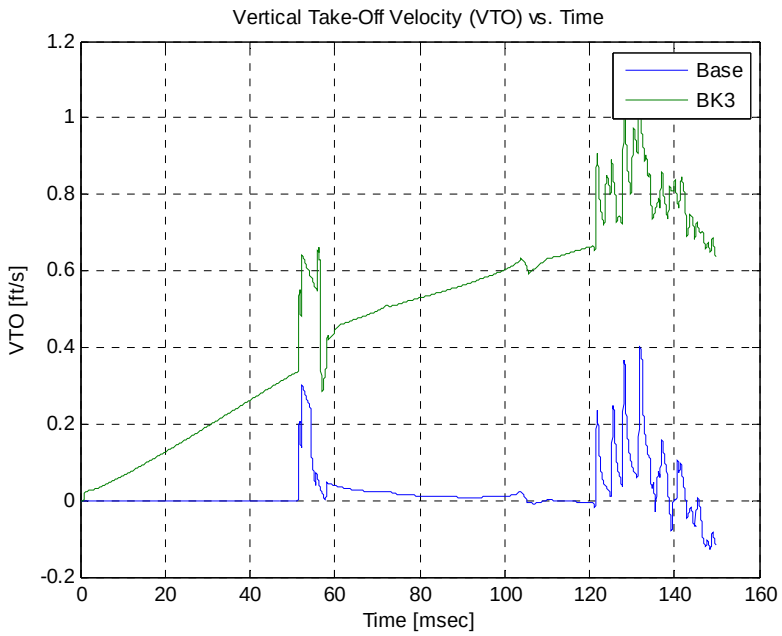

Figure 75. VTO for BK3 and Base Case

4. Bulk Cavitation Analysis

The BC results for all blocked cell cases are depicted in Figure 76. Similar characteristics to previous cases are still observed, where BC is initiated at 10msec when initial shockwave reaches water-air interface, reaches its maximum radius at approximately 35msec, dissipates completely by 60msec and additional cavitation observed near 120msec where BB reaches water-air interface to invoke this phenomenon. Two distinctly different patterns emerge for BK2 where the BC starts to collapse 22msec with another increase near 40msec when local cavitations are invoked and completes dissipation near 60msec. For BK3, lack of local cavitation reduces the overall BC volume; hence, its collapse prior to 60msec can also be observed. All four cases experienced additional cavitation formations starting at 120msec when BB shockwave emerged to initiate another set of BC near water-air interface.

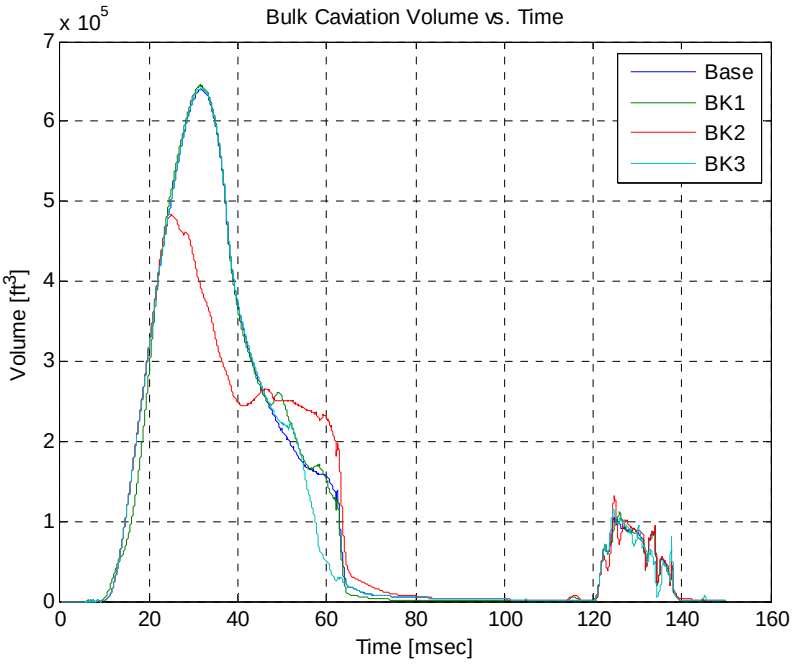

Figure 76. Bulk Cavitation Volume for Blocked Cell Cases

VIII. CONCLUSION AND RECOMMENDATION FOR FURTHER STUDIES

A. CONCLUSIONS

An in-depth analysis and characterization of littoral ocean domain (LOD) were conducted for transient phase of UNDEX by analyzing resulting parameters such as initial shock wave, vertical take-off velocity and bulk cavitation. Implementing various conditions such as ocean depth, charge size and depth, boundaries for bottom and side conditions of fluid domain and even including a small rigid body, these results were compared and contrasted to the current Eulerian fluid model.

First, results of varying ocean depths show clear distinction in UNDEX characterization at depth shallower than 300ft. At this depth, multiple shockwaves and resulting vertical take-off velocity exists due to additionally induced cavitation resulting from the reflecting pressure wave from the shallower bottom. The reflecting shockwave and energy contained within are the main culprit of shallow UNDEX characteristics.

Second, the results of varying charge size and depth showed that charge size of less than or equal to 300lbs showed linear relationships and as the charge depth reached water-air or water-bottom interface, the characteristics of resulting UNDEX parameters became increasingly amplified and chaotic. The combined bottom bounce and initial shockwave for charge depth at water-bottom interface showed combined effects of its resulting UNDEX parameters with greater BC volume while delayed initial response.

Third, results of varying lateral boundary conditions show that as the lateral boundary distance is brought closer to the detonation source, inside the radius of bulk cavitation, its behavior and the rest of the UNDEX parameters also become increasingly amplified due to similar effects seen in shallower bottom depths. Varying its reflectivity also amplified UNDEX reactions; however, differences in reflectivity between free and 50% lateral boundary condition inside and outside the radius of BC showed negligible changes in the UNDEX results.

Lastly, adding blocked cells prior to a full scale coupled run showed that fluid behaves more erratically as these blocked cells are situated within the radius of forming BC. As fluid behaves differently around the existing small rigid blocks, so too are the UNDEX parameters due to reflective energy from these rigid blocks, invoking energy back into the fluid domain. As a result, a precursor to how fluid may behave starts to emerge for a fluid structure interaction or fully coupled run cases.

As a result, recommended characterization and boundaries of LOD for UNDEX studies start to emerge. From this study, the ocean depth of 300ft, lateral boundary distance of greater than 1/3 radius distance from the edge of bulk cavitation, charge weight of 300lbs or less and its placement at minimum of 1/3 distance away from the existing boundaries, such as bottom or lateral wall are recommended. For fully coupled runs, the placement of Lagrangian solid within the bulk cavitation radius and inclusion of various bottom sediments to increase realism with caveats of setting its reflectivity condition to rigid or wall are also recommend for LOD. Although cyclic bubble was not studied extensively during this research, the obvious choice of bubble setting is to pick a charge size that will produce an initial bubble size consistent with previous LOD boundaries. If purpose is to study the transient phase of UNDEX then this is not a huge factor. However, if whipping analysis is of interest, choosing a charge size that will invoke a bubble radius of at minimum of less than chosen LOD depth is recommended.

B. RECOMMENDATION FOR FURTHER STUDIES

While this study shed some light on the benefits of establishing the boundaries of LOD for future coupled runs of various Lagrangian models or an actual LCS FE model, due to the sheer size of the problem in computing time and efficiency, other parts of Eulerian characteristics such as implementing viscous code, adding shelves within the fluid domain to study the effects of its angle and further study of steady state UNDEX phenomena like cyclic bubbles and its effect are recommended.

APPENDIX A. COMBINED DYSMAS/GEMINI SIMULATED CASES

Case #	Run Mode	Euler Dimesions (X, Y, Z) [ft]	Target Depth [ft]	Target Distance [ft]	Charge Type [ft]	Charge Weight [lbs]	Charge Depth [ft]	Bottom Type	B1 [zmax]	B2 [xmax]	B3 [zmin]	B4 [xmin]	Grid Size [ft]	Remarks
1	2D, Euler	800, 1, 1000	0.820	100	HBX-1	25	50	Clay	Free	Free	Wall	Wall	0.656	Varying Ocean Depth from 1000ft to 75ft deep. All other UNDEX parameters, including charge size and charge depth maintained constant.
2	2D, Euler	800, 1, 900	0.820	100	HBX-1	25	50	Clay	Free	Free	Wall	Wall	0.656	
3	2D, Euler	800, 1, 800	0.820	100	HBX-1	25	50	Clay	Free	Free	Wall	Wall	0.656	
4	2D, Euler	800, 1, 700	0.820	100	HBX-1	25	50	Clay	Free	Free	Wall	Wall	0.656	
5	2D, Euler	800, 1, 600	0.820	100	HBX-1	25	50	Clay	Free	Free	Wall	Wall	0.656	
6	2D, Euler	800, 1, 500	0.820	100	HBX-1	25	50	Clay	Free	Free	Wall	Wall	0.656	
7	2D, Euler	800, 1, 400	0.820	100	HBX-1	25	50	Clay	Free	Free	Wall	Wall	0.656	
8	2D, Euler	800, 1, 300	0.820	100	HBX-1	25	50	Clay	Free	Free	Wall	Wall	0.656	
9	2D, Euler	800, 1, 200	0.820	100	HBX-1	25	50	Clay	Free	Free	Wall	Wall	0.656	
10	2D, Euler	800, 1, 175	0.820	100	HBX-1	25	50	Clay	Free	Free	Wall	Wall	0.656	
11	2D, Euler	800, 1, 150	0.820	100	HBX-1	25	50	Clay	Free	Free	Wall	Wall	0.656	
12	2D, Euler	800, 1, 125	0.820	100	HBX-1	25	50	Clay	Free	Free	Wall	Wall	0.656	
13	2D, Euler	800, 1, 100	0.820	100	HBX-1	25	50	Clay	Free	Free	Wall	Wall	0.656	
14	2D, Euler	800, 1, 75	0.820	100	HBX-1	25	50	Clay	Free	Free	Wall	Wall	0.656	
15	2D, Euler	800, 1, 500	0.820	100	HBX-1	100	50	Clay	Free	Free	Wall	Wall	0.656	Varying Charge Size. All other UNDEX parameters maintained constant.
16	2D, Euler	800, 1, 500	0.820	100	HBX-1	200	50	Clay	Free	Free	Wall	Wall	0.656	
17	2D, Euler	800, 1, 500	0.820	100	HBX-1	300	50	Clay	Free	Free	Wall	Wall	0.656	
18	2D, Euler	800, 1, 500	0.820	100	HBX-1	400	50	Clay	Free	Free	Wall	Wall	0.656	
19	2D, Euler	800, 1, 500	0.820	100	HBX-1	500	50	Clay	Free	Free	Wall	Wall	0.656	
20	2D, Euler	800, 1, 500	0.820	100	HBX-1	100	100	Clay	Free	Free	Wall	Wall	0.656	Varying Charge Depth. All other UNDEX parameters maintained constant.
21	2D, Euler	800, 1, 500	0.820	100	HBX-1	100	200	Clay	Free	Free	Wall	Wall	0.656	
22	2D, Euler	800, 1, 500	0.820	100	HBX-1	100	300	Clay	Free	Free	Wall	Wall	0.656	
23	2D, Euler	800, 1, 500	0.820	100	HBX-1	100	400	Clay	Free	Free	Wall	Wall	0.656	
24	2D, Euler	800, 1, 500	0.820	100	HBX-1	100	500	Clay	Free	Free	Wall	Wall	0.656	
25	2D, Euler	230, 1, 300	0.820	100	HBX-1	25	50	Clay	Free	Free	Wall	Wall	0.656	Base Case, free boundary @ xmax
26	2D, Euler	164, 1, 300	0.820	100	HBX-1	25	50	Clay	Free	Wall	Wall	Wall	0.656	Varying Case, wall boundary @ xmax. For 26.1 & 26.2, varied reflectivity 50% & free for boundary located inside BC zone.
26.1	2D, Euler	164, 1, 300	0.820	100	HBX-1	25	50	Clay	Free	0.50	Wall	Wall	0.656	
26.2	2D, Euler	164, 1, 300	0.820	100	HBX-1	25	50	Clay	Free	Free	Wall	Wall	0.656	
27	2D, Euler	197, 1, 300	0.820	100	HBX-1	25	50	Clay	Free	Wall	Wall	Wall	0.656	
28	2D, Euler	230, 1, 300	0.820	100	HBX-1	25	50	Clay	Free	Wall	Wall	Wall	0.656	
29	2D, Euler	300, 1, 300	10	15, 105, 255	HBX-1	25	50	Clay	Free	Free	Wall	Wall	0.164	Base Case, No Blocked Cell
30	2D, Euler	300, 1, 300	10	15	HBX-1	25	50	Clay	Free	Free	Wall	Wall	0.164	Blocked cell at position (1)
31	2D, Euler	300, 1, 300	10	105	HBX-1	25	50	Clay	Free	Free	Wall	Wall	0.164	Blocked cell at position (2)
32	2D, Euler	300, 1, 300	10	255	HBX-1	25	50	Clay	Free	Free	Wall	Wall	0.164	Blocked cell at position (3)

THIS PAGE INTENTIONALLY LEFT BLANK

APPENDIX B: BULK CAVITATION THEORY

The following section describes how the method of Arons is used to map out the bounds of the cavitated region that forms when surface cutoff tries to lower the absolute pressure below the cavitation pressure. A continuation from section II. B. 2 of this study, it is a direct summary from the critical sections within the technical paper published by Costanzo and Gordon in May 1983, titled "A Solution to the Axisymmetric Bulk Cavitation Problem" and for that I am grateful for its use and many thanks to Contanzo and Gordon for use of their work as primary reference in characterizing BC for this study [9].

A. DERIVATION OF METHODS OF ARONS AND TANGENT RULE

The target pressure (P) at its location of (X, Y) is assumed to be the absolute pressure prior to arrival of the reflected wave from water-air interface. This pressure is culmination of overpressure generated by SW, atmospheric and hydrostatic pressure. Now, let P be function of radial (r) and angular (α) coordinate originating from the image charge, W_i, as shown in Figure 20. The upper cavitation boundary is defined as the locus of points at which the absolute pressure drops to the cavitation pressure upon arrival of the rarefaction wave [9]. At this point, water at cavitation will remain cavitated as long as the absolute pressure does not rise above the vapor pressure of water. For all practical purpose for the method of Arons, the vapor and cavitation pressure are assumed to be zero. Thus, the equation defining the upper cavitation boundary is

$$P(\alpha, r) + P_r = 0 \tag{B.1}$$

If P_r, the reflected wave, is expressed in terms of the charge weight and standoff using the method of images, then $P_r = -A(W^{1/3}/r)^B$. Substituting this expression into Equation (B.1) gives

$$P(\alpha, r) - A\left(\frac{W^{1/3}}{r}\right)^B = 0 \tag{B.2}$$

Where, A and B are constants specific to the charge or explosive types. Now, before the cavitation boundary is discussed, the term breaking pressure must be defined. The breaking pressure is the magnitude of the rarefaction wave (or relief wave, as commonly termed) which reduces the absolute pressure at a point to the cavitation pressure. In other words, since the cavitation pressure is taken to be 0 psi absolute, the breaking pressure has a magnitude equal to the absolute pressure at a point prior to the occurrence of cavitation at that point. The equation of the lower cavitation boundary is derived from consideration of the propagation of this breaking pressure into the uncavitated water beneath this boundary. Let $P_r = P(\alpha, r)$ be the breaking pressure for a point lying at the lower cavitation boundary. At this lower boundary, $P(\alpha, r)$ must propagate into uncavitated water with spherical attenuation resulting in $P_r = P(\alpha, r)(R/r)^B$. This is represented in Figure 77.

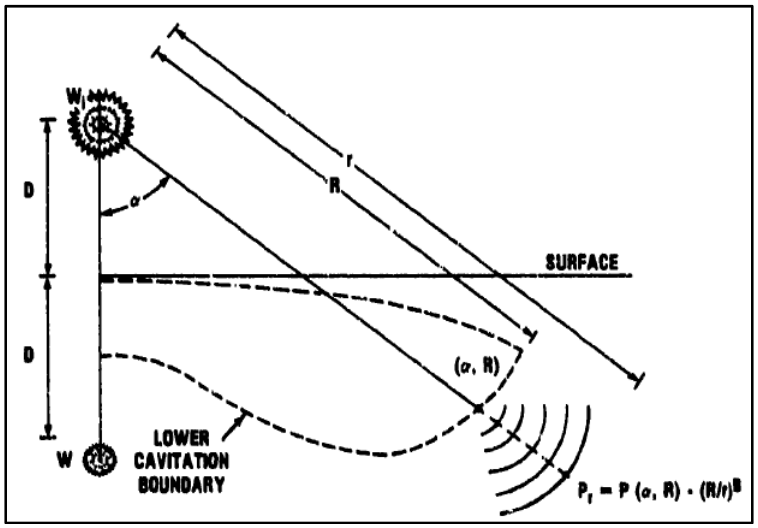

Figure 77. Propagation of Breaking Pressure into Uncavitated Water, from [9]

This pressure expression must have a faster decay rate than the general expression for absolute pressure, $P = P(\alpha, r)$, or the water located along the dashed line extending below the lower cavitation boundary will continue to cavitate. Thus, at a point on the

lower cavitation boundary, the decay rate of both of these pressure expressions is the same. Therefore:

$$\frac{d}{dr}\left[P(\alpha,r)(R/r)^{B}\right]_{r=R}=\frac{d}{dr}\left[P(\alpha,r)\right]_{r=R} \tag{B.2.a}$$

If all terms of this equation are shifted to one side of the equal sign and r^{-B} is factored out, then application of the chain rule to differentiation of a product results in:

$$\frac{d}{dr}\left[\left(r^{B}\right)P(\alpha,r)-P(\alpha,r)(R^{B})\right]_{r=R}=0 \tag{B.2.b}$$

This expression may be simplified further by recognizing that the product, $P(\alpha,r)(R^{B})$, pertains to a specific point and thus may be treated as a constant when differentiating. Therefore, this equation becomes:

$$\frac{d}{dr}\left[\left(r^{B}\right)P(\alpha,r)\right]_{r=R}=0 \tag{B.3}$$

where r = R, the point at the lower cavitation boundary for a given α. Equation (B.3) is the method of Arons for determining the lower cavitation boundary.

In Figure 78, the general shape of the BC envelope as determined by the method of Aron is given. It is of fundamental interest to the BC problem to locate the point at which a line drawn from the image charge is tangent to the upper cavitation boundary. For the derivation of this tangent point, both sides of Equation (B.2) are multiplied by r^{B} and the resulting equation and its total derivation with respect to *r* are written below as equations (B.4) and (B.5), respectively.

$$\left(r^{B}\right)P(\alpha,r)-A\left(W^{1/3}\right)^{B}=0 \tag{B.4}$$

$$\frac{d}{dr}\left[\left(r^{B}\right)P(\alpha,r)-A\left(W^{1/3}\right)^{B}\right]=\frac{\partial}{\partial r}\left[\left(r^{B}\right)P(\alpha,r)\right]+\frac{\partial}{\partial\alpha}\left[\left(r^{B}\right)P(\alpha,r)\right]\left(\frac{\partial\alpha}{\partial r}\right)=0 \tag{B.5}$$

For a given value of dα/dr, the simultaneous solution of these two equations gives the corresponding values of α and *r*. When the ray extending from the image charge is tangent to the upper cavitation boundary, α is a maximum and dα/dr = 0. When this value for dα/dr is substituted into Equation (B.5), the following is obtained:

$$\frac{\partial}{\partial r}\left[\left(r^{B}\right)P\left(\alpha,r\right)\right]=0 \tag{B.6}$$

Therefore, the simultaneous solutions of Equations (B.4) and (B.6) give the value of α and r at the tangent point. Equation (B.6) also happens to be equivalent to Equation (B.3), the equation whose solution determines the lower cavitation boundary. This indicates that the lower and upper cavitation boundaries intersect at the point at which a line drawn from the image charge is tangent to the upper boundary. This rule of tangency is also illustrated in Figure 78.

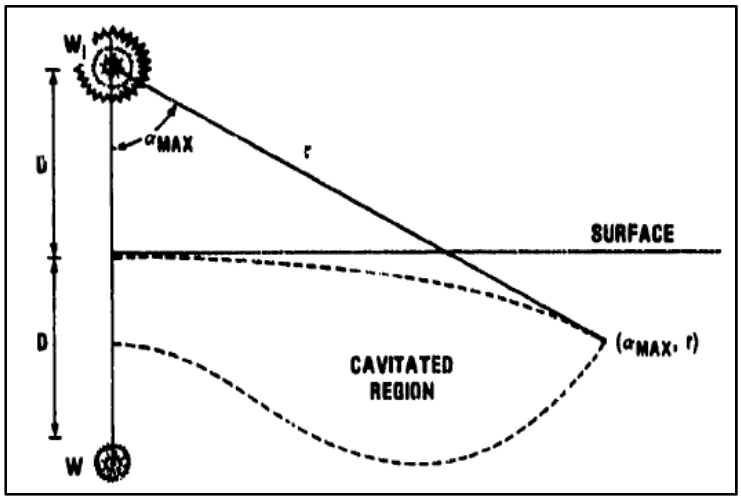

Figure 78. Bulk Cavitation Bounds and Rule of Tangency, from [10]

B. DEVELOPMENT OF THE CLOSURE MODEL

1. General Description

The general representation of a point which lies within the cavitated region is given in Figure 79. Upon the arrival of the relief wave at this point, the vertical component of the instantaneous water particle velocity is the vector sum of the vertical

components of the two velocity vectors as shown. This vector sum is termed the vertical water particle kickoff velocity or vertical take-off velocity (VTO) at point (X, Y) and is dependent solely upon the magnitude and directions of the incident and reflected acoustic water particle velocities. The directions of these velocities are defined by the unit vectors, $\tilde{i}$ and $\tilde{j}$, as shown in the figure.

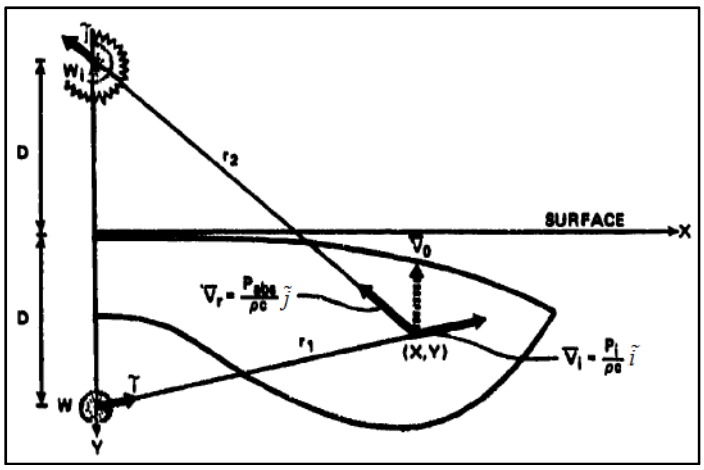

Figure 79. Point Lying in the Cavitated Region, from [9]

At every horizontal range within the extent of the BC envelope, there exists a column of water which lies between the surface and the upper cavitation boundary. Since this water does not cavitate, it is assumed that all water particles contained in this vertical column are kicked off simultaneously with kickoff velocity of the water particle located at the upper cavitation boundary. This is illustrated in Figure 80. This surface layer, which is kicked off at the time of relief wave arrival at the upper cavitation boundary with an initial velocity, $\bar{V}_0$, is decelerated by atmospheric pressure and gravity. At a short time later, the water particle lying directly beneath this surface layer is kicked off with an initial velocity, $\dot{Z}_0$.

Since this particle lies within the cavitated region and is kicked off after the surface layer, it becomes separated from the surface layer and therefore has no atmospheric pressure acting upon it. Thus, only gravity decelerates this particle. Eventually, this water particle will collide with the surface layer above it. In the

development of the closure model, it is assumed that this is a perfectly inelastic collision. Thus, this particle and the surface layer above it now form an augmented surface layer which has a velocity derived from the conservation of momentum consideration. As with the original surface layer, this augmented surface layer has atmospheric pressure and gravity acting to decelerate it.

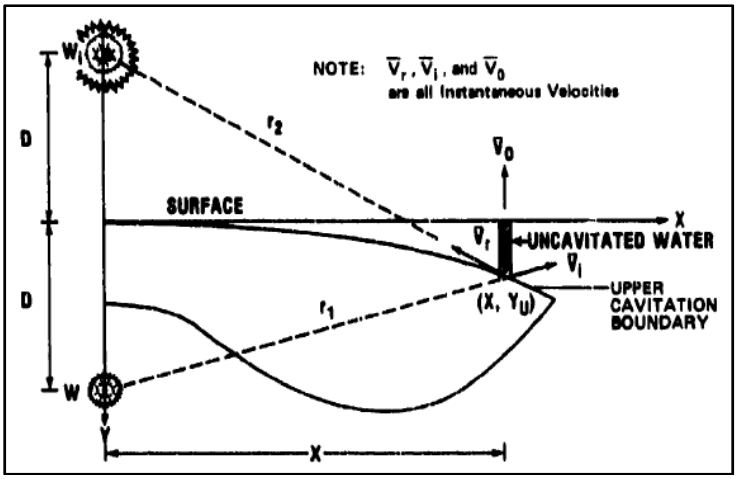

Figure 80. Kickoff Velocity of the Surface Layer, from [9]

Since the particles lying below the original surface layer are all kicked off at different times with different vertical kickoff velocities, inelastic collisions will occur one at a time between the growing surface layer and the particles directly below it. This process is known as accretion. If the surface layer displacement history at a horizontal range, X, is plotted with t=0 referring to the time of explosives charge detonation, the curve in Figure 81 is obtained. This curve is not quite a perfect parabola due to the fact that the surface layer mass is changing. Also note that this curve accounts for the initial displacement of the surface layer due to the incident SW prior to relief wave arrival at the upper cavitation boundary.

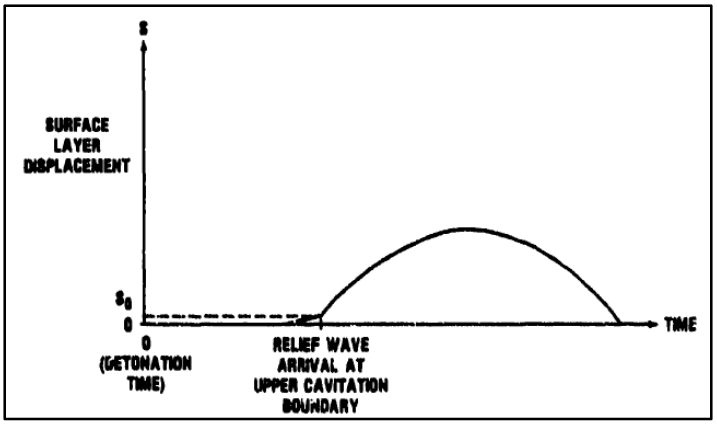

Figure 81. Surface layer Displacement, from [9]

The vertical component of the water particle velocity for the point which lies at the lower cavitation boundary at this same horizontal range, X, also must be determined. Since cavitation does not extend below this point, separation will not occur between the underlying water particles. Hence, the water which lies below this point at the lower cavitation boundary will have a vertical velocity component which is dependent upon the varying velocities $\bar{V}_r$ and $\bar{V}_i$ and their corresponding afterflow terms. This is depicted for point (X, Y_L) in Figure 82.

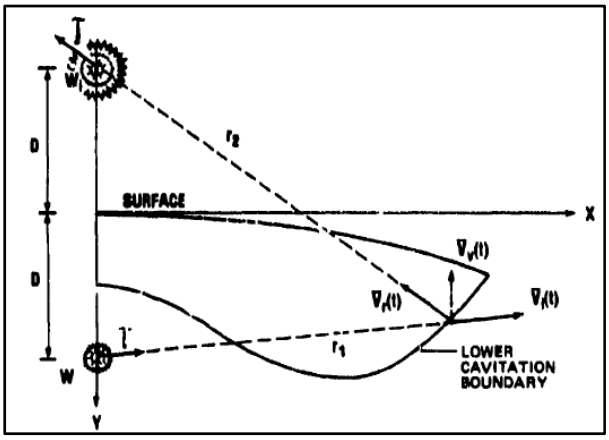

Figure 82. Velocity of a Point at the Lower Cavitation Boundary, from [9]

2. Bulk Cavitation Closure Pulse

The magnitude of the pressure pulse generated by the collision of the accreting lower cavitation boundary at closure will now be determined. Since in the closure model, the vertical components of the velocities of both the surface layer and the lower cavitation boundary for a particular horizontal range, X, are known at the time of closure, the closure pressure pulse magnitude, P_c, can be calculated by multiplying one half the relative velocity of impact of these two water masses by the characteristic impedance of the medium. That is:

$$P_C = \frac{\rho C}{2}(V_L - V_U) \tag{B.7}$$

where V is positive upward and V_U and V_L refer to the vertical velocity components at closure of the surface or upper layer and the lower cavitation boundary, respectively. The closure pressure pulse consists of two compressive waves of magnitude, P_C; one that travels upward and one that travels downwards. These closure pressures are most readily superimposed upon the incident SW and reflected pressure at the horizontal range at which closure first occurs, since at the range, the direction of propagation of the closure pulse is vertical. At other horizontal ranges, the direction of propagation of the closure pulse varies from the vertical direction by an angle ψ, as shown in Figure 83. According to the work done by Cushing [10], if C is the sound speed in water and V_C is the speed at which the cavitated region is closing at some horizontal range, X, then:

$$\sin\psi = \frac{C}{V_C} \tag{B.8}$$

Thus, the magnitude of the pressure pulse which propagates along a path oriented at this angle ψ is determined by dividing the expression of Equation (B.7) by cos ψ. That is:

$$P_C = \frac{\rho C(V_L - V_U)}{2\cos\psi} \tag{B.9}$$

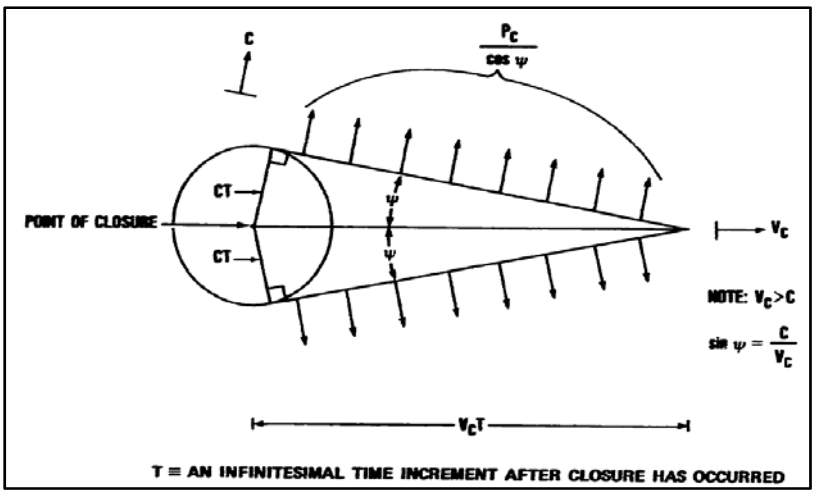

Figure 83. Closure Pulse at a Horizontal Range Different from that of First Closure, from [9]

The duration time of the closure pulse at the depth of closure is determined by the method of images and is expressed by:

$$t_{duration} = \frac{2D_C}{C}\cos\psi \tag{B.10}$$

where D_C is the depth of closure at the horizontal range of interest, X. Thus, regardless of the angle of propagation of the closure pulse, the impulse (pressure X duration) associated with cavitation closure at a particular horizontal range is the same and may be expressed as shown in Equation (B.10).

$$\text{Im } pulse = \rho(V_L - V_U)D_C \tag{B.11}$$

THIS PAGE INTENTIONALLY LEFT BLANK

APPENDIX C. BULK CAVITATION CASE STUDIES

Following case studies were conducted in order to better characterize behaviors of bulk cavitation prior to its inclusion into shallow water or littoral ocean domain environments. The MATLAB codes used for this study is included in the Appendix of this report.

1. Comparison of 2-D BC Zone, varying charge type, charge weight and charge detonation depth (Appendix C contains MATLAB codes for 2D BC Zones):

a. <u>200 lb charges of HBX-1, TNT and PETN at a depth of 25 ft</u>:

Figure 84 is a 2D representation of the bulk cavitaion zone of a 200lbs charge denotated at a depth of 25ft. The charge lies along the left vertical edge of each subplot. Each subplot represents a different explosive type as titled. This figure was created for the sole purpose of comparing the BC zone of the three different types of explosive with the other variables (depth of charge, weight of charge) held constant.

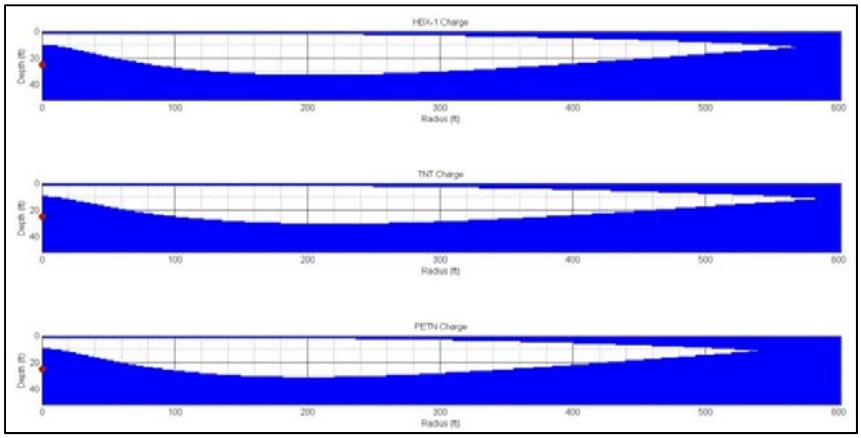

Figure 84. 2-D Bulk Cavitation of 200lbs of HBX-1, TNT and PETN @ 25ft

Since water cannot support a tension (i.e. negative pressure), cavitation occurs at points in the water column where the sum of the pressures at that point are less than or equal to zero. This pressure is sum of atmospheric, water depth, incident shock pressure, and rarefaction wave pressure. As can be clearly seen from the above figure, even

though all the explosive charge weights and detonation depths are the same, each explosive charge type creates a different BC region in both depth and radial distance outward. This is due to the fact that they have different constants (K_1, K_2, A_1, A_2) associated with them that are used in the calculation of their maximum pressure and their decay constant.

The Pentolite (PETN) ultimately had the lowest K_2 and A_2 thus causing it to have the deepest but shortest BC zone. TNT and HBX-1 are very similar in their K_2 value however TNT's A_2 value is significantly smaller than HBX-1, causing it to "reach" further outward from point of detonation. In addition, the difference in A_1 and A_2 values seems to be the major driving factor for how far out radially the BC zone expands. The Pentolite had the largest difference and thus the smallest radial distance, while TNT has the smallest difference and thus the largest radial distance of the BC zone.

b. <u>100 lb, 200 lb, and 300 lb charges of HBX-1 at 50 ft:</u>

Figure 85 is a 2D representation of the bulk cavitaion zone of a HBX explosive charge of varying weights (100lb, 200 lb, and 300lb) detonated at a constant depth of 50 feet. Once again the location of explosive depicted in the left vertical axis of each subplot. The purpose of the plot is to represent the effect of charge weight on the bulk caviation zone with other variables (charge type, detonation depth) held constant. As expected, as the charge weight is increased while the detonation depth and charge type are held constant, both the depth and breadth of the BC zone are increased.

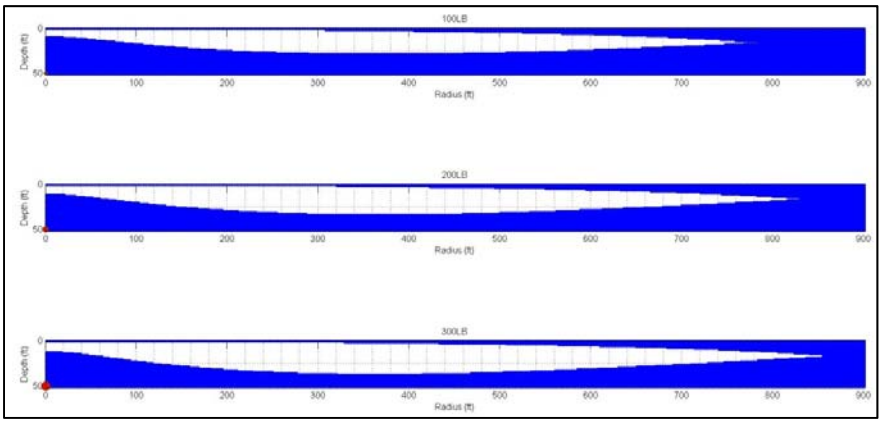

Figure 85. 2-D Bulk Cavitation of 100, 200, and 300lbs of HBX-1@ 50ft

c. 250 lb charge of TNT detonated at varying depths (5, 50 and 500ft):

Figure 86 is a 2D representation of the bulk cavitaion zone of a TNT explosive charge of 250lbs detonated at varying depths of 5, 50, and 500 ft. Figure 87 shows extended range of 250 lb at 500ft for obvious reason. Once again, the explosive is depicted along the left vertical axis of each subplot. Again, the purpose of the plot is to represent the effect of charge weight on the bulk caviation zone with other variables (charge type, detonation depth) held constant.

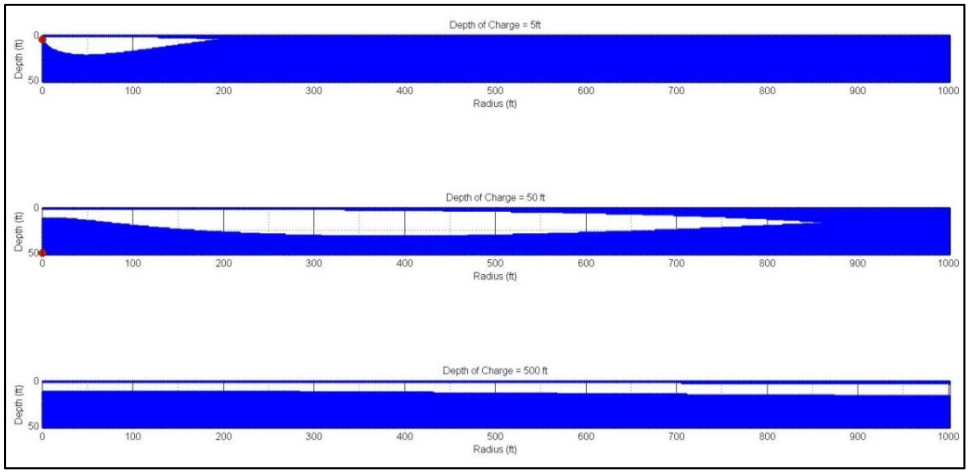

Figure 86. 2-D Bulk Cavitation of 250lbs TNT detonated @ 5, 50 and 500ft

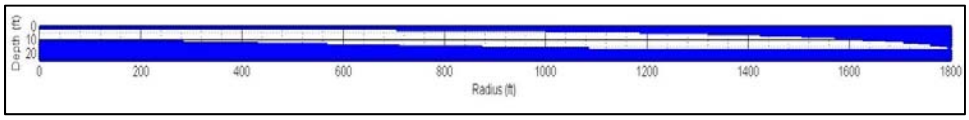

Figure 87. Extended View of 250lbs TNT detonated @ 500ft

As expected, as the depth of the detonation point of a charge varies, with the weight and type of charge being held constant, the BC region grows both in depth and breadth, with the exception of the 500' depth charge. This charge does have massive radial distance (more than twice the radial distance of charge at 50ft) compared to the other two and the thickness of the BC zone seems to grow radially rather than maximum thickness being at or near the center of the BC zone. This is most likely due to the fact that the pressure from incident and image charges are very low (having decayed

significantly already as it traveled vertically 500ft) and are at a relatively shallow depth. Therefore, the total pressure at this water column, although significantly lower than other two depth cases, is enough to create a cavitation while the surrounding pressure rises to the vapor pressure of the water (about 0.3 psi). In addition, the SW that causes the pressure havoc in this water column and causes the BC has traveled significantly farther than shallower depth charges.

2. 3-D visualization of the BC space for an underwater explosion resulting from the detonation of a 1,000lbs charge of TNT located at a depth of 25ft: (Appendix C contains MATLAB codes for 3D TNT BC Zone):

Figures 88 and 89 depict the 2D and 3D representation of 1,000lbs charge of TNT located at 25ft depth. The growth and shape of the BC zone follows the same pattern observed previously in section 1 of this report. Figure 5 below shows regional and line depiction of the BC region. Following the same trend of BC formation, the maximum thickness appears at 200ft radial distance from "ground zero" or point of detonation with about 40ft thickness. The radial length of the BC region is about 650ft.

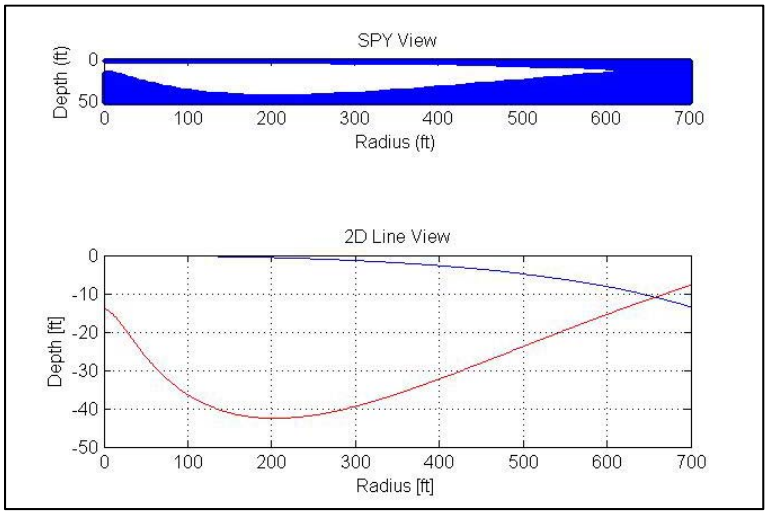

Figure 88. SPY and Line View of 1,000lbs TNT at 25ft Depth

Figure 89 is a 3D representation of BC. The overall shape is almost like a flying saucer with a dip on the bottom side of the disc. For the below representations, the top of the BC region was removed to show the contour shape within the region. The figure on

the right depicts “ground zero” and shows the radial expansion of the explosion below the BC zone. The usual maximum dip that is represented at the center of the BC zone is also depicted in both figures almost like an upside down bell.

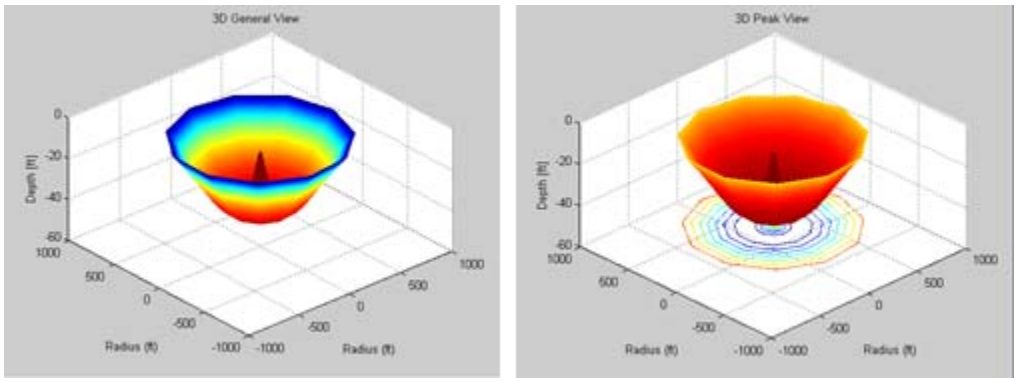

Figure 89. 3D General Top and Peak Top View of 1000lbs TNT at 25ft Depth

THIS PAGE INTENTIONALLY LEFT BLANK

APPENDIX D. BULK CAVITATION MATLAB CODES

```
% ========================================================================
%                     Computation of Bulk Cavitation Zone
%                          for Underwater Explosions
%                                    By
%                               LT Dean Ahn, USN
% ========================================================================
% This program is used to develop the BC envelope for an
% underwater charge of TNT at various 1000 lbf charge weights, 25ft depth
% and plot them in 2D & 3D.
% ========================================================================
%% Prep Matlab workspace
clear all;
clc; close all;

% 2-D SPY:  BC visualization of UNDEX, 1000 lb charge TNT @25ft
clear all;
clc;

% Constants
Pa = 14.7; % Atmpospheric pressure (psi)
Gamma = 62.5/144; % Weight density of water (lb/ft^3)
C = 5; % Acoustic velocity of water (ft/msec)

K1 = 22505; % Pmax
A1 = 1.18; % Pmax
K2 = 0.058; % Decay constant
A2 = -0.185; % Decay constant

% Plotting BC in 2D, TNT, 1000 lb @ 25ft:
counter = 0;
i = 1;
for W = [1000]; % Equivalent charge weights (lb)
    for D1= [25]; % Charge location depths (ft)
    counter = counter+1;
    A=zeros(50,700);
    for y = 1:51;
        for x = 1:701;
            R1 = sqrt((D1 - (y-1))^2 + (x-1)^2);
            % Distance from charge to desired location (ft)
            R2 = sqrt((D1 + (y-1))^2 + (x-1)^2);
            % Distance from image charge to desired location (ft)
            theta = K2*(W^(1/3))*(((W^(1/3))/R1)^(A2));
            % Decay Constant (msec)
            Pi = (K1*(W^(1/3)/R1)^(A1))*(exp(-(R2 -R1)/(C*theta)));
            % Incident Pressure Wave (psi)
            Ph = Gamma*(y-1); % Hydrostatic Pressure at y (psi)
            Pr = (K1*((W^(1/3)/R2)^(A1))); % Refelcted Pressure Wave (psi)
            F = Pi + Pa + Ph - Pr; % Upper Bulk Caviataion Boundary
            G1  =  -Pi/(C*theta)*(1+(((R2-2*D1*((D1+(y-1))/R2))/R1)*(A2*R2/R1-A2-
1)));
            G2 = -(A1*Pi/R1^2)*(R2-2*D1*((D1+(y-1))/R2));
            G3 = Gamma*((D1+(y-1))/R2) ;
            G4 = (A1/R2)*(Pi+Pa + Ph);
            G = G1 + G2 + G3 + G4; % Lower BC Boundary
            if F > 0.001; % Combine BC Boundaries
                if G < 0;
                    A(y,x) = 1;
```

```
                end
            end
            if G > 0;
                A(y,x) = 1;
            end
        end
    end
    temp(:,:,counter) = A;
    end
    charge=num2str(W);
   i=i+1;
end
    figure4=figure('NumberTitle',  'off',  'Name',  'Bulk  Cavitation  Region:
1000LB TNT Charge UNDEX at 25FT Depth', 'PaperOrientation', 'Landscape');

    subplot1=subplot(2,1,1,'Parent',figure4);
    box(subplot1,'on');
    hold(subplot1,'all');
    spy(temp(:,:,1))
    title('SPY View')
    xlabel('Radius (ft)')
    ylabel('Depth (ft)')
    plot(figure4)

%% 2-D Line
gamma=0.03703;   % seawater weight density (lb/in^3)
pa=14.7;         % atmospheric pressure (psi)
c=5;             % acoustic velocity (ft/msec)

charge_type = 2;
D = 25;
W = 1000;

% TNT Data:
    chg_name='TNT charge';
    depth=num2str(D);
    weight=num2str(W);
    K1=22505;
    A1=1.18;
    K2=0.058;
    A2=-0.185;
    ub_data=[];
    lb_data=[];

% Calculation of the upper boundary:
    for x=0:700
        for y=0:0.1:510
             r1=sqrt((D-y)^2+x^2);
            r2=sqrt((D+y)^2+x^2);
    theta=K2*W^(1/3)*(W^(1/3)/r1)^A2 ;
    F1=K1*(W^(1/3)/r1)^A1*exp(-(r2-r1)/(c*theta));
    F2=(gamma*y*12)-K1*(W^(1/3)/r2)^A1+pa ;
    F=F1+F2 ;
    if F<=0
        ub_data=[ub_data;F x -y];
        break
    end
        end
    end

% Calculation of the lower boundary:
for x=0:700
```

```
    for y=0:0.1:510
            r1=sqrt((D-y)^2+x^2);
            r2=sqrt((D+y)^2+x^2);
      theta=K2*W^(1/3)*(W^(1/3)/r1)^A2;
     pi=K1*(W^(1/3)/r1)^A1*exp(-(r2-r1)/(c*theta));
     G1=-(pi/(c*theta))*(1+(((r2-(2*D*(D+y)/r2))/r1)*(((A2*r2)/r1)-A2-1)));
     G2=-((A1*pi)/r1^2)*(r2-2*D*((D+y)/r2));
     G3=(gamma*12)*((D+y)/r2);
     G4=(A1/r2)*(pi+pa+(gamma*y*12));
     G=G1+G2+G3+G4;
     if G>=0
         lb_data=[lb_data;G x -y];
         break
     end
    end
end

% Plot upper and lower boundary data in 2D:
subplot(2,1,2)
plot(ub_data(:,2),ub_data(:,3),'b',lb_data(:,2),lb_data(:,3),'r')
xlabel('Radius [ft]')
ylabel('Depth [ft]')
title(['2D Line View'])
grid on

%% 3D Mesh & Peak Mesh:  BC View of 1000 lbf TNT Charge at 25ft
figure
r = ub_data(:,2) ;
z = lb_data(:,3) ;
w = ub_data(:,3) ;
theta = 0:pi/20:2*pi;
X = bsxfun(@times,r,cos(theta));
Y = bsxfun(@times,r,sin(theta));
Z = repmat(z,1,length(theta));
W = repmat(w,1,length(theta));
grid on
% subplot(1,2,1)
mesh(X, Y, Z, W)
title('3D General View ')
    xlabel('Radius (ft)')
    ylabel('Radius (ft)')
    zlabel('Depth [ft]')
% subplot(1,2,2)
figure
meshc(X, Y, Z, W)
title('3D Peak View')
    xlabel('Radius (ft)')
    ylabel('Radius (ft)'
    zlabel('Depth [ft]')
```

THIS PAGE INTENTIONALLY LEFT BLANK

APPENDIX E. SAMPLE GEMGRID CODES

```
format=00003

 <X GRID LINES>
   DatumIndex=1
   Datum=0.
   NCells=na  SizeFirstCell=20.  SizeLastCell=20.  Ratio=na  Width=24384.      #800ft
 <END X GRID LINES>

 <Y GRID LINES>
   DatumIndex=1
   Datum=0.
   NCells=1  SizeFirstCell=na  SizeLastCell=na  Ratio=1.  Width=1.             #2D Run
   # NCells=na  SizeFirstCell=20.  SizeLastCell=20.  Ratio=na  Width=9144.     #300ft
 <END Y GRID LINES>

 <Z GRID LINES>
   DatumIndex=1
   Datum=-16002.
   NCells=na  SizeFirstCell=20.  SizeLastCell=20.  Ratio=na  Width=762.        #25ft clay
   NCells=na  SizeFirstCell=20.  SizeLastCell=20.  Ratio=na  Width=15240.      #500ft
water
   NCells=na  SizeFirstCell=20.  SizeLastCell=20.  Ratio=na  Width=762.        #25ft clay
 <END Z GRID LINES>

 <OPTIONS>
  #Plot=DysmasP
 <END OPTIONS>
```

THIS PAGE INTENTIONALLY LEFT BLANK

APPENDIX F. SAMPLE PREGEMINI CODES

```
format=00017

 <OPTIONS>
   Mode=start                       # PreGemini mode (Start/Rezone/Overlay/Repartition)
   StartTime=0.                     # Set initial time (REAL/precalc)
   Gravity=1g                          # Gravity, positive upward (REAL/1g)
 <END OPTIONS>

 <GRID>
   Coordinates=cylindrical          # Coordinates: CARTESIAN, CYLINDRICAL, or SPHERICAL
   xCells=1219   dx=0. xDatum=0.
   yCells=1      dy=0. yDatum=0.
   zCells=838    dz=0. zDatum=0.
   GridFile=./grid/grid.asc         # File name for grid file specify (none/STRING)
 <END GRID>

 <SUBGRIDS>
   XSubGrids=4  XPartition=auto
   YSubGrids=1  YPartition=auto
   ZSubGrids=3  ZPartition=auto
 <END SUBGRIDS>

 <BOUNDARY CONDITIONS>
   xmin=wall xmax=free              # wall2/wall/freeng/free/REAL
   # ymin=wall ymax=free
   zmin=wall zmax=free
 <END BOUNDARY CONDITIONS>

 <MATERIALS>
   MaterialID=he_solid    File=hbx_1solid.mtl
   MaterialID=he_gas      File=hbx_1.mtl
   MaterialID=water               File=tillwater.mtl
   MaterialID=air                 File=air.mtl
   MaterialID=clay                File=clay.mtl
 <END MATERIALS>

 <BURN>
   Unburned=he_solid  Burned=he_gas  Time=0. RefPt=(0., 0., -1524.) #50ft z-deep 2D Run
 <END BURN>

 <HYDROSTATIC FIELD>
   pRef=1.0e+6    zRef=0.  zMax=max         # Ref pressure, ref location, zMax (must be
1st line)
   Material=air   ei=eref  zMin=0.  # top state
   Material=water         ei=eref  zMin=-15240.      # 2nd state
   Material=clay  ei=eref  zMin=-16002.      # bottom state
 <END HYDROSTATIC FIELD>


 <INITIAL STATES>    # state     matl      g    frac   rho         e        p   a0   u
v   w
   StateID=he_solid  Material=he_solid      Rho=rhoref       ei=eref  EOSvar=(0.)      #
explosive state
   StateID=water          Material=water    Rho=rhoref       ei=eref  EOSvar=(0.)      #
water state
   StateID=air    Material=air      Rho=rhoref       ei=eref  EOSvar=(0.)      #
atmosphere state
   StateID=clay           Material=clay     Rho=rhoref       ei=eref          EOSvar=(0.)
 <END INITIAL STATES>

 <FLOWFIELD>
   Option=hydrostatic
   Option=ball    state=he_solid    mass=11340.      RefPt=(0., 0., -1524.)   #25lb @ 50ft
 <END FLOWFIELD>

 <TEXT OUTPUT>
    imin=1  imax=1  jmin=1  jmax=1  kmin=1  kmax=1
 <END TEXT OUTPUT>
```

THIS PAGE INTENTIONALLY LEFT BLANK

APPENDIX G. SAMPLE GEMINI CODES

```
format=00015

 <CASE>
   StartFile=./pregemini/restart_000000_xxx.bin  # Start file  (use "_xxx.bin" extension
for parallel runs)
   Title=500ft                  # Title (Limit 40 characters)
   Mode=fluid                      # Run mode (Fluid/Coupled)
 <END CASE>

 <TERMINATE>
   EndStep=999999                  # Termination step (INT/none)
   EndTime=.15                     # Termination time (INT/none)
   dtMin=1.e-12                    # Terminate if step size is less than this value
(sec)
   <TRAP>
   #  x=608.44 j=1 z=-123.86 Var=p Dif=0.01
   <END TRAP>
 <END TERMINATE>

 <INTEGRATION>
   CFL=.45                         # CFL safety factor (0.9 for 1D, 0.45 for 2D and 3D)
   CFLInit=.05                     # Initial step CFL factor
   Limiter=2.                      # Limiter: 0.0 - 2.0
   LagEqualize=sou                 # Equalize after Lagrange step
   RemapEqualize=on                # Equalize after remap step
   Protect=1                       # Protect (=0 off, >0 on)
 <END INTEGRATION>

 <CELL HISTORY>
  i=1        j=0. k=-1524.             #charge center at 50ft z-deep

  x=3048.    y=0.         z=-25.                    #at x=25cm z-deep
  x=4572.    y=0.         z=-25.
  x=6096.    y=0.         z=-25.                #plus every 100ft to 800ft
  x=7620.    y=0.         z=-25.
  x=9144.    y=0.         z=-25.                    #except at 150, 200, 250, 300, 350,
400ft
  x=10668.   y=0.         z=-25.
  x=12192.   y=0.         z=-25.
  x=15240.   y=0.         z=-25.
  x=18288.   y=0.         z=-25.
  x=21336.   y=0.         z=-25.
  x=24384.   y=0.         z=-25.

  x=3048.    y=0.         z=-1524.         #at x=50ft z-deep
  x=4572.    y=0.    z=-1524.
  x=6096.    y=0.         z=-1524.             #plus every 100ft to 800ft
  x=7620.    y=0.    z=-1524.
  x=9144.    y=0.         z=-1524.
  x=10668.   y=0.    z=-1524.
  x=12192.   y=0.         z=-1524.
  x=15240.   y=0.         z=-1524.
  x=18288.   y=0.         z=-1524.
  x=21336.   y=0.         z=-1524.
  x=24384.   y=0.         z=-1524.

  x=3048.    y=0.         z=-2134.                  #at x=70ft z-deep
  x=4572.    y=0.    z=-2134.
  x=6096.    y=0.         z=-2134.             #plus every 100ft to 800ft
  x=7620.    y=0.    z=-2134.
  x=9144.    y=0.         z=-2134.
  x=10668.   y=0.    z=-2134.
  x=12192.   y=0.         z=-2134.
  x=15240.   y=0.         z=-2134.
  x=18288.   y=0.         z=-2134.
  x=21336.   y=0.         z=-2134.
  x=24384.   y=0.         z=-2134.

 <END CELL HISTORY>
 <CONTOUR PLOTS>
   StepFreq=3000                  # Plot step frequency (INT/none/table)
   TimeFreq=0.001                 # Plot time frequency (REAL/none/table)
```

```
 <TARGET PLOT STEPS>
  3000
 <END TARGET PLOT STEPS>

 <TARGET PLOT TIMES>
  0.0001
  0.001
  0.025
  0.030
  0.035
  0.040
  0.045
  0.050
  0.055
  0.060
  0.065
  0.070
  0.075
  0.080
  0.085
  0.090
  0.095
  0.100
  0.105
  0.110
  0.120
  0.130
  0.140
  0.150
 <END TARGET PLOT TIMES>
 <END CONTOUR PLOTS>

 <RESTART>
   StepFreq=1000                    # Restart file output step frequency (INT/none)
   SaveFreq=100                     # Retention interval (ex: use 1 to save every file,
use 2 to delete every other file)
 <END RESTART>

 <TEXT OUTPUT>
   StepFreq=500                     # Output step frequency (INT/none)
   TimeFreq=1000.                   # Output time frequency (INT/none)
   imin=1 imax=1 jmin=1 jmax=1 kmin=1 kmax=1
 <END TEXT OUTPUT>

 #<COUPLED>
   #Units=cm-g-s
   #BackPressure=0.e+6               # Back pressure inside SWI bodies (d/cm^2)
   #LoadFailedSWI=on                 # Load failed SWI elements (on/off)
   #BodyOrigin=(0., 0., 0.)          # Location of Body coordinate system in Fluid mesh
(cm)
   #BodyXAxis=(1., 0., 0.)           # Vector along Body coordinate system x axis in
Fluid coordinates (cm)
   #BodyYAxis=(0., 1., 0.)           # Vector along Body coordinate system y axis in
Fluid coordinates (cm)
   #BodyZAxis=(0., 0., 1.)           # Vector along Body coordinate system z axis in
Fluid coordinates (cm)
 #<END COUPLED>

 #<ELEMENT HISTORY>
  #1
  #2
  #3
 #<END ELEMENT HISTORY>

 #<NODE HISTORY>
 #1
 #2
 #3
 #4
 #<END NODE HISTORY>
```

APPENDIX H. SAMPLE GEMFIELD CODES

```
Format=00004

<Case>
DirOut=./             # Subdirectory for output files.  (Required.  Make optional?)
                        # Use "./" for current working directory.
Series=xyz             # Series: Output file identifier (1-10 characters or "").
(Optional)

  FileFormat=DysmasP                                  # DysmasP (latest format), DysmasP2010
or DysmasP2007
#
#  FileFormat=Tecplot     FileSplit=Single           # Tecplot (latest format), Tecplot10,
or Tecplot9
#  FileFormat=Tecplot     FileSplit=ByVar            # Tecplot (latest format), Tecplot10,
or Tecplot9
#  FileFormat=Tecplot     FileSplit=ByTime           # Tecplot (latest format), Tecplot10,
or Tecplot9
#  FileFormat=Tecplot     FileSplit=ByVarAndTime     # Tecplot (latest format), Tecplot10,
or Tecplot9
#  FileFormat=vtkxml      FileType=binary            # vtkxml (ascii or binary) or
vtklegacy (ascii only)
#  FileFormat=vtkxml      FileType=ascii             # vtkxml (ascii or binary) or
vtklegacy (ascii only)
#  FileFormat=vtklegacy                              # vtkxml (ascii or binary) or
vtklegacy (ascii only)

<End Case>


#Note: all vars are optional
<TIME>
  tBeg=-1.000    tEnd=.25      # tBeg,tEnd: Time window for output (sec) (before scaling
or offset)
                               # Default: Entire simulation time
  tOffset=0.00   tScale=1.00  # tOffset, tScale: Offset and scaling for time (Default:
tOffset=0, tScale=1)
                               # t <== tScale*(tOffset+t)
  MaxTimeRecords=50000         # Max number of time records to generate.
     #Note: These target times are in ADDITION to any data at times within the time
window (tBeg, tEnd)
     #specified above.  If you want only the target times then set tBeg and tEnd negative
(or very large).
  <TIME STEP TARGETS>
    #1815
    #6000
  <END TIME STEP TARGETS>
<END TIME>


<OPTIONS>
  ShowFailed=on    # Show failed body elements (on or off, default is on)
                   # (Use "on" to preserve correct element numbering in Tecplot)
  Verbosity=1      # Amount of screen output (Default=1)
<END OPTIONS>


# At least one plot variable is required
# Default units are cgs
<FLUID VARIABLES>
##These vars are only available as cell-averaged quantities
  Var=p                 Units=psi      #Units: psi, ksi, Pa, MPa, bar  or scaling factor
  Var=u                 Units=1.       #Units: m/s, ft/s, in/s  or scaling factor
  Var=v                 Units=1.       #Units: m/s, ft/s, in/s  or scaling factor
  Var=w                 Units=ft/s     #Units: m/s, ft/s, in/s  or scaling factor
  Var=ekin                             #Units: J, MJ  or scaling factor
##These vars are available as cell-averaged (MatNum=0) or per material (MatNum>0)
  Var=r     MatNum=0    Units=1.0      #Units: kg/m^3  or scaling factor
  Var=r     MatNum=1    Units=1.0      #Units: kg/m^3  or scaling factor
  Var=r     MatNum=2    Units=1.0      #Units: kg/m^3  or scaling factor
  Var=e     MatNum=0    Units=1.0      #Units: J, MJ  or scaling factor
  Var=e     MatNum=1    Units=1.0      #Units: J, MJ  or scaling factor
  Var=e     MatNum=2    Units=1.0      #Units: J, MJ  or scaling factor
  Var=eint  MatNum=0    Units=1.0      #Units: J, MJ  or scaling factor
```

```
  Var=eint  MatNum=1    Units=1.0      #Units: J, MJ  or scaling factor
  Var=eint  MatNum=2    Units=1.0      #Units: J, MJ  or scaling factor

##These vars are only available per material (MatNum>0)
  Var=f     MatNum=1                   #No units
  Var=f     MatNum=2                   #No units
<END FLUID VARIABLES>

<BODY NODE VARIABLES>
#  Var=u                 Units=1.       #Units: m/s, ft/s, in/s  or scaling factor
#  Var=v                 Units=1.       #Units: m/s, ft/s, in/s  or scaling factor
#  Var=w                                #Units: m/s, ft/s, in/s  or scaling factor
<END BODY NODE VARIABLES>

<BODY ELEMENT VARIABLES>
#  Var=p                 Units=Pa       #Units: psi, ksi, Pa, MPa, bar  or scaling factor
#  Var=pPos              Units=Pa       #Units: psi, ksi, Pa, MPa, bar  or scaling factor
#  Var=pNeg              Units=Pa       #Units: psi, ksi, Pa, MPa, bar  or scaling factor
<END BODY ELEMENT VARIABLES>


  #Optional. If left unspecified, the entire domain will be output
<SUBDOMAIN>
  iMin=1     iMax=9999999     iDelta=1
  yMin=0.    yMax=0.          jDelta=1
  kMin=1     kMax=9999999     kDelta=1
  Offset=(0.,0.,0.)
<END SUBDOMAIN>


#########################################################
# The following is a Key to the Plottable Variables
#########################################################
#   Variable:                       allowed MatNum (0...NMat)
# all =  all point variables             NA
#   u = velocity in r,x-dir              0
#   v = velocity in y,theta-dir          0
#   w = velocity in z-dir                0
#   p = pressure                         0
#   r = density                          any
#   e = total specific energy            any
# eint= internal energy                  any
# ekin= kinetic energy                   0
#   t = temperature                      0
#   f = volume fraction                  >0
#   i = impulse intensity (time in sec)   0   (for his only)
# eos#= EOS variable number #            0    (only 1 material allowed to have this
feature, it is picked automatically
#                                            (currently only available for P-alpha EOS)
# stat= status of cell (active/blocked)  0    (for field only)
# mat = material id                      NA

#############################################################
# The following are Scaling Factors for some common units
#############################################################
# Pressure
#  1.450377e-005  #psi
#  1.450377e-008  #ksi
#  0.1            #Pa
#  1.e-007        #MPa
#  1.e-006        #bar
# Force
#  1.e-005        #N
#  1.e-008        #kN
#  2.248089e-006  #lbf
# Acceleration
#  0.01       #m/s^2
#  0.0328083  #ft/s^2
#  0.3937008  #in/s^2
# Velocity
#  0.01       #m/s
#  0.0328083  #ft/s
#  0.3937008  #in/s
# Distance
#  0.01       #m
#  0.0328083  #ft
#  0.3937008  #in
# Volume
#  1.e-006        #m^3
```

```
#  3.531467e-005  #ft^3
#  0.06102374     #in^3
# Density
#  1000       #kg/m^3
# Energy
#  1.e-007    #J
#  1.e-013    #MJ
# Mass
#  0.001      #kg
# Impulse intensity
#  0.1            #Pa*s
#  1.e-007        #MPa*s
#  1.e-006        #bar*s
#  1.450377e-005  #psi*s
#  1.450377e-002  #psi*ms
```

THIS PAGE INTENTIONALLY LEFT BLANK

APPENDIX I. SAMPLE GEMHIS CODES

```
Format=00004

<Case>
DirOut=./             # Subdirectory for output files.  (Required.  Make optional?)
                        # Use "./" for current working directory.
Series=""             # Series: Output file identifier (1-10 characters or "").
(Optional)

  FileFormat=dysmasp                                  # DysmasP (latest format), DysmasP2010
or DysmasP2007
#
#  FileFormat=Tecplot   FileSplitPt=Single      FileSplitGbl=Single     # Tecplot (latest
format), Tecplot10, or Tecplot9
#  FileFormat=Tecplot   FileSplitPt=Single      FileSplitGbl=ByVar      # Tecplot (latest
format), Tecplot10, or Tecplot9
#  FileFormat=Tecplot   FileSplitPt=ByVar          # Tecplot (latest format), Tecplot10,
or Tecplot9
#  FileFormat=Tecplot   FileSplitPt=ByPt           # Tecplot (latest format), Tecplot10,
or Tecplot9
#  FileFormat=Tecplot   FileSplitPt=ByVarAndPt     # Tecplot (latest format), Tecplot10,
or Tecplot9
#
#  FileFormat=plain   FileSplitPt=ByVarAndPt     #
<End Case>


#Note: all vars are optional
<Time>
  tBeg=-1.000    tEnd=.15       # tBeg,tEnd: Time window for output (sec) (before scaling
or offset)
                                # Default: Entire simulation time
  tOffset=0.00  tScale=1.00     # tOffset, tScale: Offset and scaling for time (Default:
tOffset=0, tScale=1)
                                # t <== tScale*(tOffset+t)
MaxTimeRecords=500000           # Set max num of time records (used for array allocation)
(default=500000)
RemoveOverlap=on                # Flag for removing oldest data if there is a time
overlap (on or off, default is on)
<End Time>


# Default units are cgs
<Point Variables>
##These vars are only available as cell-averaged quantities
  Var=p                 Units=1.       #Units: psi, ksi, Pa, MPa, bar  or scaling factor
  Var=u                 Units=1.       #Units: m/s, ft/s, in/s  or scaling factor
  Var=v                 Units=1.       #Units: m/s, ft/s, in/s  or scaling factor
  Var=w                 Units=1.       #Units: m/s, ft/s, in/s  or scaling factor
  Var=ekin                             #Units: J, MJ  or scaling factor
  Var=i                                #No units
##These vars are available as cell-averaged (MatNum=0) or per material (MatNum>0)
  Var=r     MatNum=0    Units=1.0      #Units: kg/m^3  or scaling factor
  Var=r     MatNum=1    Units=1.0      #Units: kg/m^3  or scaling factor
  Var=r     MatNum=2    Units=1.0      #Units: kg/m^3  or scaling factor
  Var=e     MatNum=0    Units=1.0      #Units: J, MJ  or scaling factor
  Var=e     MatNum=1    Units=1.0      #Units: J, MJ  or scaling factor
  Var=e     MatNum=2    Units=1.0      #Units: J, MJ  or scaling factor
  #Var=e     MatNum=3    Units=1.0      #Units: J, MJ  or scaling factor
  Var=eint  MatNum=0    Units=1.0      #Units: J, MJ  or scaling factor
  Var=eint  MatNum=1    Units=1.0      #Units: J, MJ  or scaling factor
  Var=eint  MatNum=2    Units=1.0      #Units: J, MJ  or scaling factor

##These vars are only available per material (MatNum>0)
  Var=f     MatNum=1                   #No units
  Var=f     MatNum=2                   #No units
<End Point Variables>


####################################
#The remaining sections are optional
####################################
```

```
<Options>
ChargeScale=1.        # Scaling for specie (EnergyInt, Energy, Mass, Volume, Radius)
(default=1.)
Verbosity=1           # IVerbose: Screen output (0=no, 1=some, 2=lots)
pRefImp=-5.00e7       # Impulse intensity ref pressure (dynes/cm^2) (if unset then use
value from 1st record in file)
<End Options>

<Global Variables>
#Note: MatNum=0 is for total of all materials
   Var=radius       MatNum=1      Units=1.     #Units: m, ft, in  or scaling factor
   Var=volcav          MatNum=3      Units=1.     #Cavitation volume in water

#for body/block fixed mesh option
#   Var=BodyCG-X
#   Var=BodyCG-Y
#   Var=BodyCG-Z
#   Var=BodyVel-X
#   Var=BodyVel-Y
#   Var=BodyVel-Z
#   Var=BodyF-X
#   Var=BodyF-Y
#   Var=BodyF-Z
<End Global Variables>



<Body Global Variables>
 Var=force-x
 Var=force-y
 Var=force-z
 Var=force
#Var=impulse
<End Body Global Variables>

<Body Element Variables>
   Var=p
#  Var=i
<End Body Element Variables>

<Body Node Variables>
Var=force-x
Var=force-y
Var=force-z
Var=force
Var=u
Var=v
Var=w
Var=vel
Var=x
Var=y
Var=z
<End Body Node Variables>



#######################################################
# The following is a Key to the Global Variables
#######################################################
#   Variable:                     allowed MatNum (0...NMat)
# all =  all global variables            NA
# dt = Gemini time step size             NA
# mass = mass                            any
# energy = total energy                  any
# radius = equivalent radius             >0
# vol = volume                           >0
# volcav = cavitated volume              >0
# BodyVel-[xyz]                          NA   (for body/block fixed mesh option)
# BodyCG-[xyz]                           NA   (for body/block fixed mesh option)
# BodyF-[xyz]                            NA   (for body/block fixed mesh option)
#
#######################################################
# The following is a Key to the Point Variables
#######################################################
#   Variable:                     allowed MatNum (0...NMat)
# all =  all point variables             NA
#   u = velocity in r,x-dir              0
#   v = velocity in y,theta-dir          0
#   w = velocity in z-dir                0
```

```
#   p = pressure                          0
#   r = density                           any
#   e = total specific energy             any
# eint= internal energy                   any
# ekin= kinetic energy                    0
#   t = temperature                       0
#   f = volume fraction                   >0
#   i = impulse intensity (time in sec)    0   (for his only)
# eos_#= EOS variable number #            0    (only 1 material allowed to have this
feature, it is picked automatically
#                                             (currently only available for P-alpha EOS)
# stat= status of cell (active/blocked)  0    (for field only)
# mat = material id                     NA

#######################################################
# The following is a Key to the Body Global Variables
#######################################################
# force-x = Total body force in r,x-dir       (sum of node forces)
# force-y = Total body force in y,theta-dir   (sum of node forces)
# force-z = Total body force in z-dir         (sum of node forces)
# force   = Total body force magnitude        (sum of node forces)
# impulse = Impulse (time in sec)

#######################################################
# The following is a Key to the Body Element Variables
#######################################################
#   p = Element pressure (net)
#   i = Impulse intensity (time in sec)
#   ppos = Element pressure on "positive" side (normal points toward "eye") of coupling
interface element
#   pneg = Element pressure on "negative" side (normal points away from "eye") of
coupling interface element

#######################################################
# The following is a Key to the Body Node Variables
#######################################################
# force-x = Node force in r,x-dir
# force-y = Node force in y,theta-dir
# force-z = Node force in z-dir
# force   = Node force magnitude
#   u = Node velocity in r,x-dir
#   v = Node velocity in y,theta-dir
#   w = Node velocity in z-dir
# vel = Node velocity magnitude
#   x = Node position (r,x-dir)
#   y = Node position (y,theta-dir)
#   z = Node position (z-dir)

#############################################################
# The following are Scaling Factors for some common units
#############################################################
# Pressure
#   1.450377e-005  #psi
#   1.450377e-008  #ksi
#   0.1            #Pa
#   1.e-007        #MPa
#   1.e-006        #bar
# Force
#   1.e-005        #N
#   1.e-008        #kN
#   2.248089e-006  #lbf
# Acceleration
#   0.01       #m/s^2
#   0.0328083  #ft/s^2
#   0.3937008  #in/s^2
# Velocity
#   0.01       #m/s
#   0.0328083  #ft/s
#   0.3937008  #in/s
# Distance
#   0.01       #m
#   0.0328083  #ft
#   0.3937008  #in
# Volume
#   1.e-006        #m^3
#   3.531467e-005  #ft^3
#   0.06102374     #in^3
# Density
#   1000       #kg/m^3
```

```
# Energy
#   1.e-007    #J
#   1.e-013    #MJ
# Mass
#   0.001      #kg
# Impulse intensity
#   0.1            #Pa*s
#   1.e-007        #MPa*s
#   1.e-006        #bar*s
#   1.450377e-005  #psi*s
#   1.450377e-002  #psi*ms
```

APPENDIX J. SAMPLE MATERIAL FILE

```
format=00002

 <OPTIONS>
   title="sand eos using miegrunisen eos"
   eosType=mieg
 <END OPTIONS>

 <REFERENCE>
   rhoRef=2.023
   eiRef=0.
   cRef=260000.0
 <END REFERENCE>

 <LIMITS>
   rhoMin=1.e-02
   eiMin=-9.9e+99
   pMin=2.e+4
 <END LIMITS>

 <EOS VARS>
   gamma0=.97
   S=1.86
   rho0=2.023
   ei0=0.0
   p0=0.0
   c02=4.048e+10
 <END EOS VARS>
```

THIS PAGE INTENTIONALLY LEFT BLANK

LIST OF REFERENCES

[1] A. P. Walters, "Investigation of an explicitly modeled solid ocean floor on a shallow water UNDEX event," M.S. thesis, ME Dept., Naval Postgraduate School, Monterey, CA, 2011.

[2] C. Cavas.(2014, Feb. 24). Pentagon changes course, halts LCS at 32 ships. *Defense News* [Online]. Available: http://www.defensenews.com/article /20140224/DEFREG02/302240026/Pentagon-Changes-Course-Halts-LCS-32-Ships

[3] L. D. Santiago, "Fluid-interaction and cavitation effects on a surface ship model due to an underwater explosion," M.S. thesis, ME Dept., Naval Postgraduate School, Monterey, CA, 1996.

[4] S. M. Arbogast, "The influence of shock-induced air bubble collapse resulting from underwater explosive events," M.S. thesis, ME Dept., Naval Postgraduate School, Monterey, CA, 2012.

[5] "Naval Ship shock design and analysis," lecture notes for ME4525, ME Dept., Naval Postgraduate School, 2012.

[6] R. H. Cole, *Underwater Explosion*, Vicksburg: U.S. Army Corp of Engineers, 2007, pp. 3–13.

[7] *Wikipedia*, s.v. "Blast Injury" [Online]. Available: http://en.wikipedia.org/wiki/Blast_injury

[8] H. G. Snay, "Underwater explosion phenomena: The parameters of migrating bubbles," U.S. Naval Ordnance Laboratory, White Oak, MD, Tech. Report NAVORD 4185, 1962.

[9] J. D. Gordon and F. A. Costanzo, "A solution to the axisymmetric bulk cavitation problem," *The Shock and Vibration Bulletin,* vol. 53, part 2 of 4, pp. 41–51, 1983.

[10] V. J. Cushing, "On the theory of bulk cavitation," Engineering Physics Company, Rockville, MD,1969.

[11] A. Wardlaw and R. Llami, "Simulation of underwater explosion cavitation phenomena," Naval Surface Warfare Center, Indian Head Division, Indian Head, 2004.

[12] Office of Naval Research, *DYSMAS, User's Manual*, Office of Naval Research, Arlington, VA, 2012.

[13] Office of Naval Research, *GEMINI: The DYSMAS Eulerian Solver Theory Manual*, Office of Naval Research, Arlington, VA, 2012.

[14] G. R. Prendergast, "Whipping analyses of the ddg-51 class full ship model," M.S. thesis, ME Dept., Naval Postgraduate School, Monterey, CA, 2004.

[15] T. S. Joergensen, "U.S. Navy operations in littoral waters: 2000 and beyond," *Naval War College Review,* vol. 51, no. Spring 1998, pp. 20–29.

[16] *Wikipedia*, s.v. "Littoral zone," [Online]. Available: http://en.wikipedia.org/wiki/Littoral_zone.

[17] D. Hinrichsen, *Coastal Waters of the World: Trends, Threats, and Strategies*, Washington, DC: Island Press, 1998.

[18] NOAA. (June 2014) "Satellite mapping of the ocean bottom," [Online]. Available: http://www.nnvl.noaa.gov/MediaDetail.php?MediaID=572&MediaTypeID=1

[19] B. M. Dobratz and P. C. Crawford, *LLNL Explosive Handbook: Properties of Chemical Explosives and Explosive Simulants*, Livermore: Lawrence Livermore National Laboratory, 1985.

[20] R. Buxton, "The effects of porous sea bottoms on the propagation of underwater shock waves using the p-alpha equation of state," M.S. thesis, CE Dept., Pennsylavnia State University, University Park, PA, 2009.

[21] N. Lu, T. H. Kim and W. J. Likos, "Tensile strength of unsaturated sand," *Journal of Engineering Mechanics ASCE, Vol. 135,* pp. 1401–1419, 2009.

[22] B. M. Das, *Principles of Geotechnical Engineering*, Pacific Grove: Brooks/Cole, 2002.

[23] E. Zywicz and J. Lin, "DYNA3D: A nonlinear, explicit, 3d finite element code for solid & structural mechanics," Methods Development Group, 2011.

INITIAL DISTRIBUTION LIST

1. Defense Technical Information Center
   Ft. Belvoir, Virginia

2. Dudley Knox Library
   Naval Postgraduate School
   Monterey, California